MICROCOPY RESOLUTION TEST CHART

NATIONAL BUREAU OF STANDARDS 1963 A

DTIC

FEB 1 4 1986

D

A SCHLIEREN AND HOT-WIRE
INVESTIGATION OF KARMAN
VORTEX STREETS

THESIS

John B. Wissler
First Lieutenant, USAF

AFIT/GAE/AA/85D-18

DEPARTMENT OF THE AIR FORCE

AIR UNIVERSITY

AIR FORCE INSTITUTE OF TECHNOLOGY

Wright-Patterson Air Force Base, Ohio

86 2 14 009

AFIT/GAE/AA/85D-18

DTIC
SELECTE
FEB 1 4 1986
S   D
D

A SCHLIEREN AND HOT-WIRE
INVESTIGATION OF KARMAN
VORTEX STREETS

THESIS

John B. Wissler
First Lieutenant, USAF

AFIT/GAE/AA/85D-18

AFIT/GAE/AA/85D-18

A SCHLIEREN AND HOT-WIRE INVESTIGATION

OF KARMAN VORTEX STREETS

THESIS

Presented to the Faculty of the School of Engineering

of the Air Force Institute of Technology

Air University

In Partial Fulfillment of the

Requirements for the Degree of

Master of Science in Aeronautical Engineering

John B. Wissler, B.S.

First Lieutenant, USAF

December 1985

Accesion For		
NTIS CRA&I	☒	
DTIC TAB	☐	
Unannou.ced	☐	
Justification		
By		
Di_t ib tio. /		
Availability Codes		
Dist	Avaii a.·d / or Special	
A-1		

Preface

This thesis began life as a study of the inter-
action between turbulent eddies and normal shock waves.
Von Karman Streets behind a cylinder were to be used to
provide a regular eddy pattern, and both hot-film anemometer
measurements and schlieren photographs were used to gain
information on the Karman Street vortices before, during,
and after the shock's passage. However, the further along
Lieutenant Colonel Jumper, my advisor, and I progressed,
the more we realized that we really did not understand
what the anemometer data was telling us about the character
of the vortices passing by it. Consequently, we delved
into the problem of how to characterize each individual
vortex based on the data from a single hot-film anemometer
and a schlieren photograph of the vortex. The result of
that effort is this thesis; unfortunately, due to time
constraints, we never did study the shock-wave/vortex
interaction.

I would like to thank my advisor, Lieutenant
Colonel Eric Jumper, for his support and encouragement
through the inevitable highs and lows of a thesis effort,
and my committee members, Dr. William Elrod and Dr. James
Hitchcock, for their assistance. My appreciation also to

Leroy Cannon, Jay Anderson, and Nick Yardich, of the

Department of Aeronautics and Astronautics Laboratory for

their help and their patience with an experimental neophyte,

and to Carl Shortt and Ron Ruley of the AFIT Shop for the

excellent machine fabrication support. Finally, I would

like to thank John Anthony, my son, and most importantly

of all, Beth, my wife, for their patience over the last

few months. They deserve a break from school more than

I do.

<div align="right">— John B. Wissler</div>

Table of Contents

List of Figures

List of Tables

x

List of Symbols

B_i	theoretical flow value	$lbm/(ft^2\text{-}s)$
c_1	vortex constant	$in\text{-}lbm/(ft^2\text{-}s)$
c_2	vortex constant	in^{-2}
D	cylinder diameter	in
D_1, D_2	rotational direction	+1 = counter-clockwise -1 = clockwise
f	frequency (also used as an arbitrary function)	sec^{-1}
fd	density factor	
$\vec{H}_f$	Hessian Matrix	
k	ratio of specific heats	1.4
m	coefficient for fourth order polynomial curve fit	
P	pressure	in Hg or psi
R	gas constant	53.3 ft-lbf/(lbm-R)
r	radius	in
T	temperature	deg-F
t	time	sec or msec
u	tangential velocity	ft/sec
$\bar{V}$	translational velocity	ft/sec
z	sum of squares of error between theoretical and experimental flows	

Γ_o	circulation	ft^2/sec
γ	angle	radians
θ	angle between upstream horizontal and radius from vortex center to anemometer	radians
ρ	density	lbm/ft^3
(ρu)	tangential mass flow per unit area	$lbm/(ft^2\text{-}s)$
(ρV)	measured mass flow per unit area	$lbm/(ft^2\text{-}s)$
$(\overline{\rho V})$	convective mass flow per unit area	$lbm/(ft^2\text{-}s)$
μ	viscosity	$lbm/ft\text{-}s$
ν	kinematic viscosity	ft^2/s

AFIT/GAE/AA/85D-18

Abstract

This investigation involved taking schlieren and
hot-film anemometer data on Karman vortex streets, then
developing a means of characterizing the individual
vortices in a street using a schlieren picture and the
corresponding anemometer trace. A ThermoSystems, Inc.
IFA-100 anemometer system, with a Tektronix 425 oscillo-
scope was used to record an anemometer trace. The trace
was captured on photographic film. The oscilloscope also
fired a Cordin Model 5401 Spark Lamp, which provided, via
a schlieren optical system, a physical picture of the
Karman Streets formed behind a 5/16-inch dia cylinder in a
2-inch by 2-inch square cross-section test region with a
Mach 0.43 flow. Distance and angle information were
obtained from the schlieren photographs, and timing and
anemometer output voltage were obtained from the anemometer
trace photograph using an HP-9874A digitizer. The data
was analyzed using a Newton-Raphson method to solve for
two constants, c_1 and c_2, which should have completely
characterized the vortices in the vortex street, assuming
the vortices followed the theoretical equation for a com-
bined free and forced vortex. It was assumed that the
superposition of two vortices plus the mean flow were the

parameters influencing the flow at any point in space and time. The core supremacy principle, which says that in a vortex core only one vortex contributes to the flow, was used in the data analysis. It was found that generally close fits between the theoretical data using the solved for constants c_1 and c_2, and the experimental data from the anemometer were possible, thus indicating reasonable vortex characterization.

A SCHLIEREN AND HOT-WIRE INVESTIGATION

OF KARMAN VORTEX STREETS

I.   Introduction

An object immersed in a flow of fluid, under cer-
tain conditions, will give rise to a phenomenon known as
the Karman vortex street, an alternating series of eddies
or vortices being periodically shed from the downstream
side of the object (Figure 1). This phenomenon occurs in
compressible or incompressible flow, and has been exten-
sively investigated over the years both experimentally and
theoretically (1; 2; 3; 4).

Because the Karman street is such a regular, and
hence readily characterized pattern of vortices, one could
conceivably use a Karman street to investigate turbulence.
Weston attempted to use the vortices to investigate tur-
bulence effects on laser beam propagation (5). However,
difficulties in getting a reliable Karman street led to a
further study by Clark on how to consistently generate a
vortex street (6). By subjecting a vortex street to
shocks of varying strengths, one could conceivably gain
information on turbulent energy transfer and eddy effects.

With these thoughts in mind, the following objec-
tives were devised as the focus of this research:

1

Fig. 1. Karman Street Vortex Behind a
Wedge from Clark (6:5)

1. Design and construct a facility capable of generating a Karman vortex street and subjecting the street to a normal shock wave.

2. Starting with the successful results of Clark (5), develop a means of characterizing the vortices in the Karman vortex street using both schlieren photography and hot-wire anemometry.

The rest of this research report focuses on the approach taken and the results of the investigation. Section II discusses the theory and approach. Section III describes the experimental apparatus and Section IV details the experimental procedure. Section V discusses the results of the research and Section VI lists the conclusions drawn. Finally, Section VII contains a list of recommendations for further work.

II. Theory and Approach

As mentioned before, vortices have been investi-
gated extensively, including their interaction with shock
waves. Some definitions and derivations will be recalled
for background, then some ideas with respect to experi-
mental analysis of Karman Streets will be developed.

Vortices and Their Formation

Broadly defined, a vortex is a "finite volume of
rotational fluid, bounded by irrotational fluid or solid
walls" (9:1). Schlichting shows a theoretical vortex as
having an approximately linear velocity profile for a
certain distance out from its center (the rotational core),
surrounded by a transition region and a velocity profile
varying inversely with r (4:89). The theoretical profile
for an incompressible vortex, shown in Figure 2, is well
supported by experimental results, an example of which is
shown in Figure 3, which is based on dynamic-stall-induced
vortices over airfoils (7:119). The radial decay outside
the core is due to viscous effects, which also cause the
vortex to flatten out and dissipate with time. The vortex
of Figure 2 is described by the equation (4:89)

$$u(r,t) = \frac{\Gamma_o}{2\pi r} \left(1 - \exp(-r^2/4\nu t)\right) \tag{1}$$

4
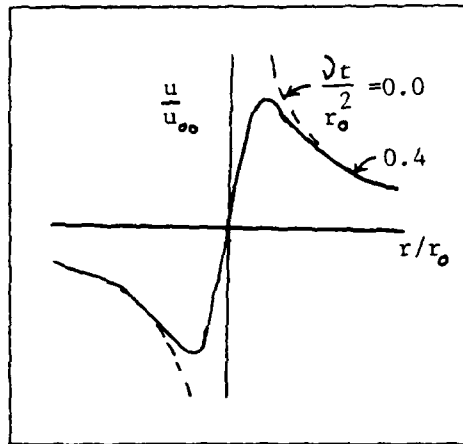
Fig. 2. Theoretical Profile for an
Incompressible Vortex
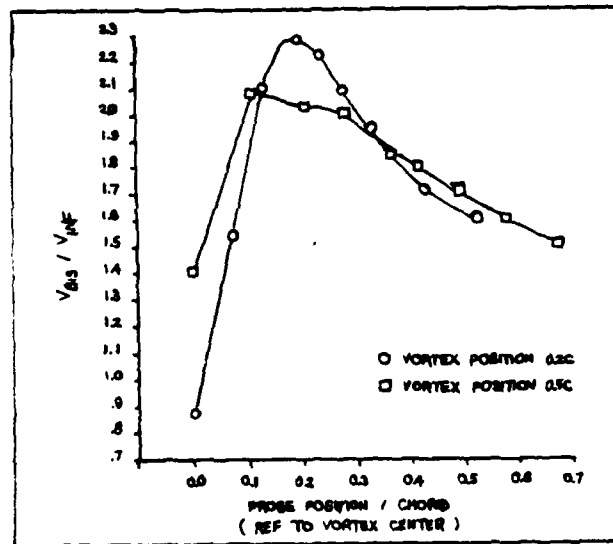
Fig. 3. Dynamic-Stall-Induced Vortex

5

where

u = tangential velocity

Γ_o = circulation of vortex at time = 0

ν = dynamic viscosity

$\bar{t}$ = time from formation as an ideal ($1/r$) vortex

Note that as r increases, $u(r,t)$ approaches a theoretical, irrotational free vortex ($u = \Gamma_o/2-r$).

Because the hot wire or hot-film anemometer is sensitive to the product of density, ρ, and velocity, u, of the fluid flowing across the wire/film (13:13), the density distribution of a vortex is also important. Starting with the incompressible equation (1) together with the radial momentum Navier-Stokes equation simplified for compressible, tangential flow (i.e. closed circular streamlines),

$$\frac{u^2}{r} = \frac{1}{\rho} \frac{\partial P}{\partial r} \tag{2}$$

one can arrive at equation (3), which gives a relationship for density variation across the vortex (8:222):

$$\frac{\rho_o - \rho}{\rho} = (1 - \frac{K}{\bar{t}})^{\frac{1}{k-1}} - 1 \tag{3}$$

where

ρ_o = density at vortex center

k = polytropic exponent (1.4 for air)

6

$\overline{t}$ = time from formation as an ideal vortex

$$K = ((k-1)/k\nu)(\Gamma_{oT}/4\pi)^2 * \rho/ P*L(\eta_a)$$

$$L(\eta_a) = \lim \int_0^{\eta_a} \frac{1}{\eta^3} [1-\exp(-1.259\eta^2)]^2 \, d\eta$$

r_o = core radius

$\eta = r/r_o$

η_a = outer (ambient) limit of vortex

Equation (3) assumes an isentropic relationship between pressure and density.
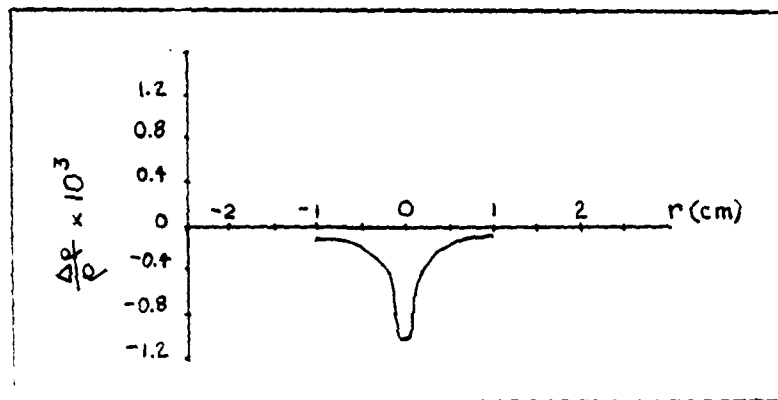
Fig. 4. Density Distribution Across a Vortex

As shown in Figure 4, the density is less in the center of the vortex, and greater on the extremities (8:221). This is due to centripetal (body) forces tending to move fluid away from the center of the vortex. This distribution form has been confirmed in other experimental and

computational studies (10; 11). Note also that the differences in densities across the vortex disappear with time, for the same reasons the rotational velocity disappears. Because the density changes are low (within 5 percent), the normal assumption is an approximately constant density across the vortex street for the purpose of mass-flow calculations.

Vortices can be formed by fluid flowing around an immersed object. Considering flow around a cylinder, as the fluid traverses the cylinder's surface it forms a boundary layer, and the pressure distribution first falls then rises (4:29). Eventually, the boundary layer separates away from the cylinder surface, and the fluid downstream of the separation point is entrained in a region of backflow, or recirculating fluid. As the velocity increases, a "bound" vortex first forms, then, with still higher velocities, breaks away, first on one side of the cylinder, then on the other, in a regular, periodic manner (3:18). Thus, the von Karman Vortex Street is formed.

The vortices are shed from a given side at a frequency which can be related to the Reynolds Number based on cylinder diameter. This relationship is given by Strouhal Number, S,

$$S = fD/V \qquad\qquad (4)$$

8

where

    f = shedding frequency from one side

    D = cylinder diameter

    V = freestream velocity

as a function of Reynolds Number, Re_D

$$Re_D = VD/\nu \tag{5}$$

where ν = kinematic viscosity. This relationship between
these parameters has been determined empirically and is
shown in Figure 5 (4:32).
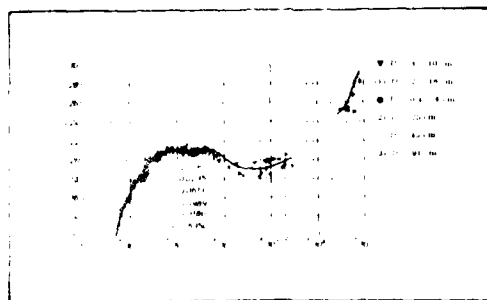
Fig. 5. Strouhal Number versus Reynolds Number
         for Flow over a Cylinder

Roshko (3) has identified four flow regimes in the
S versus Re_D curve. When the Re_D is less than 40, one has
symmetric, viscous flow behind the cylinder, where the
vortices are bound. Between Re_D values of 40 and 150,
the vortices begin to shed in a stable manner, forming a

9

stable vortex street (3:816). The vortex flow is pre-
dominantly laminar. Between Re_D values of 150 and 300,
the shedding and vortices are in transition, starting as
laminar flow immediately behind the cylinder (Figure 6).
The vortices passing into the vortex street are purely
turbulent (3:817).
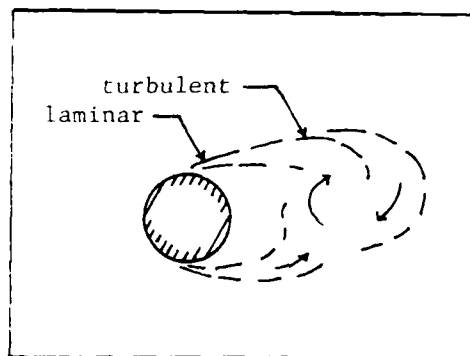
Fig. 6. Vortex Shedding

Beyond Re_D of 300, transition has occurred, and the
shedding is irregular and highly turbulent. Once the Re_D
reaches approximately 100,000, the transition occurs in the
cylinder boundary layer ahead of the separation point
(3:817) and the Karman streets no longer form.

Generation of a Vortex

To shorten the research task, Clark's successful
results with an enclosed jet over a cylinder were used
(6). Although the Re_D would suggest uncertain results in
the street pattern, Clark's experiments show regular streets

10

to be present. Further, the flow is sufficiently compres-
sible so that schlieren techniques could be used.

Flow Visualization

The well-known technique of Toeppler-schlieren
photography was used to visualize the flow. The technique
uses changes in the fluid's index of refraction caused by
changes in fluid density in order to bend a collimated
beam of light, thus varying the light intensity falling
on photographic film (5; 6).

The photographs were correlated via timing informa-
tion with hot-wire or hot-film anemometer data, so that one
could associate a mass flow per area or velocity with a
specific location in the vortex. Using this visual and
flow information, it is theoretically possible to charac-
terize the observed vortices.

Flow Measurement

As mentioned earlier, flow-rate information was
obtained using a hot-wire or hot-film anemometer. The
anemometer is simply a heated wire placed in a flowing
fluid, with the convection heat transfer rate from the wire
determined principally by the mass flow of the fluid
perpendicular to the wire axis (12:109; 13:13).

Considering an ideal vortex street "rolling" past a
wire, anemometer output consists of a steady-state value,
which is a time average of the flow past the wire, as well

11

as a fluctuating component superimposed over the steady-
state value. In the case of a series of vortices of equal
strength but alternating rotation passing by the anemometer,
the variation should be periodic though not necessarily
sinusoidal. If one uses autocorrelation and spectrum
analysis techniques on the wire output (6:10-14), one can
get a good indication of the periodicity of the vortex
street. This technique is also useful in verifying the
street's existence. If the wake of the cylinder has no
order whatsoever, the autocorrelation and spectrum analysis
would reveal no regularity or predominant frequency (the
shedding frequency).

Data Analysis

There are two major aspects to the data analysis
task: location of the data point in the vortex and inter-
pretation of anemometer output.

If one considers a schlieren photograph of a vortex
(Figure 7), it is possible to pick out a region that appears
to be a core, the semi-circular, darker area being half of
the core, surrounded by a swirling outer region. For the
purpose of this study the center of the vortex is taken to
be the center of the major diameter of the darker area.
The location of the anemometer with respect to the vortex
is determined by measuring from the vortex center using
the 1-inch scale in the picture.

12
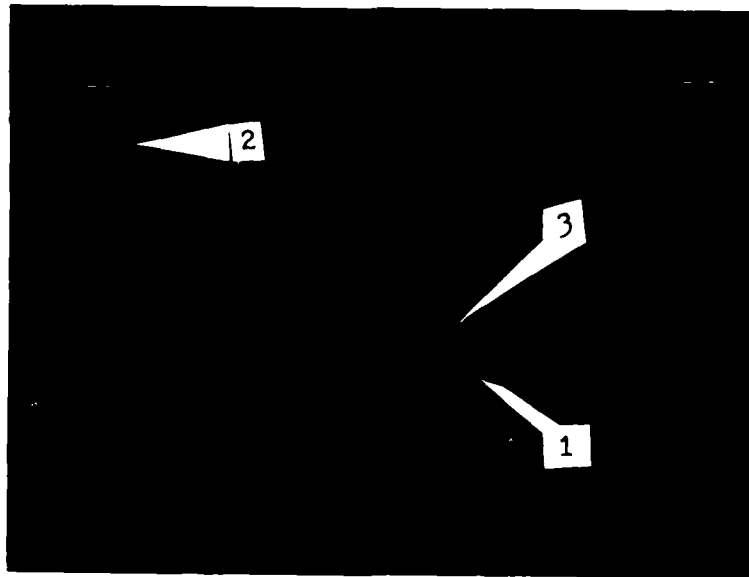
1. Half moon
2. Flow direction
3. Center

Fig. 7. Schlieren Photograph of a Vortex Street

It is possible to gain an insight into the flow
past the anemometer by conducting a thought experiment
on graph paper. One begins the experiment by constructing
a hypothetical Karman street, as shown in Figure 8. Each
vortex is assumed to have a tangential mass-flow per unit
area profile similar to Figure 2, to translate with a mass-
flow vector as shown in Figure 8, and to decay to zero
within a distance slightly greater than the vortex spacing.
By using a vector sum of the translational and the tangen-
tial flow vectors of the three nearest vortices, one can
"build" an anemometer signal similar to actual signals

13

Vortex Street Arrangement with Data Points

convective velocity of vortex centers
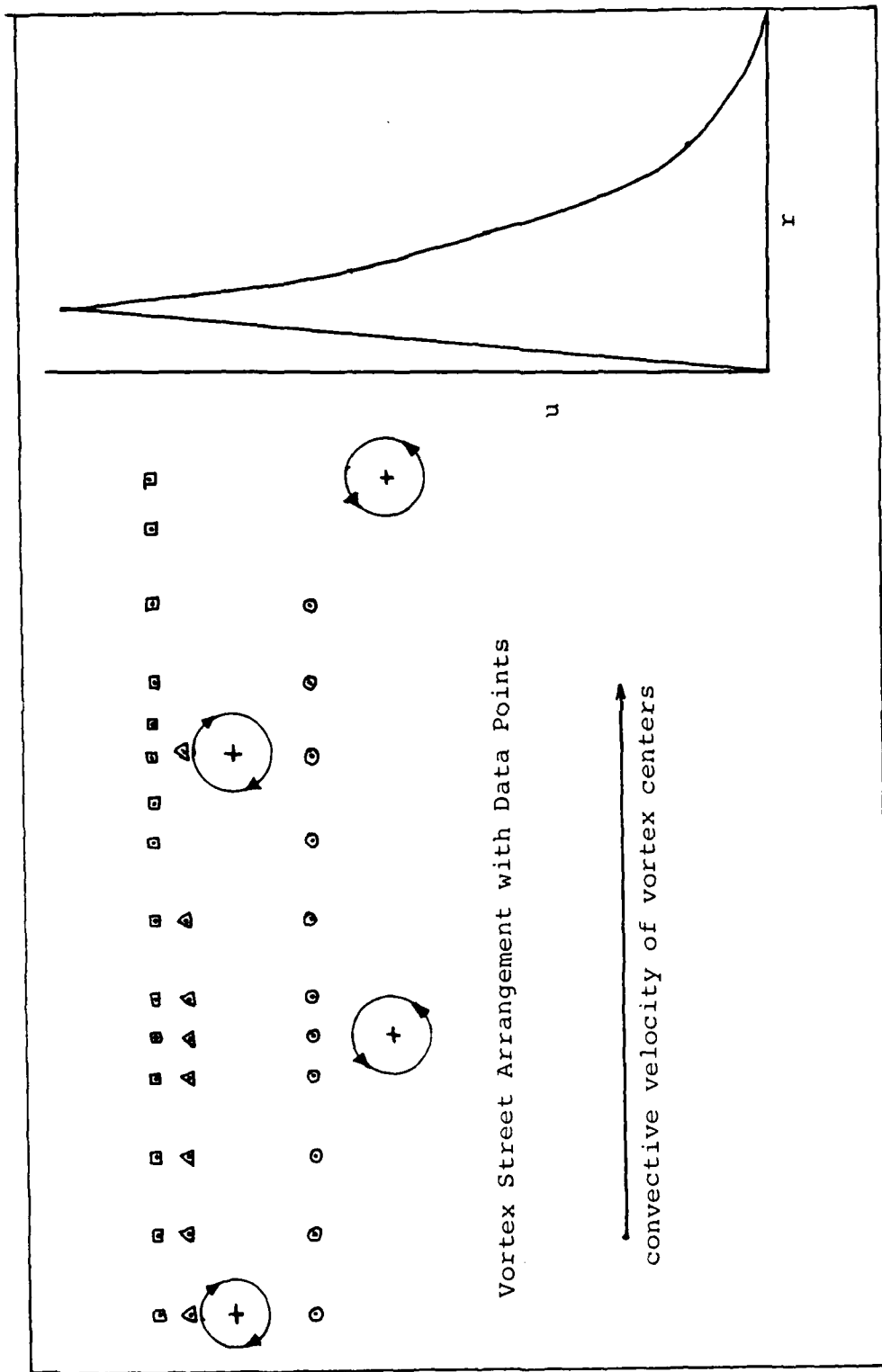
Fig. 8. Imaginary Karman Street

14

(Figure 9). This signal can then be used as "experimental data" for later thought experiments.

Because the only information available from the anemometer is magnitude and not direction, some assumptions and mathematical manipulations are necessary in order to arrive at meaningful results. Let us first examine the case of a single vortex convecting in a uniform stream. We first assume that the average flow is parallel to the test section walls. We also assume that there is no spiralling or transverse (along the long axis of the vortex) motion associated with the fluid in the vortex. In other words, any flow vector experienced by the anemometer consists only of an average flow vector plus a pure tangential flow vector.

Using the schlieren photograph, we can determine the angle θ and the distance r of the anemometer from the vortex center (Figure 10). Defining $(\overline{\rho V})$ as the convective mass flow per unit area and (ρV) as the mass flow per unit area at the instant the photograph was taken, through geometry it is possible to find (ρu), the tangential mass flow per unit area.

From Figure 10, one can derive a second angle γ such that

$$(\rho u) * \sin\theta = (\rho V) * \cos\theta - (\overline{\rho V}) \qquad (6)$$

15
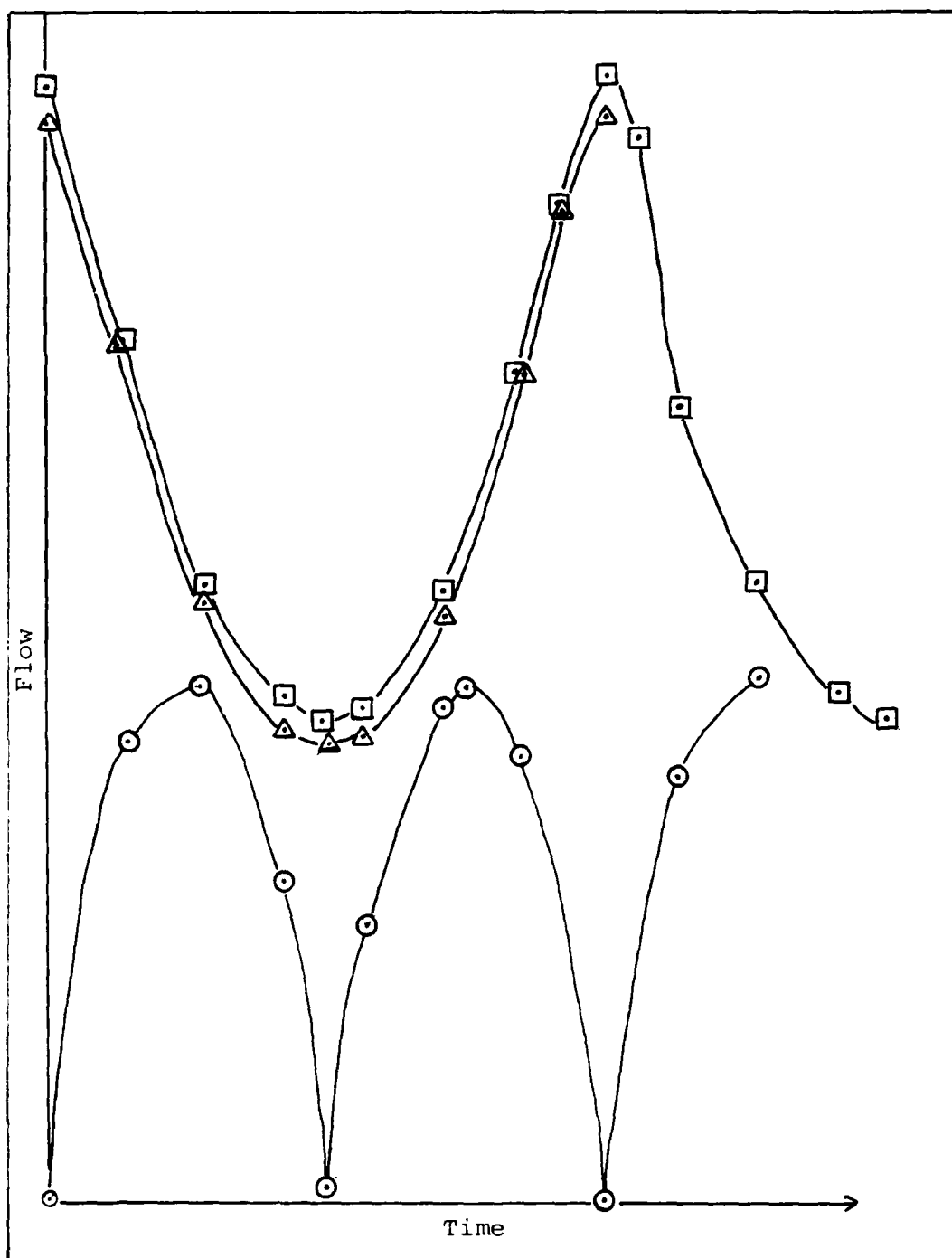
Fig. 9.   Anemometer Traces from Imaginary Street
          (i.e., "experimental data")

16
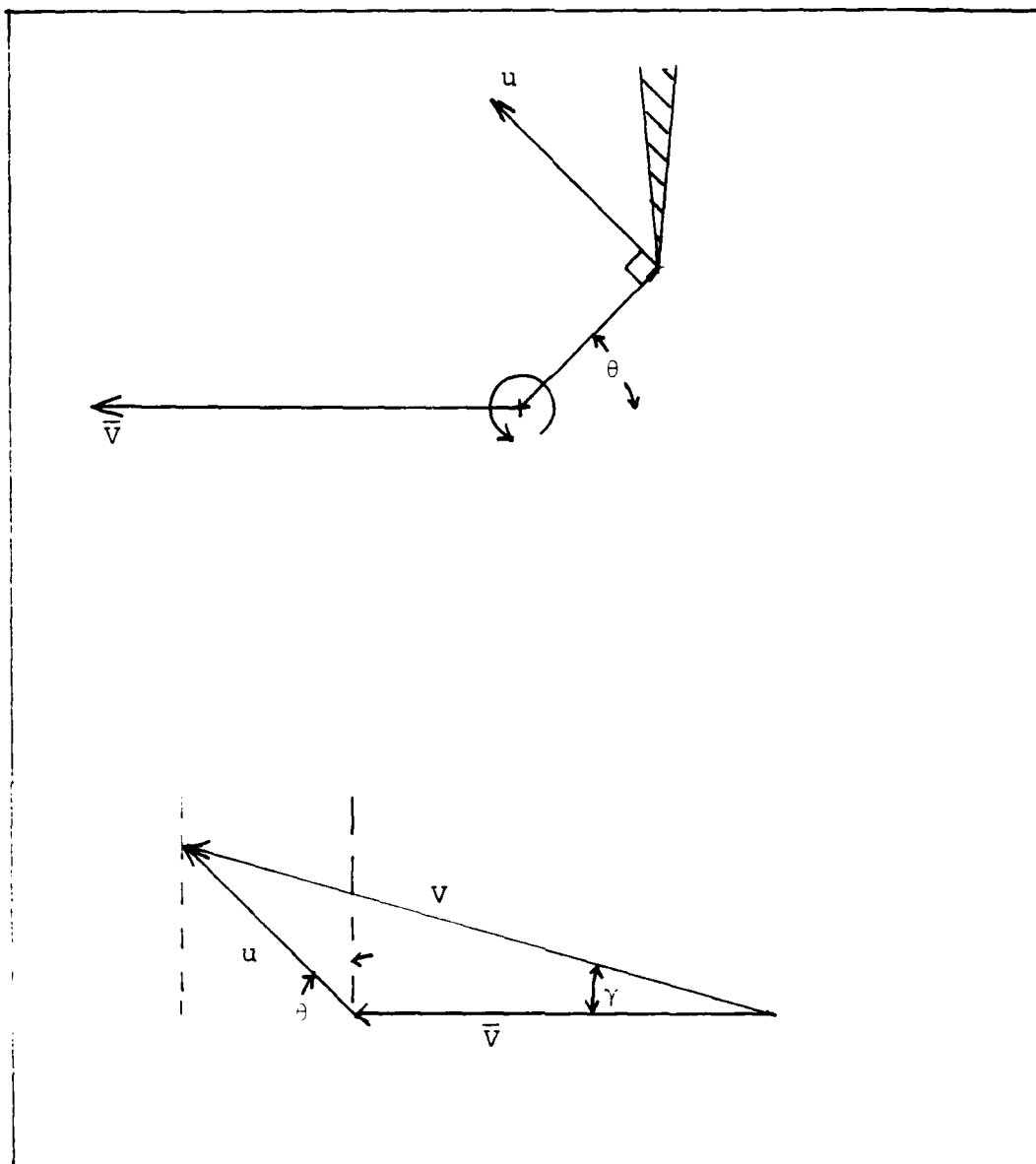
Fig. 10. Definition of Angles for
          Single-Vortex Assumption

17

and

$$\sin\gamma = (\rho u) * \cos\theta / (\rho V)$$

Recalling that

$$\cos\gamma = (1 - \sin^2\gamma)^{\frac{1}{2}} = (1 - (((\rho u) * \cos\theta) / (\rho V))^2)^{\frac{1}{2}} \qquad (7)$$

we can see, after substituting Equation (7) into Equation
(6) and simplifying, that

$$V1 = V2 * \sin\theta + (1 - V2^2 * \cos^2\theta) \qquad (8)$$

where

$$V1 = (\rho u) / (\rho V)$$
$$V2 = (\overline{\rho V}) / (\rho V)$$

Thus, it is possible to find the tangential mass flow per
unit area.

Examining the single-vortex assumption, where the
signal is assumed to be influenced only by the nearest
vortex and the translational flow, one can graphically con-
duct the mathematical analysis developed in Equations (6),
(7), and (8), and generate an "experimental" profile for
a vortex in the street. If the single vortex assumption
is correct, the processed experimental data should exactly
yield the vortex profile used to originally build the
street. Instead, the result exhibits much scatter
(Figure 11) about the exact profile. Consequently, despite

18
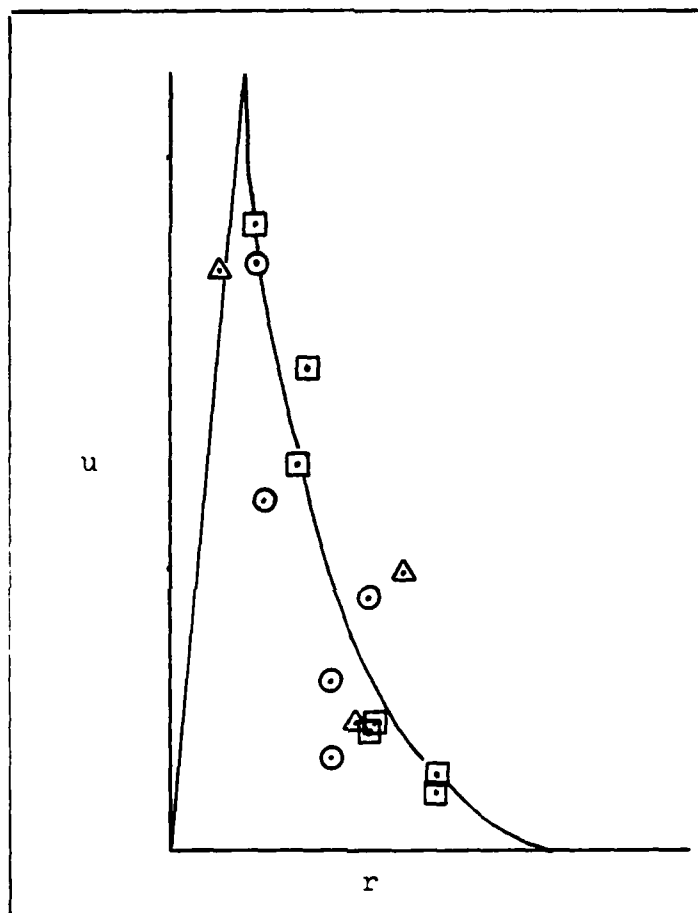
Fig. 11.   Profile Using Single Vortex Analysis

19

its simplicity, the single vortex assumption is inadequate for acceptable analysis.

The case for two vortices of equal but opposite strength is considerably more complex algebraically, and is fully developed in Appendix A. The analysis is based on the assumption that each vortex is of the form

$$(\rho u) = (c_1/r)(1-\exp(-c_2 r^2)) \qquad (9)$$

after Equation (1). Because the density variations across the vortex are not great (8:222), we assume that the mass flow per unit area profile of the vortex is not greatly different from its velocity profile. Performing another thought experiment using hypothetical velocity and density profiles, one can see that the general form should not change (Figure 12).

The tangential flow (ρu) of each vortex can be resolved into horizontal (x) and vertical (y) components. The translational velocity times average density constitutes a horizontal mean flow vector. Via the general vector relation:

$$(\text{resultant magnitude}) = ((\Sigma \text{ horizontal components})^2$$
$$+ (\Sigma \text{ vertical components})^2)^{\frac{1}{2}}$$

one arrives at the two vortex equation:

20
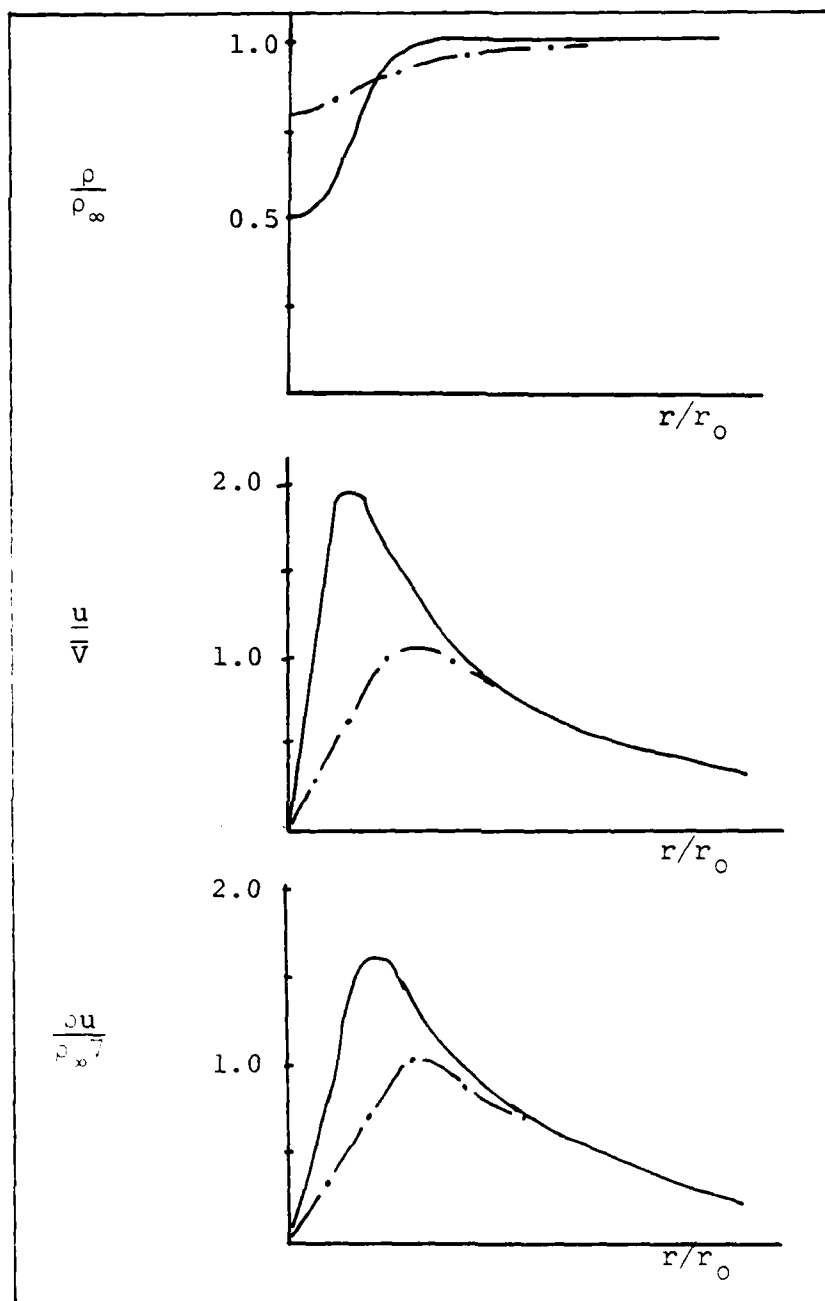
Fig. 12.   Hypothetical Density and Velocity Profiles

$$(\rho V) = \{[\frac{D_1 c_1}{r_1}(1-\exp(-c_2 r_1^{\;2}))\sin\theta_1$$

$$+ D_2 \frac{c_1}{r_2}(1-\exp(-c_2 r_2^{\;2}))\sin\theta_2$$

$$+ (\overline{\rho V})]^2 + [D_1 \frac{c_1}{r_1}(1-\exp(-c_2 r_1^{\;2}))\cos\theta_1$$

$$+ \frac{D_2 c_1}{r_2}(1-\exp(-c_2 r_2^{\;2}))\cos\theta_2]^2\}^{\frac{1}{2}} \qquad (10)$$

where r_1, θ_1, and D_1 refer to one vortex and r_2, θ_2, and D_2 refer to the other vortex. D_1 and D_2 are the directions of rotation for each vortex, being +1 for counter-clockwise and -1 for clockwise (directions of positive and negative θ, respectively).

Using the "experimental data" from the hypothetical street, one can, once again, graphically construct an "experimental" vortex profile. The contribution of each vortex is unknown before-hand; therefore, one has to use an iterative type approach as shown in Figure 13 to collapse the data from the two-vortex assumption to very close to the original profile used to generate the street. Thus, the two-vortex assumption appears to be valid in analyzing the anemometer data, assuming that the *effective* vortex radius is on the order of the spacing between con-secutive vortices.

There still remains the question of how one solves for the constants c_1 and c_2 in Equation (10), which, as

22
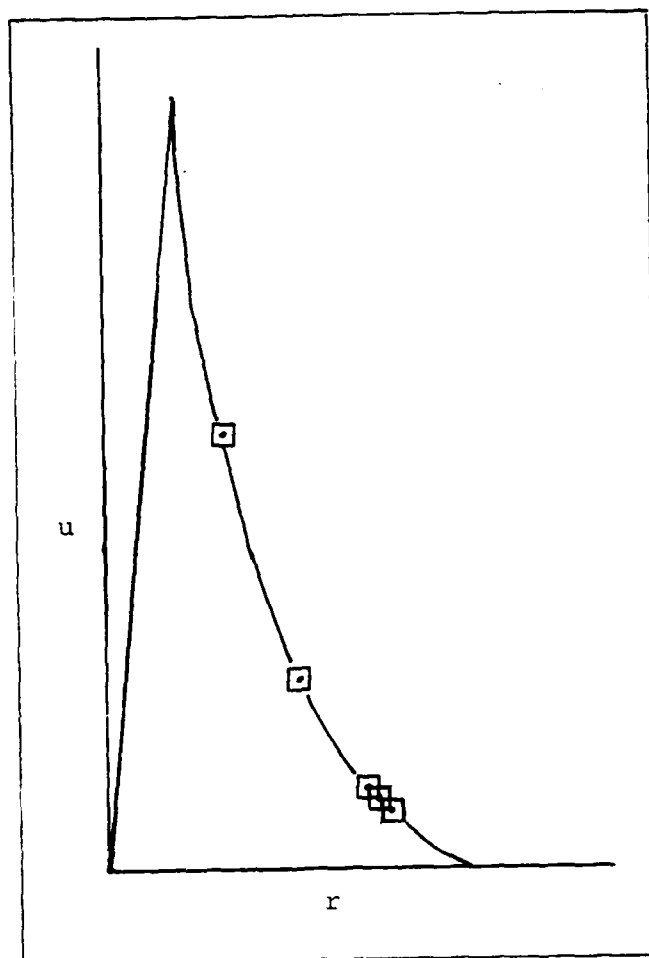
Fig. 13.   Vortex Profile Using Two-Vortex
Assumption (solid line is
original vortex profile)

written, represents one equation and two unknowns at a particular instant in time and $(r_1, \theta_1, r_2, \theta_2, (\rho V))$. However, if one considers the anemometer output, one has a complete time history of the flow both before and after the schlieren picture was made, as the vortex pair moves in space. By mathematically translating the vortex pair incrementally in time at the translational velocity, one can compute a new set of $(r_1, \theta_1, r_2, \theta_2, (\rho V))$ at each time increment. Note that (ρV) is available from the anemometer trace via the anemometer calibration. Thus, one can obtain multiple sets of data from one anemometer trace and one schlieren picture. The development of these new sets of data is based on simple geometry and is treated in Appendix A.

In theory, since we have two unknowns c_1 and c_2, we can apply Equation (14) to two sets of data to obtain the two equations needed to solve for the two unknowns. However, Equation (10) is highly nonlinear, making an explicit solution impossible. Furthermore, there are noise and experimental error associated with each set of data, so that even if an explicit solution were possible algebraically, an exact solution would be impossible due to the errors.

Because of the experimental error and nonlinearity, a nonlinear optimizational-type approach is needed. Using

24

Equation (10), and following stochastic process theory
given by Bronson (16), one can define a function f as:

$$f_i(c_1,c_2) = f_{i1}(c_1,c_2) + f_{i2}(c_1,c_2)$$
$$+ f_{i3}(c_1,c_2) + f_{i4}(c_1,c_2) \qquad (11)$$

where

$$f_{i1} = c_1^2/r_1^2 (1-\exp(-c_2 r_1^2))^2$$

$$f_{i2} = 2(\sin\theta_1 \sin\theta_2 + \cos\theta_1 \cos\theta_2) c_1^2 (1-\exp(-c_2 r_1^2))$$
$$\cdot (1-\exp(-c_2 r_2^2))$$

$$f_{i3} = c_1^2/r_2^2 (1-\exp(-c_2 r_2^2))^2$$

$$f_{i4} = 2(\rho V) c_1 (D_1 \sin\theta_1/r_1 (1-\exp(-c_2 r_1^2))$$
$$+ D_2 \sin\theta_2/r_2 (1-\exp(-c_2 r_2^2)))$$
$$+ (\overline{\rho V})^2 - (\rho V)^2$$

    i = data point corresponding to a given time

Defining

$$B_i = [f_i + (\rho V)_i^2]^{\frac{1}{2}} = B_i(c_1,c_2)$$

we can say that the error between theory and experiment
is $B_i - (\rho V)_i$. Therefore, squaring the errors and incorpo-
rating them into a function z, we arrive at:

25

$$z = - \sum_{i=1}^{N} [B(i) - (\rho V)_i]^2$$

where N is the number of data points. By finding the (c_1, c_2) pair which maximizes z, we minimize the error between theoretical and experimental data. The Newton-Raphson technique was adapted to this problem and is developed in Appendix A (16:112).

III. Experimental Apparatus

The experimental apparatus consisted of the flow device and test section, optical equipment, and the hot-wire anemometer. A list of instrumentation is contained in Appendix C.

Flow Device and Test Section

Air for the test was provided by a compressor capable of supplying approximately 0.5 lbm/sec at a nominal pressure of 85 psig. Because the test required approximately 1.5 lbm/sec, it was necessary to operate in a blow-down type of arrangement by drawing down the compressor's accumulator tank. This allowed a maximum run-time of approximately 1 minute.

After entering the laboratory bay, the air proceeded through a cyclone separator and filter, which removed dirt and water. From the separator and filter, the air flowed through 2-inch pipe to a 2-inch gate valve, which served as a master on/off control. It then passed through a Grove Company Model 83 Flex-Flo flow regulator before finally entering a stilling chamber (Figure 14).

The stilling chamber was the same as the one used in Weston's and Clark's research (5; 6). It served to stagnate the incoming flow and also contained honey-comb

27
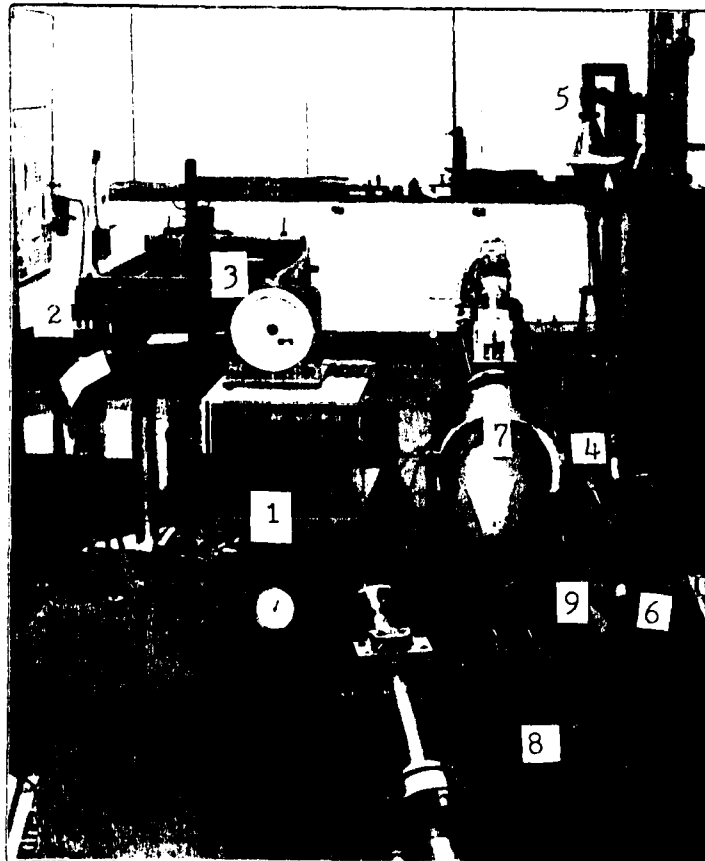
1. Instrumentation   6. 2-in Pipe
2. Camera   7. Stilling Chamber
3. Pressure Gauge   8. Gate Valve
4. Spark Lamp   9. Controller
5. Cyclone Separator

Fig. 14.   Test Apparatus

grids to smooth out any turbulence at that point. It in turn fed air into the test section via a convergent nozzle.

The test section was designed to duplicate Clark's successful design. To this end, it had a 2-inch by 2-inch square cross-section (total area of 4 square inches) with a 5/16-inch diameter circular bar mounted horizontally through its centerline (Figure 15 and 16). Penetrating the top of the section were two pressure taps and four anemometer taps. The top and bottom of the section were wood and the sides were plexiglass and optical glass. The cylinder was mounted in the plexiglass. The entire section was 4-feet long and was constructed from an existing square shock tube.

At the downstream end of the test section was the outlet assembly, constructed by the AFIT Model Fabrication Shop. It consisted of four square exit ports, each of approximately 1 square inch area, which provide an exhaust area of slightly over 4 square inches for the steady flow (Figure 17). A pneumatic annular slider was designed to close the exit ports when the shock wave was released. Closing off the ports ensures that the shock does not dissipate into the room instead of traveling upstream into the Karman street generated by the steady flow across the cylinder. The slider was configured to be initiated by bottled air through a solenoid valve.
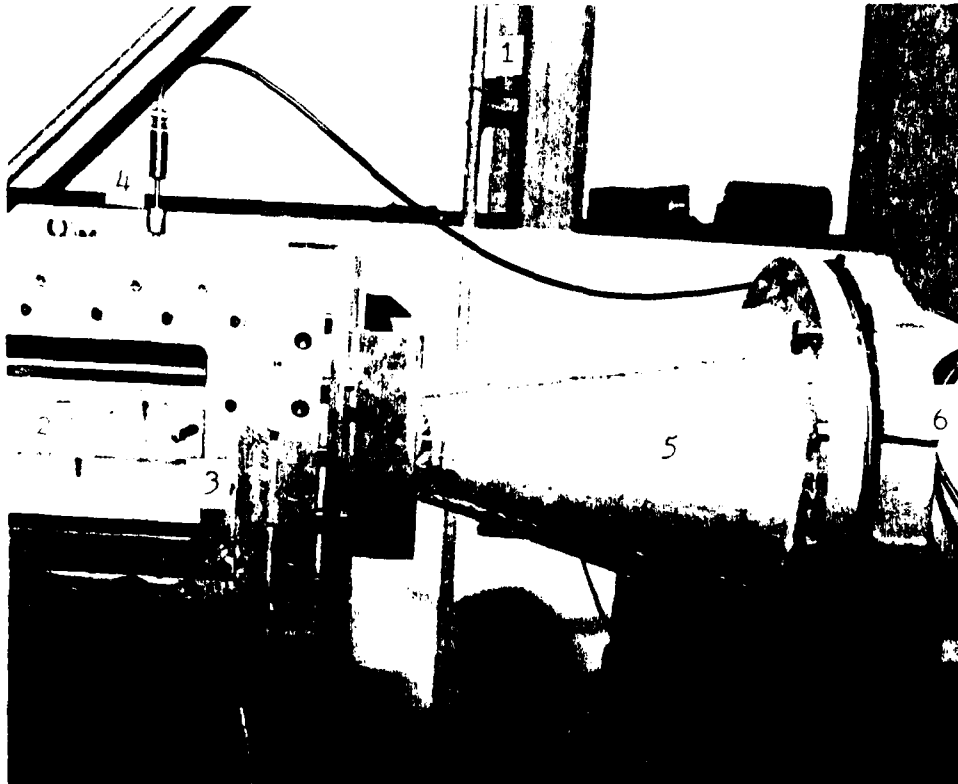
1. Flow   4. Anemometer Probe
2. 2 in x 2 in Test Section   5. Nozzle
3. Cylinder   6. Stilling Chamber

Fig. 15.   Overall View of Test Section

30
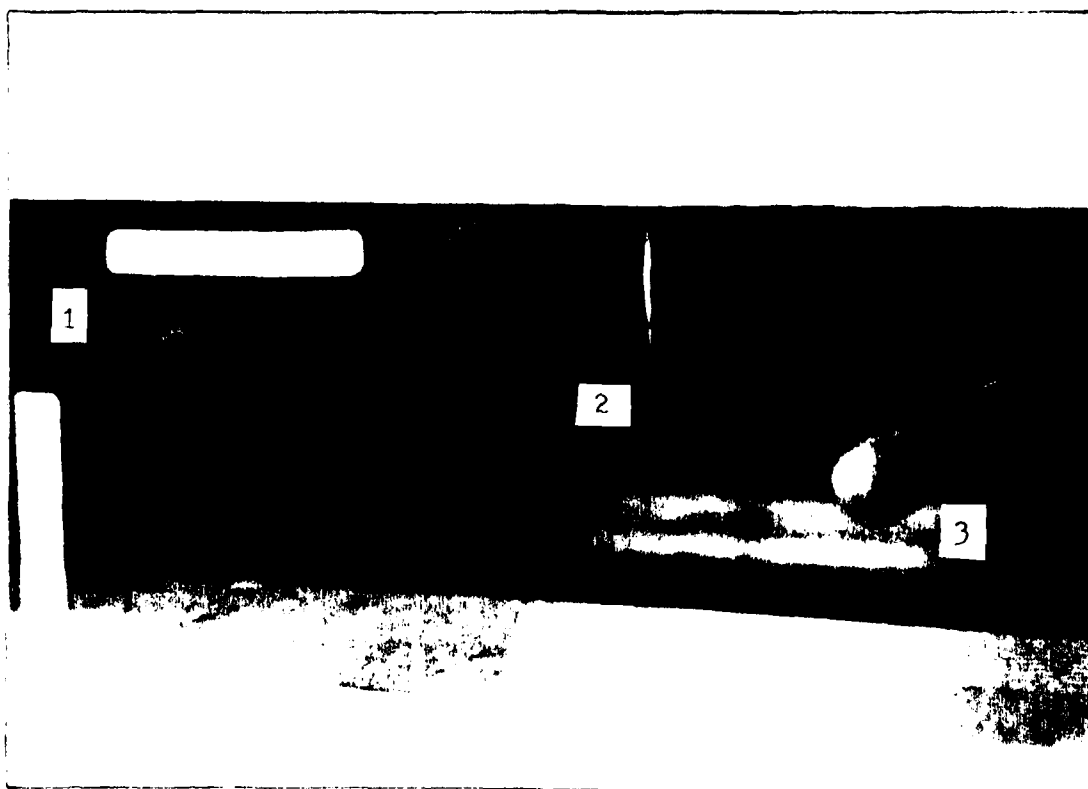
1. 1" Tape Strips
2. TSI 1214-10 Hot Film Anemometer
3. 5/16" Cylinder

Fig. 16. Close-up View of Test Section
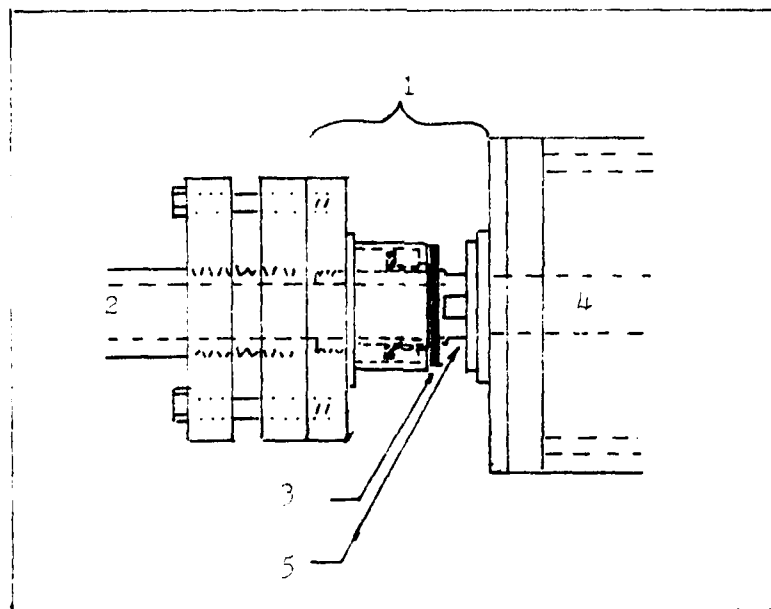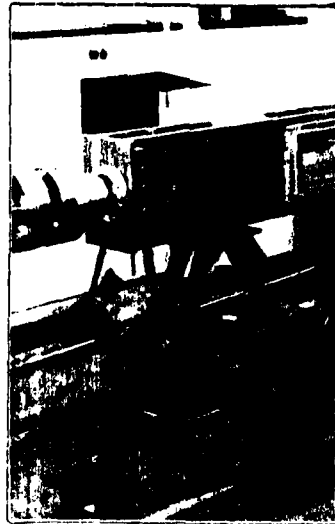
1. Outlet Assembly   4. Square Shock Tube
2. Circular Shock Tube   5. 1" Square Outlet
3. Annular Slider

Fig. 17. Outlet Assembly

The shock tube was attached to the outlet assembly. The shock tube driver was the same as that described by McQueen (13:6-10). The most notable aspect of the tube was the fact that it used the double diaphragm system of operation as opposed to a single diaphragm punctured by a needle. Each diaphragm was capable of withstanding approximately one-half of the needed pressure drop, and the pressure across the diaphragm assembly was increased in stages from low, to an intermediate level between the diaphragms, to high. When the intermediate region was vented to ambient pressure, the intermediate/high pressure diaphragm suddenly experienced a pressure nearly twice its breaking pressure, and so it burst. The low/intermediate diaphragm then found itself in the same predicament and also broke, and the resulting shock wave traveled down the tube toward the test section.

Optical System

The schlieren system originally used a Cooke Model 596-4116 spark lamp aimed through three mirrors and a knife edge to expose Polaroid Type 47 film (ASA 3000) to get a visual picture of the flow conditions behind the cylinder. The spark lamp consisted of a bank of capacitors discharging across a small gap to generate a point source of light of very short duration. A Cordin Model 5205 Power Supply (Figure 18) provided approximately 8000 Volts

33

1. CMC Counter
2. AN/USM-425 Oscilloscope
3. C-30 Camera
4. IFA-100
5. Transformer
6. Spark Lamp Power Supply
7. Trigger Box
8. Stilling Chamber
9. 30-in Hg Gauge

Fig. 18. Arrangement of Test Instrumentation

for charging the capacitors. A 200 Volt pulse triggered the spark lamp to discharge. The light traveled to a 40-inch focal length mirror, across the test section in parallel beams to a second 40-inch mirror, and to the knife edge via a plane mirror which turned the light towards the camera. After passing the knife edge, the light exposed the film. Midway through the research, a Cordin Model 5401 spark lamp became available, and it replaced the Cooke spark lamp (Figure 14).

Since it was desirable to correlate the picture with the anemometer data, the spark lamp was triggered after the anemometer oscilloscope began its trace. A 5-Volt signal came out of the delayed gate on the back of the oscilloscope, and passed to a transformer box which produced the 200-Volt signal necessary to trigger the spark lamp. The time delay was measured using a CMC Model 726C Universal Counter turned on at the start of the anemometer trace and turned off when the 200-Volt signal was triggered. Thus, it was possible to determine the point on the anemometer data corresponding to the time the schlieren picture was taken. Two 1-inch lengths of tape on the test section window served as the horizontal and vertical scales for the location of the anemometer as well as the size of the vortices. An HP-9874A digitizer/HP-85 computer system was used to read the schlieren picture for distance information.

Anemometer System

Mass flow per unit area was measured by the Thermo-Systems, Inc. (TSI) IFA-100 Intelligent Flow Analyzer, which consisted of a TSI Model 1214-10 hot film anemometer and the accompanying electronics necessary to receive and process the anemometer signal (Figure 18). To increase resolution on the oscilloscope, the IFA-100 was set for a 2-Volt offset, wherein 2 Volts was subtracted from the bridge output, and oscilloscope sensitivity was increased. Therefore, to get the actual anemometer signal magnitude, one would add 2 Volts to the magnitude of the oscilloscope signal.

A Tektronix AN/USM-425 (Tektronix Model 465M) oscilloscope with a Tektronix C30 Series oscilloscope camera was used to make a permanent record of the anemometer data. The primary reason for choosing the 425 was because it could provide the delayed 5-Volt pulse to trigger the spark lamp. Because it did not have a trace storage capability, it was necessary to photograph the oscilloscope trace as it occurred by leaving the C30 camera shutter open during the event. Exposures were also made of the zero voltage level and the grid. The oscilloscope was triggered by hand when the pressure in the stilling chamber was at the desired value for that particular test run. Unfortunately, this meant that there was no control over the vortices' position relative to the wire. The anemometer data was digitized

36

Using the HP-9874A digitizer/HP-85 computer system.
Figure 19 shows a schematic of the test instrumentation.

To verify the street's existence, in addition to
using the schlieren photography, in initial investigations
the anemometer output was fed to an HP-3721A Correlator
and an HP-3582A Spectrum Analyzer. A Fluke Model 2100A
Digital Thermometer was used to indicate temperature and
a Wallace and Tiernan Model FA145 30-in Hg Bourdon Tube
gauge was used to measure pressure inside the stilling
chamber.
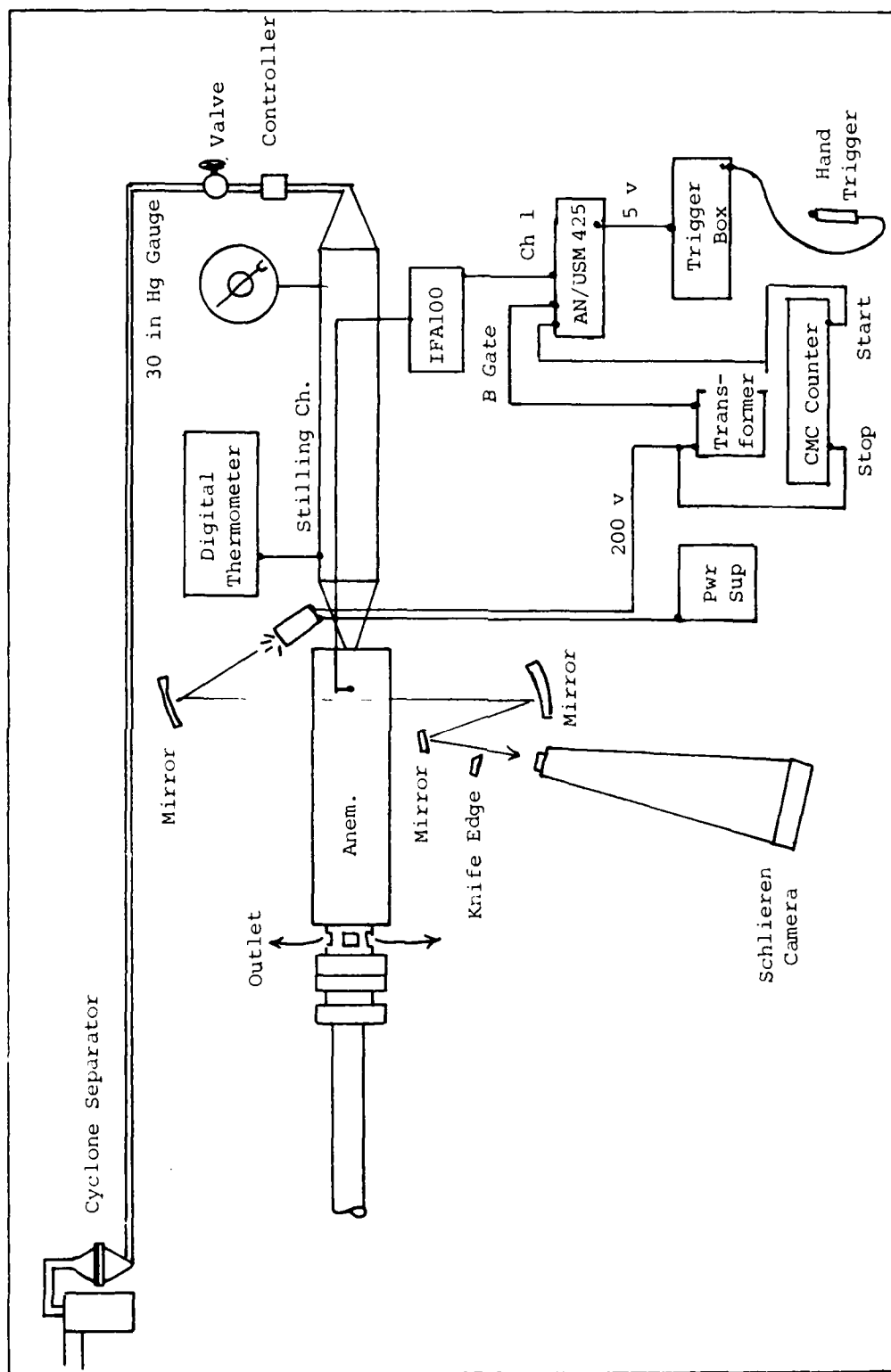
Fig. 19. Schematic of Test Instrumentation (Top View)

38

IV. Experimental Procedure

Anemometer Calibration

The anemometers were calibrated in a calibrator modeled after the TSI Model 1125 (13:17). By placing them in the exit of a nozzle fed by a stagnation chamber and varying the total-pressure and back-pressure, it was possible to closely simulate the actual experimental conditions. The anemometer output voltage, total-pressure, total-temperature, and back pressure were recorded. At least 10 calibration points were taken.

Isentropic flow equations were used to calculate the mass flow per unit area across the anemometer at each data point. The resulting mass-flow per unit area and voltage were then applied to a BASIC computer program (15:179-182) which solved for the constants m_0 through m_4 in the fourth order polynomial:

$$\rho V(E) = m_0 + m_1 E + m_2 E^2 + m_3 E^3 + m_4 E^4$$

where E is the anemometer output voltage in volts and ρV is the mass-flow per unit area in lbm/ft^2-sec. Because the total temperature never varied more than a few degrees, temperature differences were considered to have negligible effect.

39

Vortex Characterization

The general procedure for characterizing the vortices was to obtain the anemometer and schlieren data, mathematically translate it in time to obtain 20 data points, and use the Two-Vortex Assumption to approximate the constants c_1 and c_2. Errors were checked by comparing the theoretical flows with the experimental flows.

Before each experimental session, the test equipment connections were verified as shown in Figure 19 and the equipment turned on. After a suitable warm-up time, the anemometer frequency response was set using the square wave test function on the IFA-100 (13:23-24).

Once the instrumentation was ready, the room lights were turned off in order to avoid overexposing the schlieren film. The oscilloscope was set for a 5-V delay signal out (B gate on the AN/USM-425) approximately 1 msec after initial triggering. The schlieren and oscilloscope camera shutters were opened, the spark lamp armed, and the delay timer was reset. The experiment was now ready to begin.

Air flow was initiated and controlled by manually opening and adjusting the hand valve so as to maintain 20 in Hg -gauge pressure inside the stilling chamber. After several seconds the hand trigger was pressed, thus triggering the oscilloscope and, after the delay, the spark lamp. The total temperature was also noted.

After data collection, the valve was shut and the camera shutters were closed. The zero level trace and graticle on the oscilloscope were photographed and the pictures were developed.

The photographs were then processed using the HP9874A digitizer. Angle, radius, and average spacing between consecutive vortices were obtained using the schlieren picture and average time interval and voltage history were obtained using the anemometer picture. The information was then applied to the two vortex model and c_1 and c_2 were solved for iteratively. Once c_1 and c_2 were known, they were used to construct a theoretical Karman street for comparison with the experimental street over several periods.

V. Results and Discussion of Results

Initially, it was important to confirm that Karman vortex streets were being produced in the test section. Once it was found that the streets did exist, and operating conditions (stilling chamber pressure) had been selected, the streets could be investigated in detail. The raw experimental data in the form of photographs as well as a summary are located in Appendix D.

Preliminaries

Using autocorrelation and raw anemometer data, one could see that Karman vortex streets existed for stilling chamber pressure (P_{SC}) ranges of 8 to 25 in Hg -gauge. The results were similar to those obtained by Clark (6:69-74). However, at the lower pressures, the Mach numbers were too low for the vortex streets to be visible using schlieren techniques. Although the higher pressures resulted in greater turbulence, optical considerations drove P_{SC} to be from 15 to 25 in Hg -gauge. The stilling chamber pressure of 20 in Hg-gauge was selected as the operating condition. The corresponding test section static pressure (P_{TS}) at the P_{SC} = 20 in Hg was 14 in Hg-gauge, which, according to isentropic flow tables, gives a Mach 0.43 flow ahead of the 5/16-inch dia cylinder.

42

The selection of the P_{SC} of 20 in Hg-gauge created

a dilemma from an experimental point of view. In order to

get good quality schlieren pictures, there had to be some

compressibility effects. This meant the Mach number had

to be relatively high, which in turn mandated use of a

higher P_{SC}. Unfortunately, a higher Mach number also meant

a higher Reynolds number, which meant more chaotic flow

behind the cylinder. The Reynolds number based on cylinder

diameter was calculated at approximately 100,000, which,

according to Figure 4 and Roshko (3), is a region where the

Karman street is unstable and irregular. Consequently,

there were great variations in the quality of the street,

as seen on schlieren photographs and measured by the

anemometer. Frequently, only a dead wake was observed.

Since the characterization technique required clearly

defined vortices, much of the data collected was unuseable.

Initial Investigation

Early test runs were made without the anemometer

passing through the core region of the vortices. Conse-

quently, the data collected contained no information about

the core. Without information on the core one cannot, with

any degree of reliability, expect to completely charac-

terize the vortex. It was decided to place the anemometer

wire even with the top edge of the cylinder, so that the

vortex centers would pass close by the wire, thus enabling

43

information to be acquired about the core. The 20 data points used to calculate c_1 and c_2 were evenly distributed along the portion of the trace generated by the two vortices captured on the schlieren picture.

A problem which developed with the Cordin spark lamp was that every time it sparked, a spike of several tenths of a Volt was exhibited on the anemometer trace. This spike defied all attempts to get rid of it, including shielding, grounding, and filtering. Therefore, the 20 data points used in the solution to c_1 and c_2 began at the spark-lamp firing and went backward on the trace (see Appendix D). Additional points running further back were read so as to enable a comparison between the experimental trace and the theoretical trace to be made over several cycles.

A second modification to the analysis method which was made early in the research was to invoke a core supremacy principle. If one considers the vortex core as a rigid rotator, where the fluid is irrotational and spins as a more or less "monolithic" mass of fluid, super-position should not hold within the core region. The only vortex contributing to the flow inside the core should be the nearest one, or the one of which the core in question is a part. An analogy would be a string of solid cylinders spinning and convecting at the same time in a fluid. The region in between the cylinders is influenced by the nearest

44

spinning cylinders, but the region inside a solid cylinder is obviously influenced only by the cylinder itself.

The analysis program was modified by having it branch to a one-vortex solution whenever the smallest of the two radii was less than a set core radius. The radius chosen for this study was one-half the cylinder diameter, or 5/32-inch, which was approximately the average radius of the cores as observed on the schlieren pictures.

When some of the experimental data was applied to the analysis program, the resulting theoretical Karman street profile for the solved for c_1 and c_2 was almost constant (Figures 20 to 24) instead of the periodic profile exhibited by the corresponding experimental data. Independent of starting values for c_1 and c_2, the Newton-Raphson method generally converged on low values of c_1 and c_2 as approximations to the actual flow. The Run 092609 (Figure 23) did exhibit some theoretical street formation; the other runs showed simply a flat profile.

If one considers the magnitude of the theoretical street, one finds that it is approximately equal to the product of the convective velocity (V1 in the program "DATANAL8") and the free stream density (calculated as the test section static pressure divided by the product of the gas constant, R, and temperature, T), or approximately 44 lbm/ft^2 - sec. It is possible that the free-stream density is not an accurate representation of the average

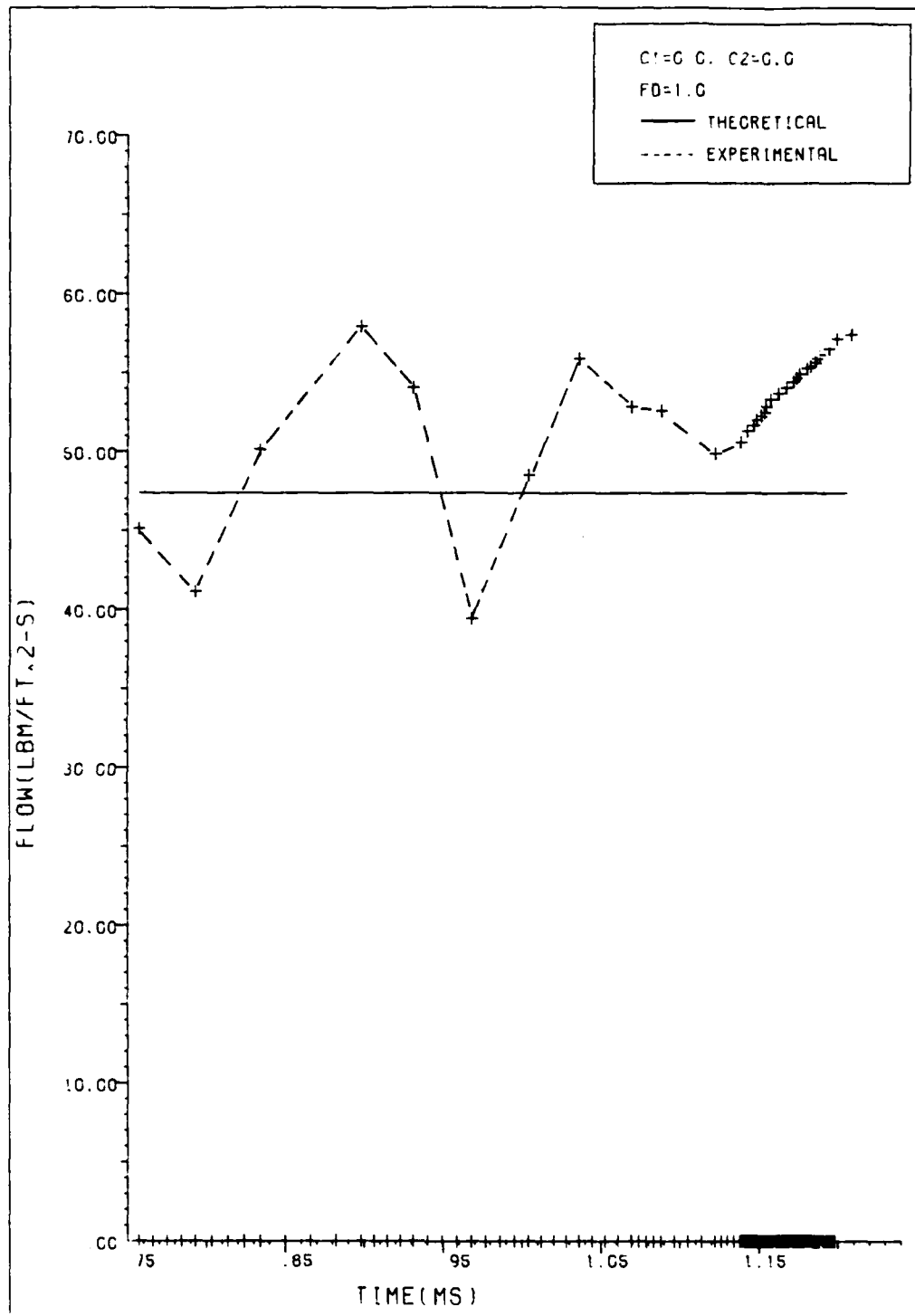Fig. 20.   Run 092502--Theoretical and
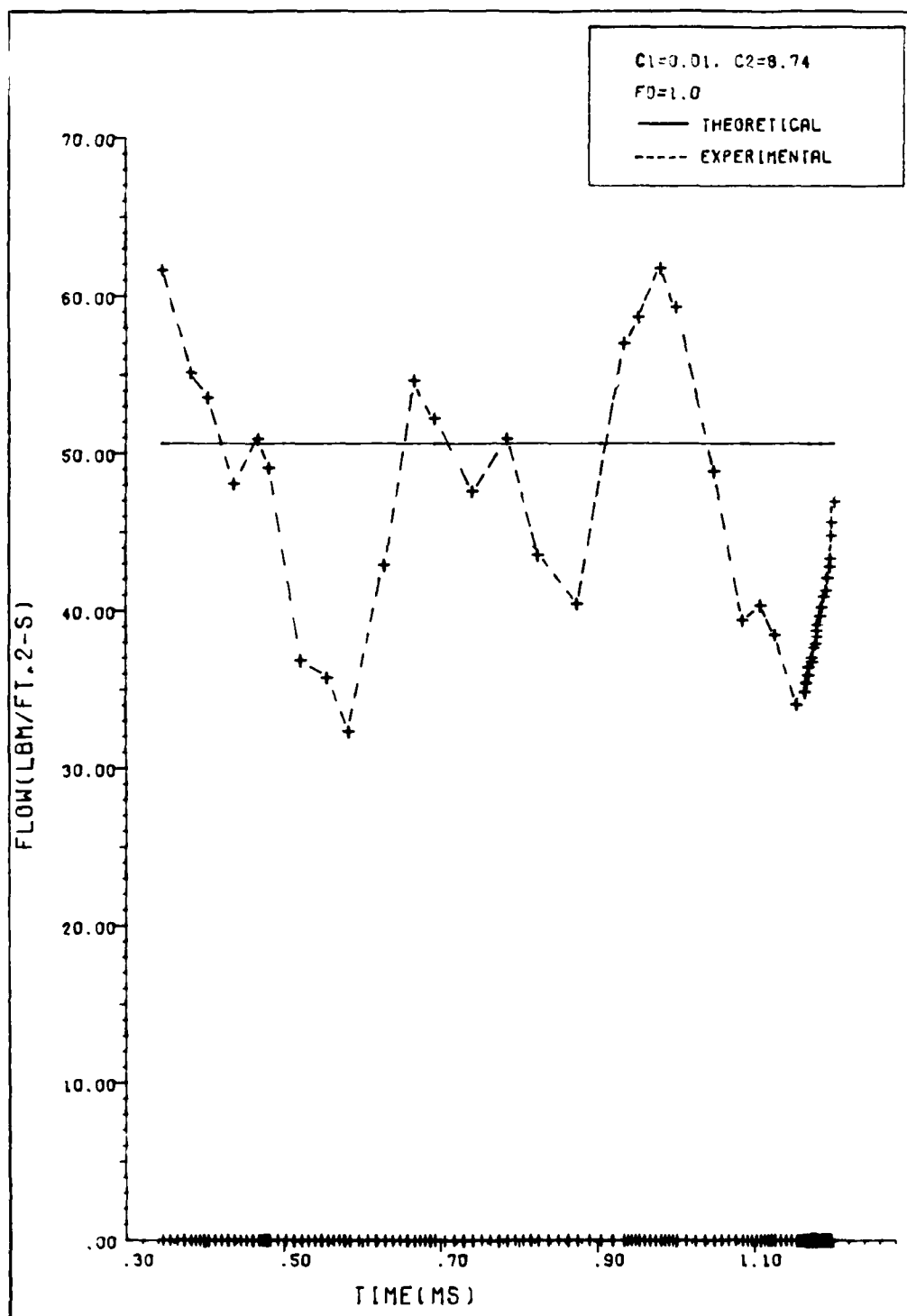   Experimental Karman Streets

46

Fig. 21. Run 092504--Theoretical and
Experimental Karman Streets
(Pradtl-Tietjens Theory Used)
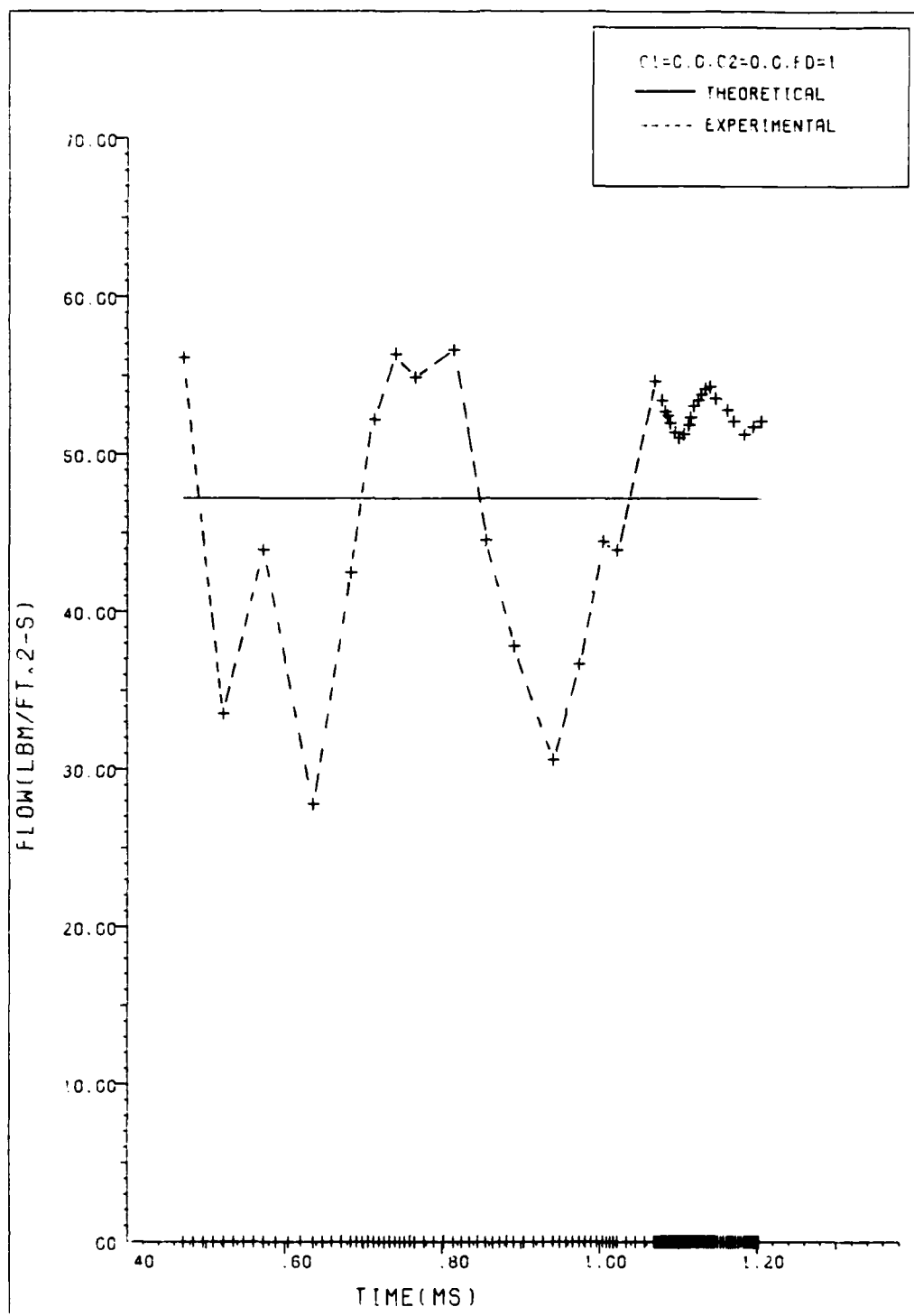
47

Fig. 22.   Run 092602--Theoretical and
Experimental Karman Streets

48

Fig. 23.   Run 092609--Theoretical and
Experimental Karman Streets

49

Fig. 24.   Run 092611--Theoretical and
            Experimental Karman Streets

50

density of the two vortex system used to find c_1 and c_2.
Use of the free-stream density appears to overwhelm any
attempts by the analysis program to solve for the vortices,
as represented by c_1 and c_2, that are known to be in
existence in the flow. The smallest error between theory
and experiment is when no vortices exist; consequently,
the analysis drives the c_1, c_2 solution towards small
values, and the profile is flat.

These results could indicate that the density,
instead of varying by several percent across a vortex,
might in fact vary by up to tens of percent. From a
mathematical perspective, a lower average density would
give the analysis program an opportunity to come to a solu-
tion with nonzero vortices.

Final Investigations

To see whether the average density was in fact
lower than the free stream density, the analysis program
was modified so as to allow an artificial reduction of
the free-stream density to some value determined by a
density factor, fd, which was set between zero and one.
The density factor entered into the computational scheme
only in the calculation of the convective mass flow per
unit area (lines 7070, 7480, 7910, 8260, 8290, 8320, 8390,
and 8430 in the program "DATANAL8"--see Appendix A). With
a lower average density, the rest of the solution adjusted

itself accordingly, and it was possible for nonzero vortex solutions to make more of a contribution to the theoretical flow, thus permitting the periodicity exhibited by the experimental flow.

As shown in Figures 25 to 36, with the proper density factor, one can match the experimental data relatively closely over several cycles. The period also matches, except for a slight phase shift. The phase shift is considered unimportant, because it does not change the essential character and profile of the vortex street.

Increasing the density factor has a dual effect on the theoretical Vortex Street. At low density factors, even large values of c_1, corresponding to stronger vortices, cannot provide enough mean flow to match the mean flow of the experimental data. Consequently, the whole theoretical curve, even though it matches the general profile of the experimental curve, appears to be offset below the experimental curve. The theoretical curve also has much larger amplitude fluctuations than the experimental curve (Figures 25, 26, 27, 31, and 37, in particular). As the density factor increases, the mean of the theoretical curve rises toward the mean of the experimental curve. However, the theoretical vortices get weaker, as manifested by the smaller amplitude fluctuations (Figures 29 and 30). By the time the factor equals one, where the average density

Fig. 25.   Run 092502--Theoretical and
Experimental Karman Streets

53

Fig. 26. Run 092504--Theoretical and
Experimental Karman Streets

54

Fig. 27. Run 092504--Theoretical and
Experimental Karman Streets
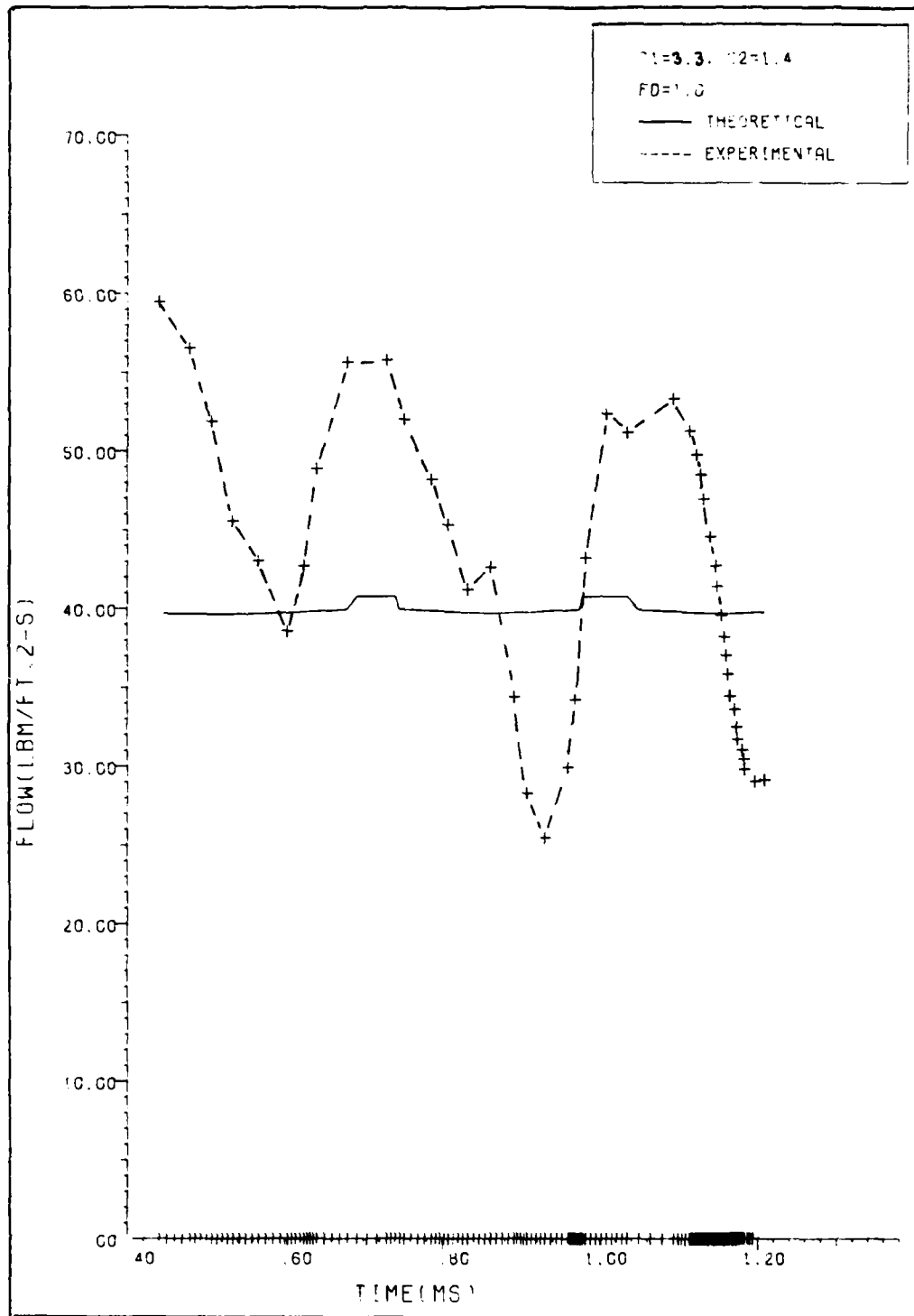
Fig. 28. Run 092601--Theoretical and
Experimental Karman Streets

56

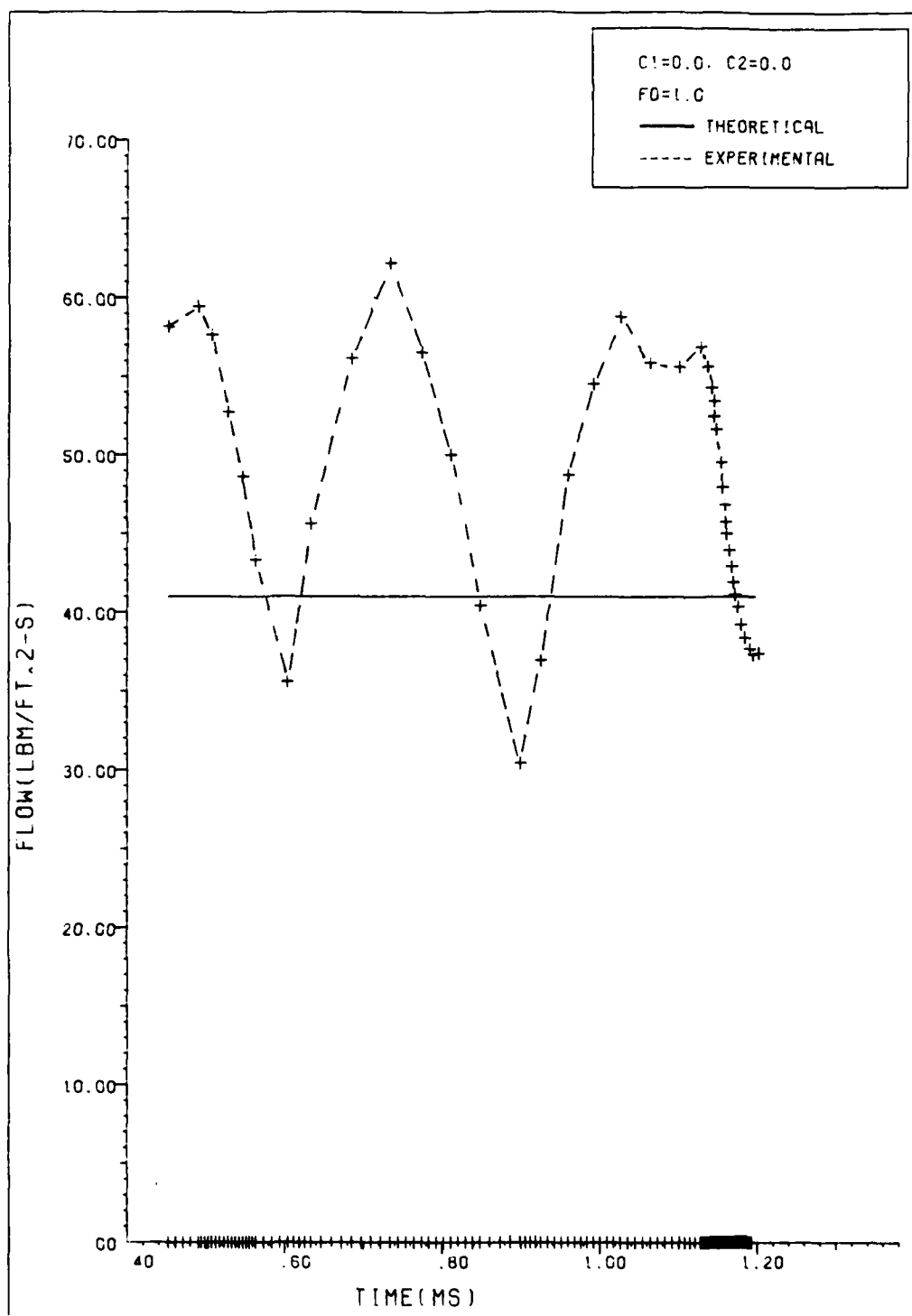Fig. 29.   Run 092601--Theoretical and
           Experimental Karman Streets

57

Fig. 30.   Run 092601--Theoretical and
Experimental Karman Streets

Fig. 31.   Run 092602--Theoretical and
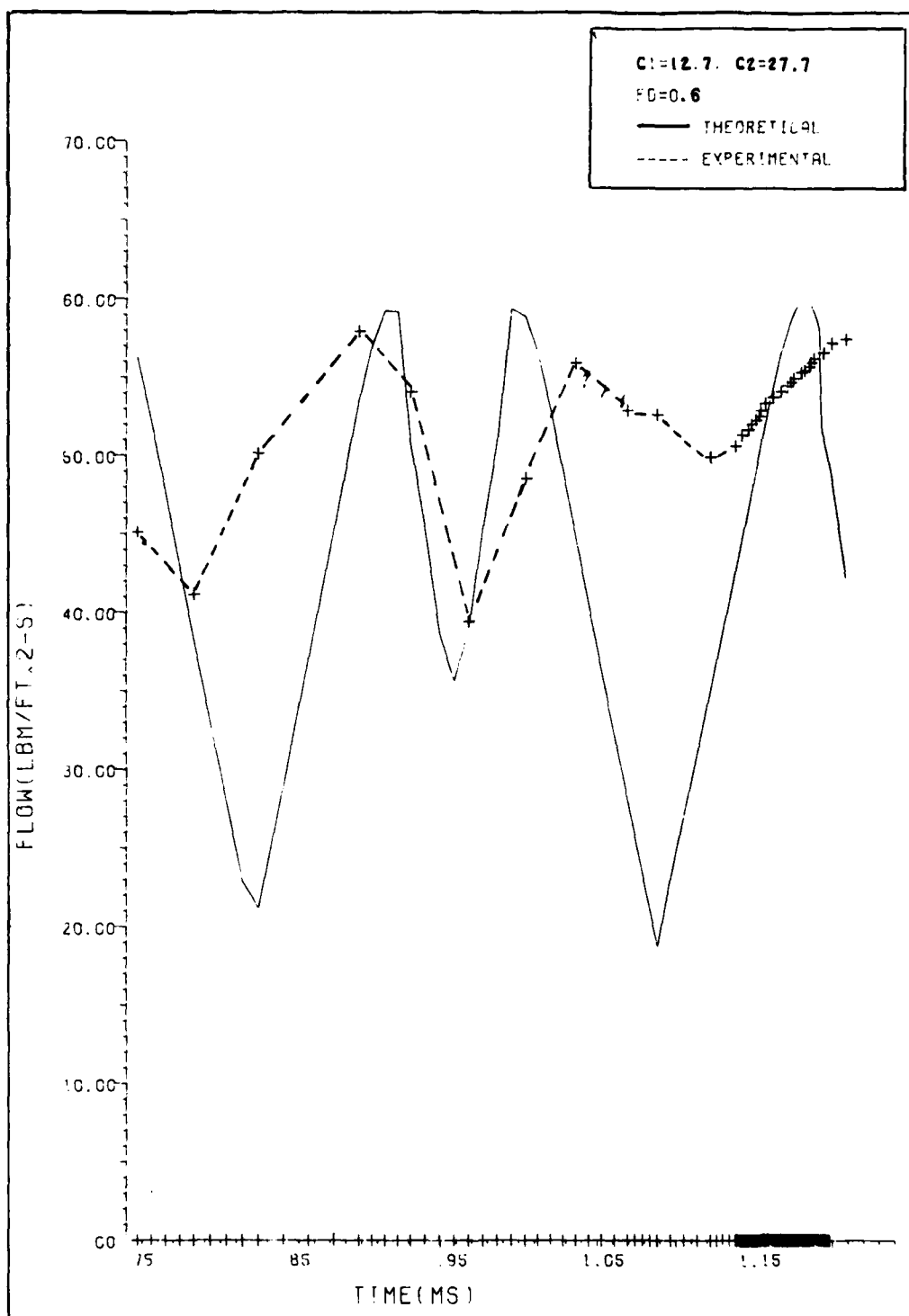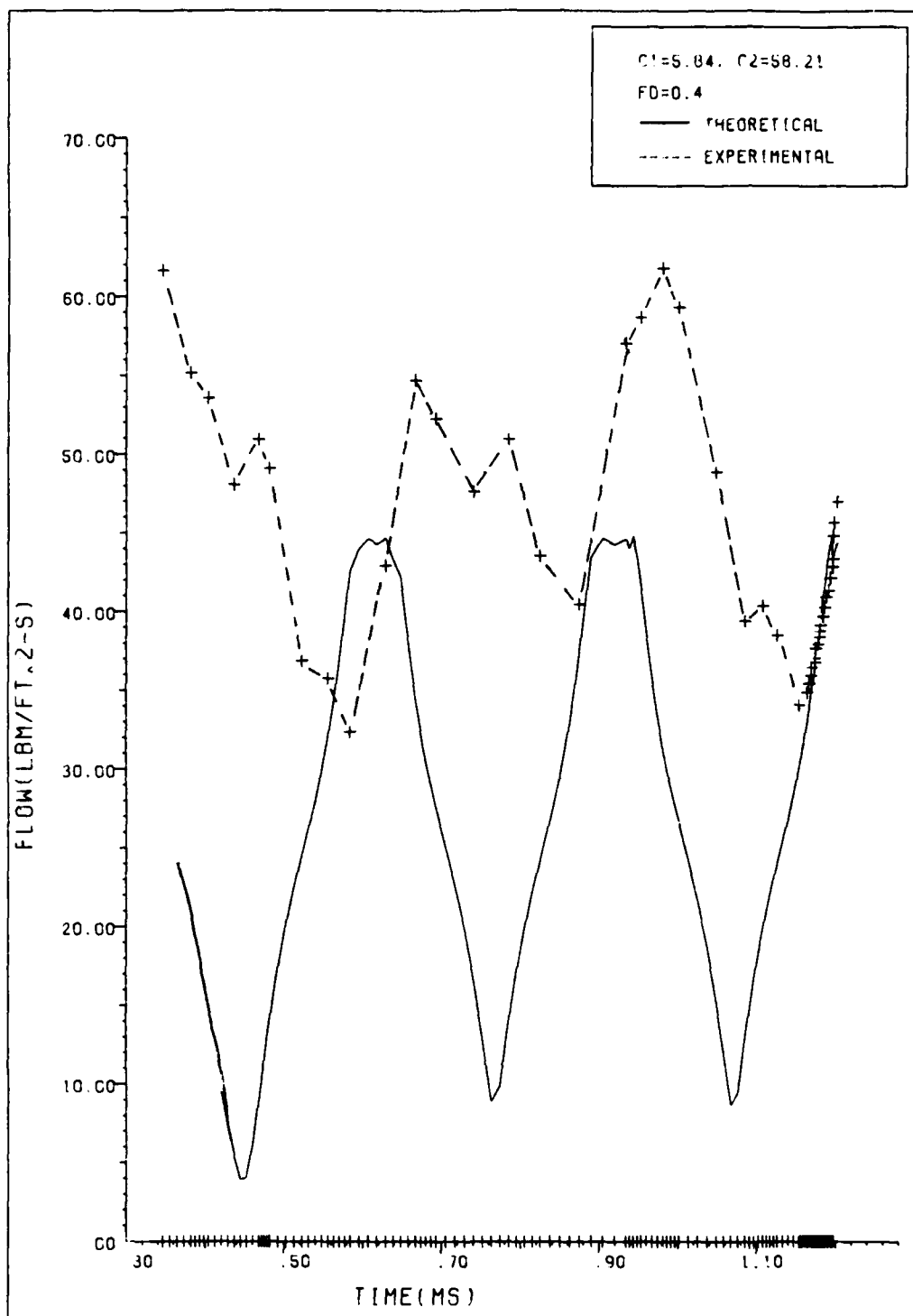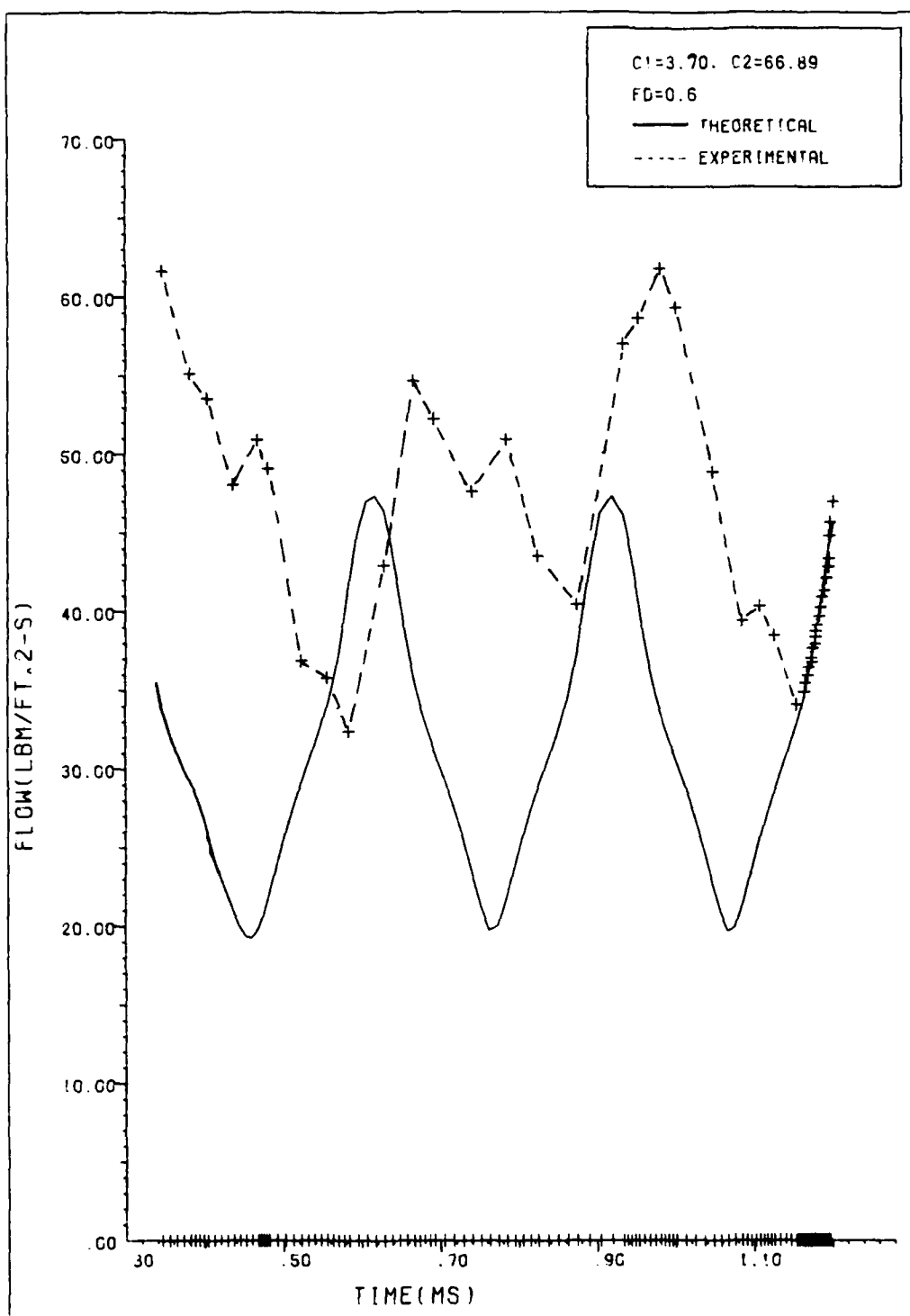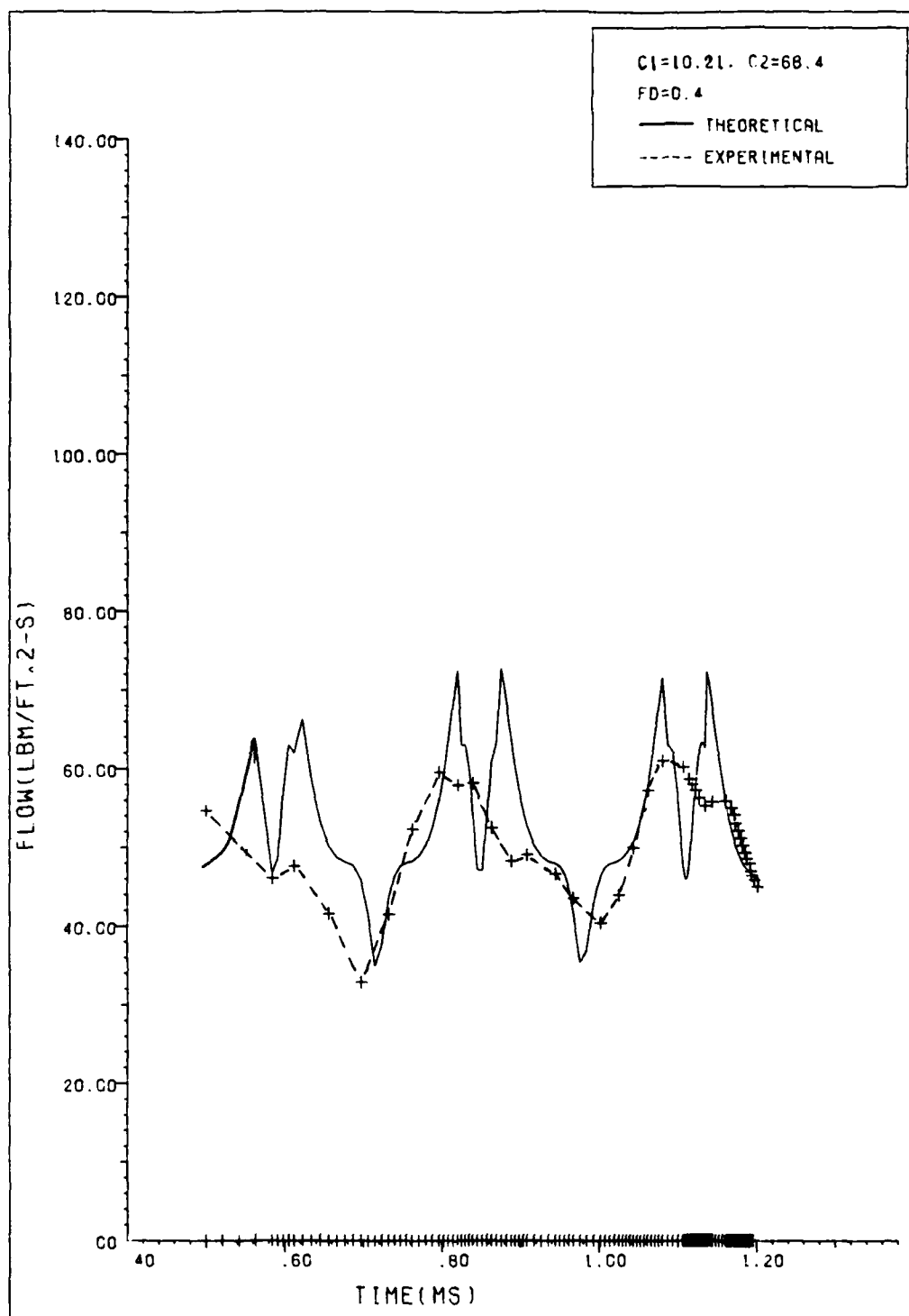Experimental Karman Streets

59

Fig. 32.   Run 092602--Theoretical and
Experimental Karman Streets

Fig. 33. Run 092606—Theoretical and
Experimental Karman Streets

61

Fig. 34. Run 092606--Theoretical and
Experimental Karman Streets

62

Fig. 35. Run 202609--Theoretical and Experimental Karman Streets

63

Fig. 36.   Run 092611--Theoretical and
            Experimental Karman Streets

64

is equal to the free-stream density, the theoretical curve is almost completely flat (Figures 31 and 32).

Over the 20 points used to calculate c_1 and c_2, the analysis yields very good agreement with the experimental data. The theoretical Karman street is very periodic, but as time values decrease, agreement with experimental data gets worse. Because the experimental Karman streets are turbulent and irregularly formed, one would expect agreement to get worse. However, the theory does appear to be capturing the essential characteristics of the flow (Figures 28, 33, 34, and 35). Note that the irregularities exhibited by the theoretical flow curves are due to the resolution of the display program.

There was another aspect to the density factor which was considered. Because the factor entered into the computational scheme as:

$$...fd*\rho*\overline{V}...$$

it could also be considered as modifying the value of $\overline{V}$ and leaving ρ constant.

Prandtl and Tietjens (17:132-133) indicate that the velocity field of a Karman street is due to the superposition of the vortices on the free-stream flow, and not on the translational flow of the vortex centers. It is this difference in velocity that appears to cause the vortices in the street to move towards the (5/16-inch)

65

cylinder from the point of view of a reference frame
attached to the free-stream flow. Thus, the magnitude of
the inertial translational velocity of the vortex centers
is less than the free-stream velocity. By using fd's
greater than 1.0, one can artificially raise $\overline{V}$ to a value
approximately equal to the free-stream velocity. Accord-
ingly, values of fd equal to 1.2, 1.4, and the ratio
of free-stream velocity (V_∞) to the measured value of $\overline{V}$
were applied to "DATANAL8." The resulting plots are shown
in Figures 37 to 48.

As can be seen, some of the best approximations
occurred for the values of fd equal to $V_\infty/\overline{V}$ (Figures 40
and 48). Contrary to previous experience, the theoretical
curves did not always flatten with increasing density
factor, although the theoretical curve for Run 092504
(Figures 21, 38, and 39) was flat for all values of fd
greater than or equal to 1.0. There appears to be an
optimum value of fd which yields the best approximation to
the data; unfortunately, the limitations of the program
"DATANAL8" prevent more than a crude estimation of that
optimum value. As shown in Figures 40 and 48, the optimum
could be the one such that:

$$fd*\rho*\overline{V} = \rho*V_\infty$$

where V_∞ is the free-stream velocity. However, there are
also indications that a different value of fd is more

66
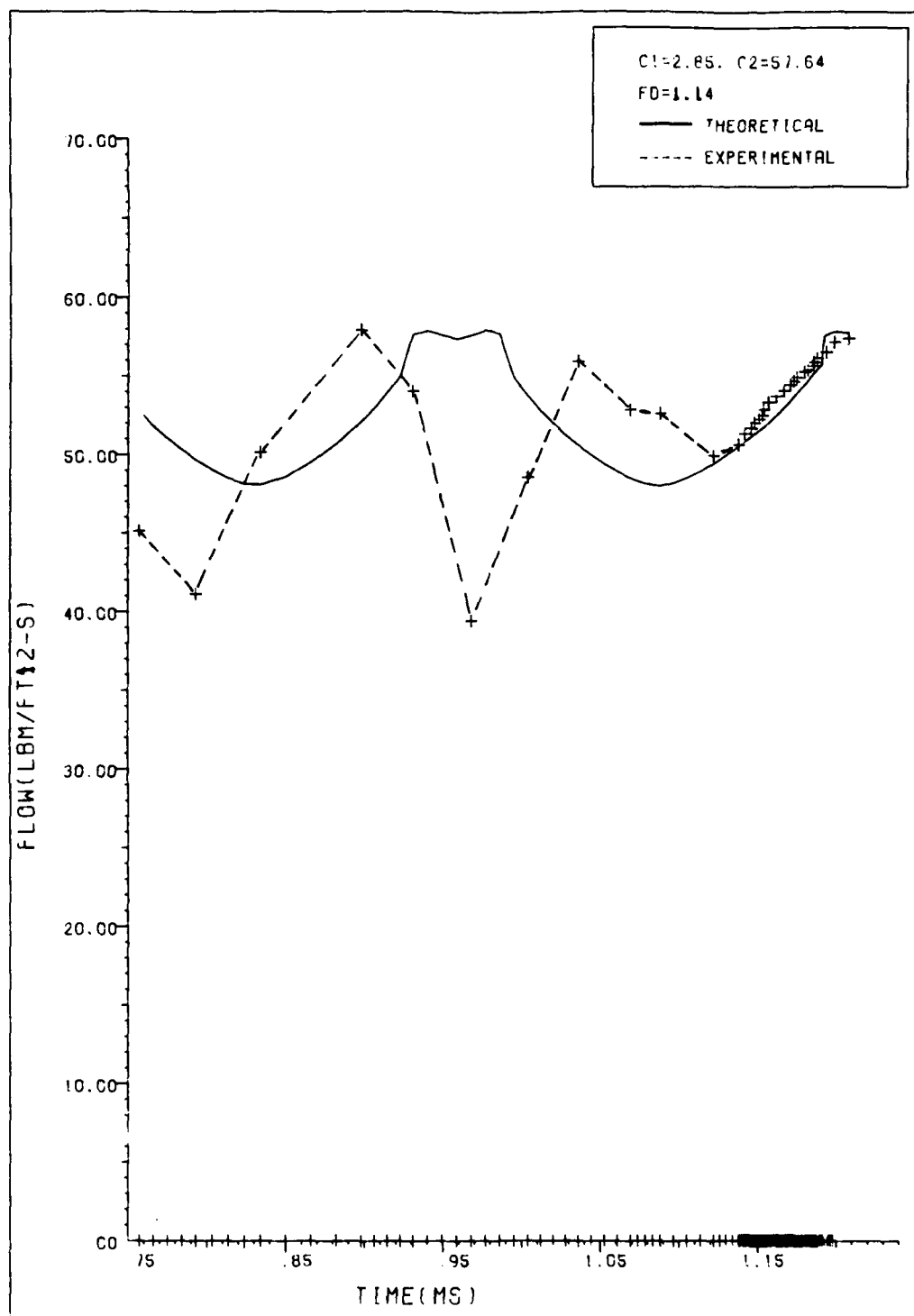
Fig. 37.   Run 092502--Theoretical and
Experimental Karman Streets
(Prandtl-Tietjens Theory Used)

67
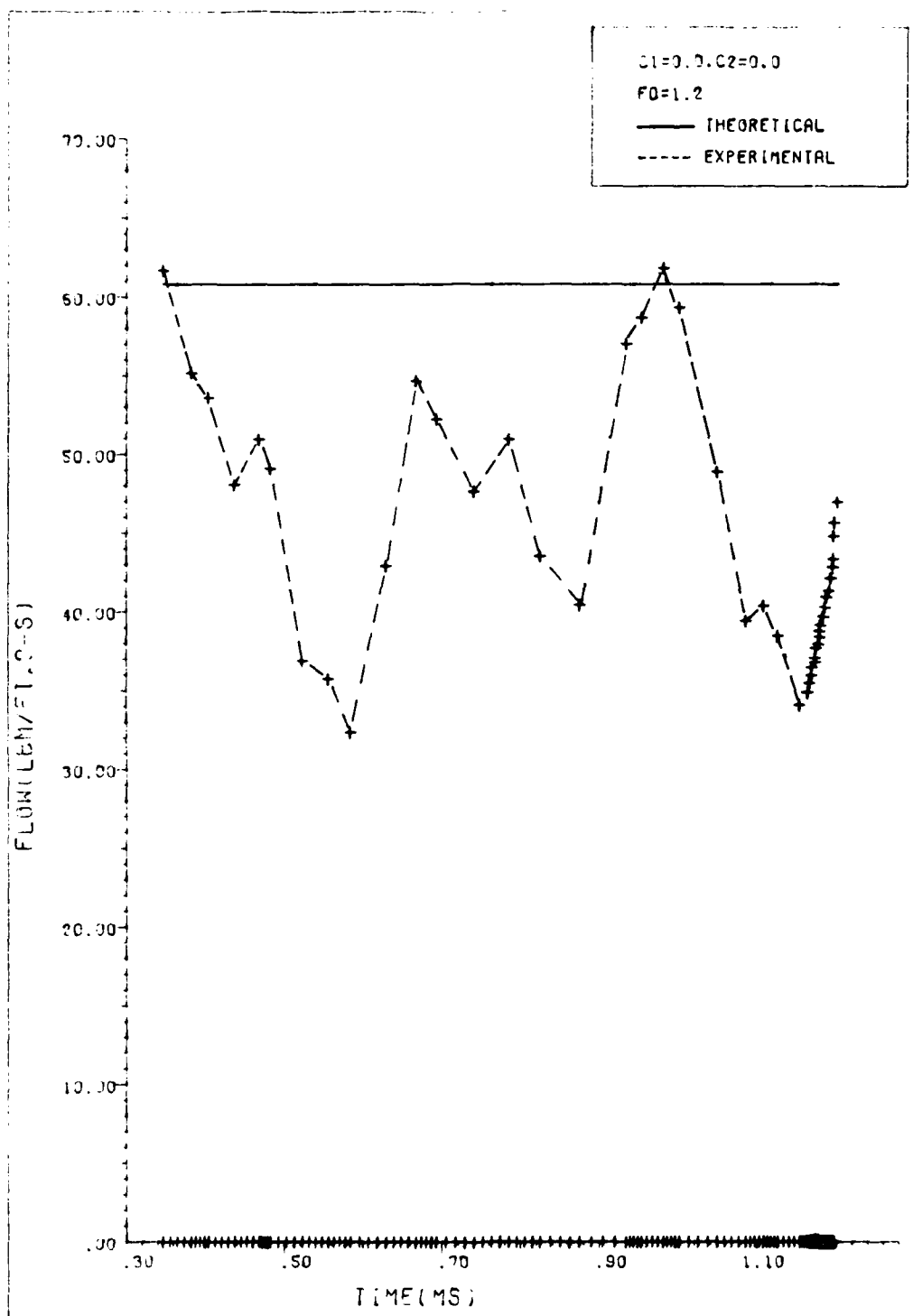
Fig. 38.   Run 092504--Theoretical and
Experimental Karman Streets

68
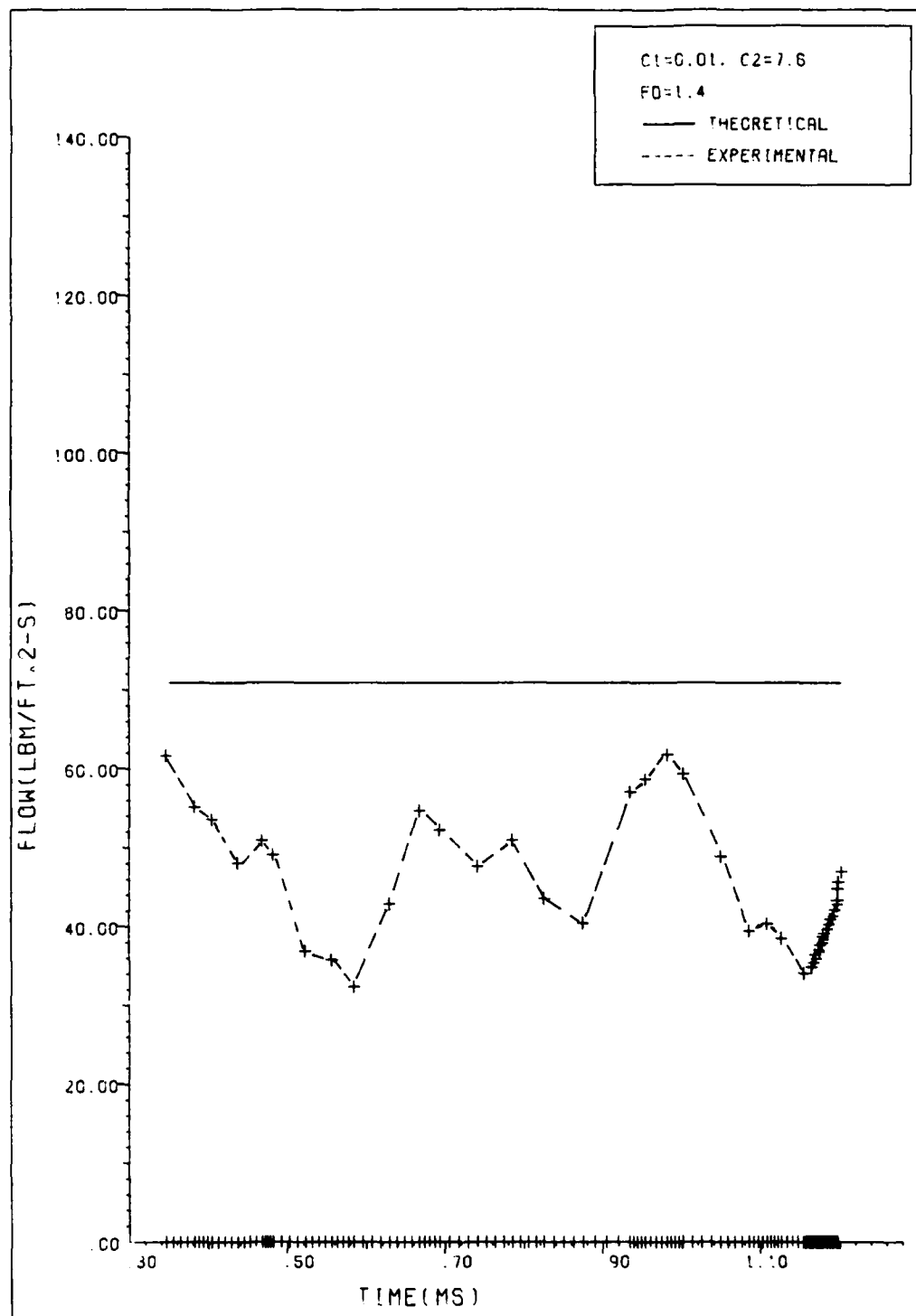
Fig. 39.   Run 092504--Theoretical and
Experimental Karman Streets

69
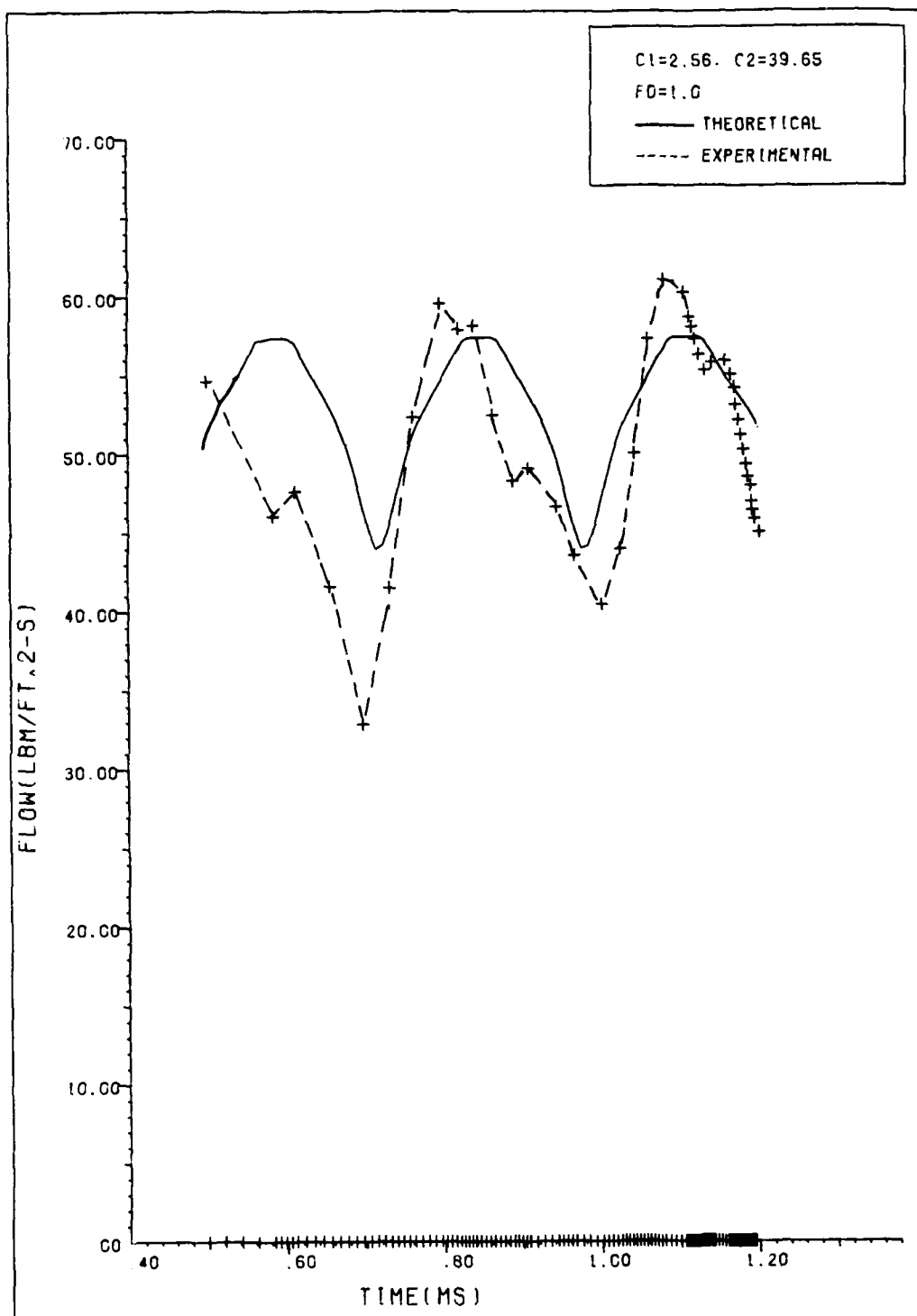
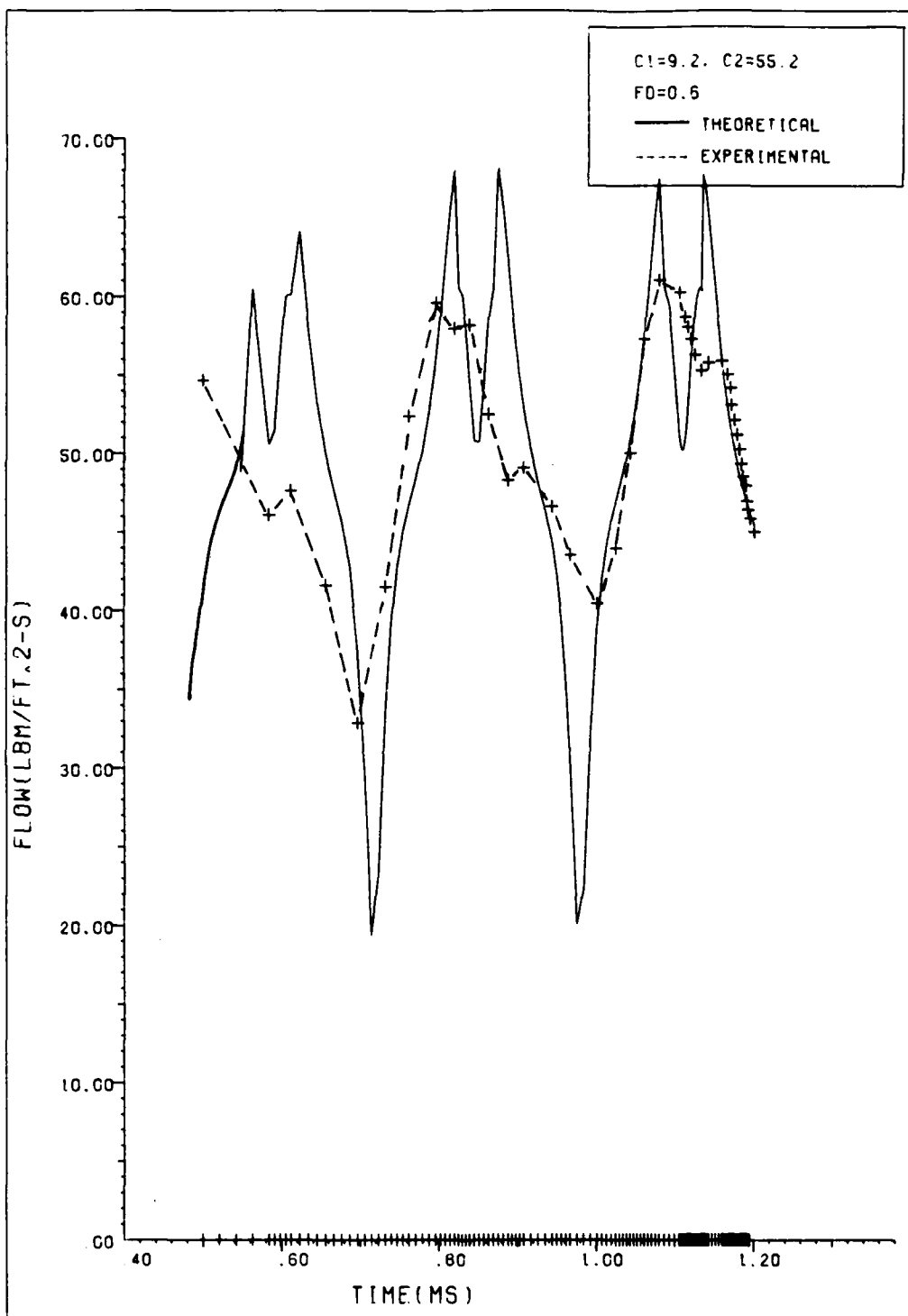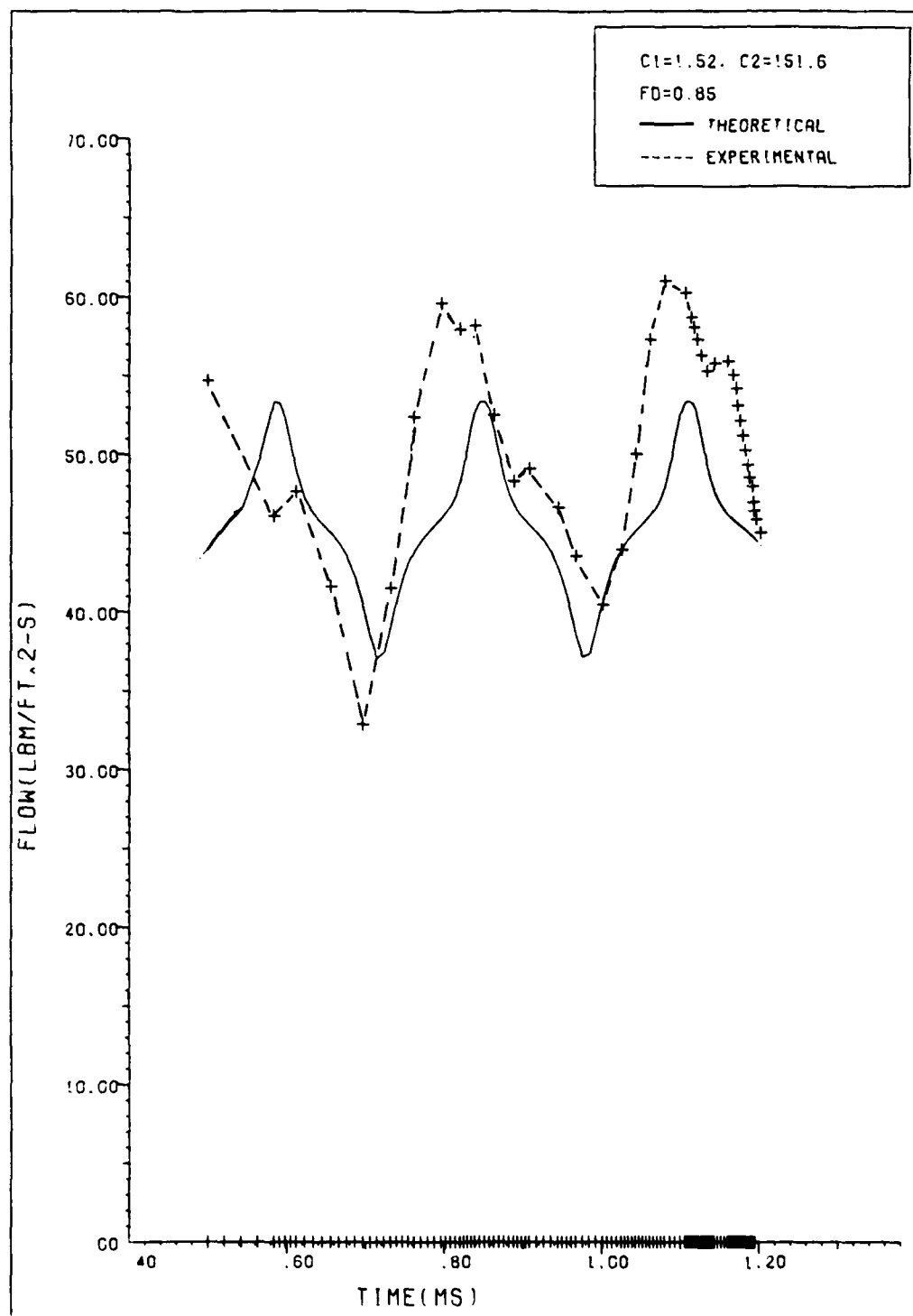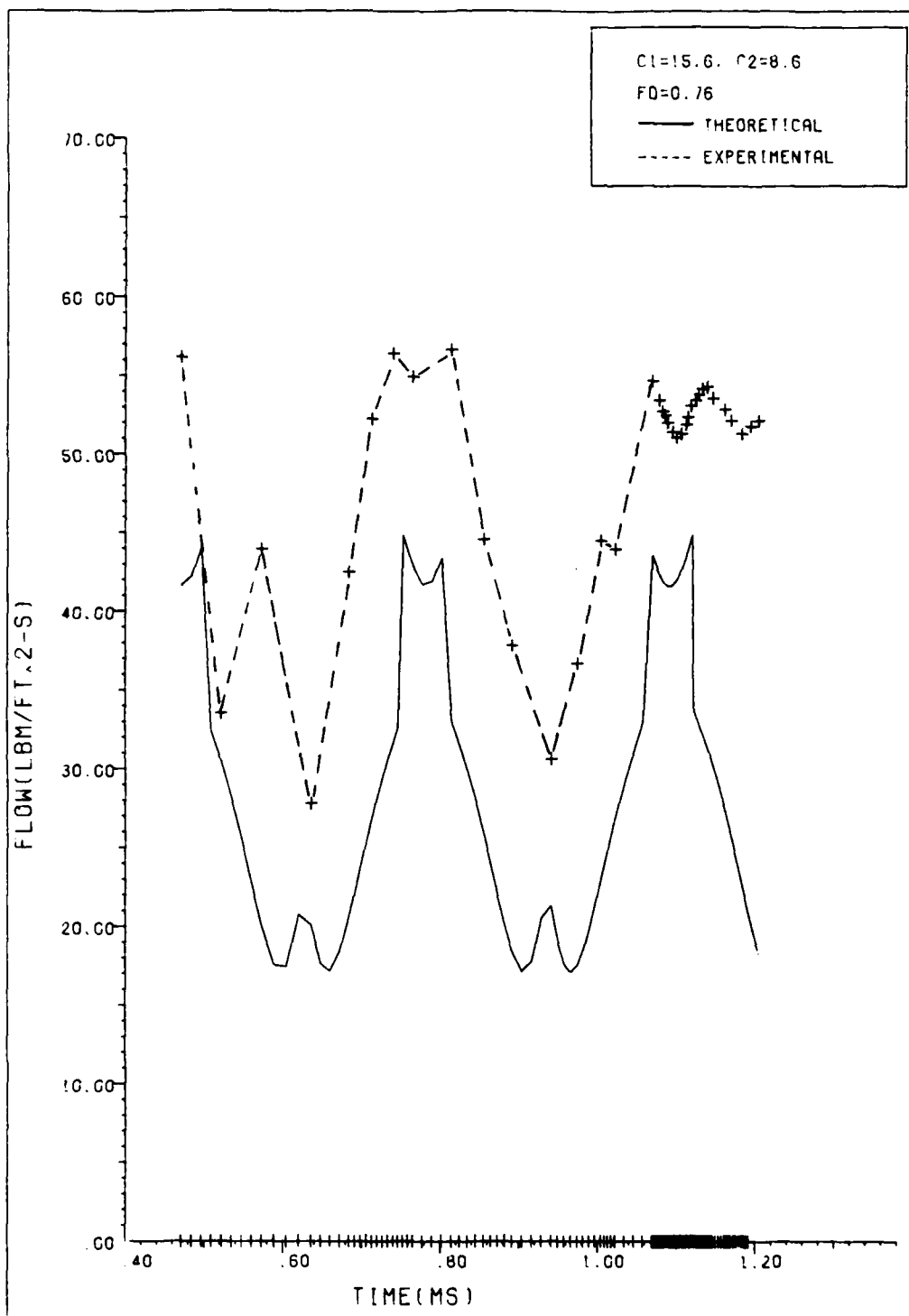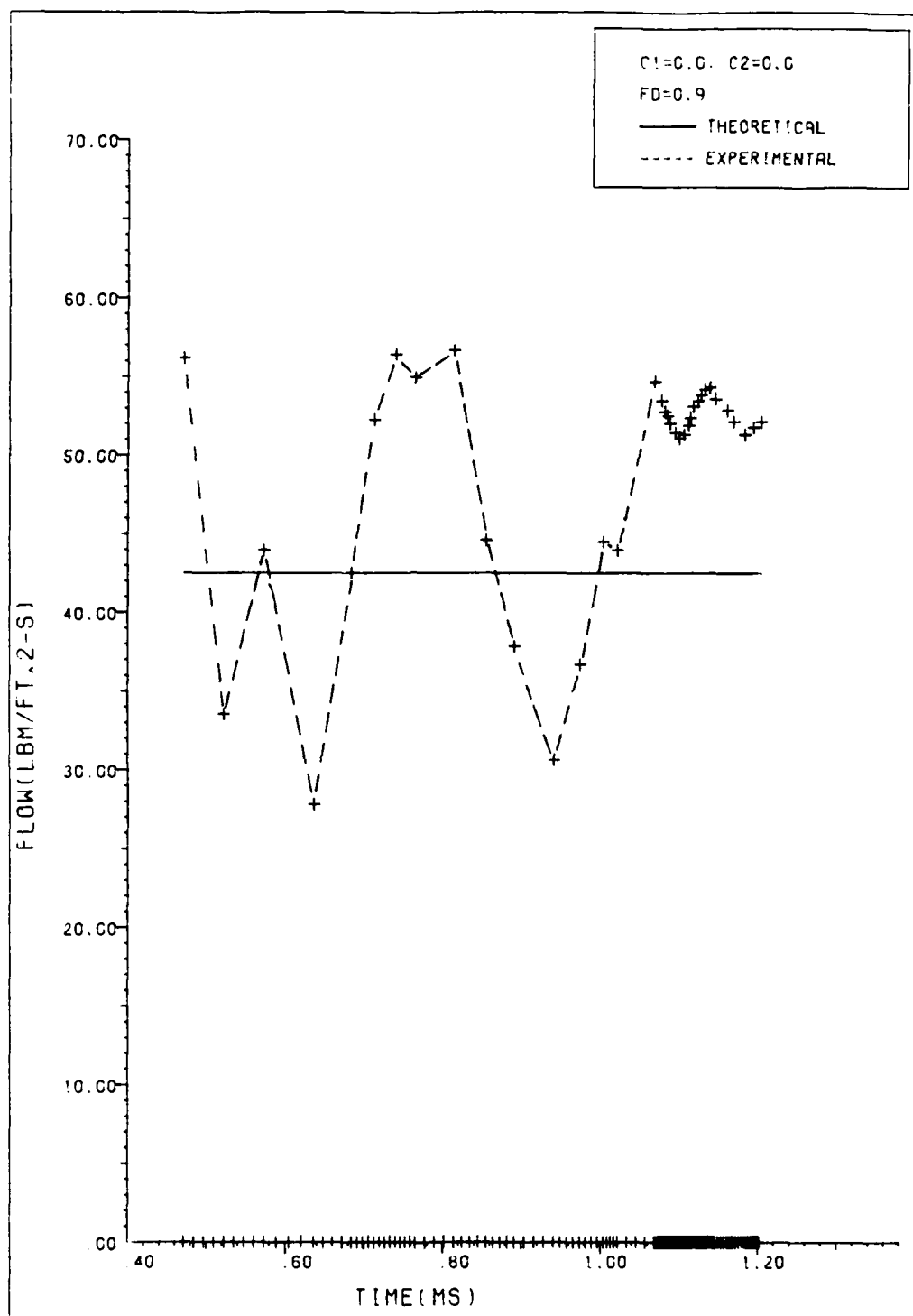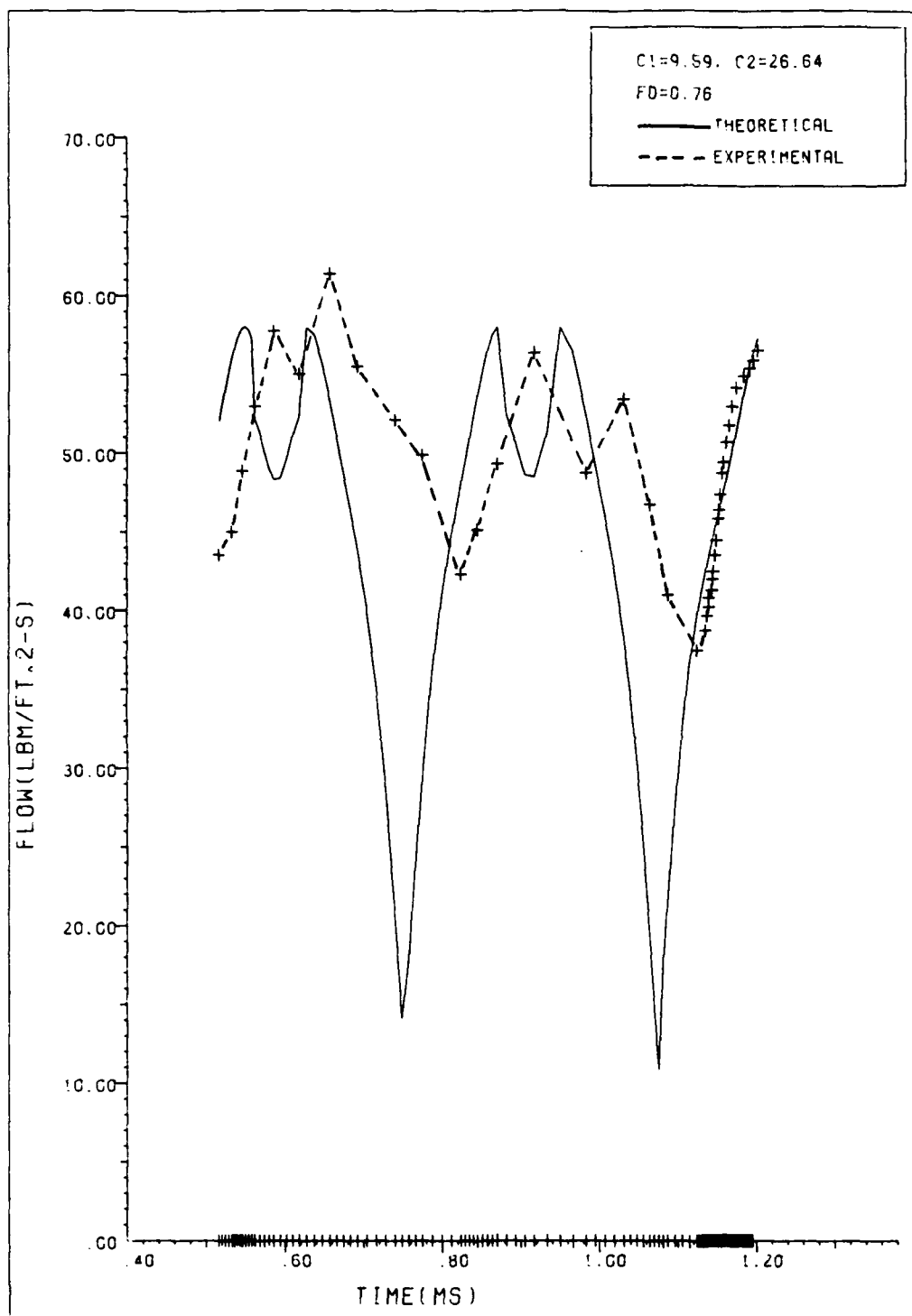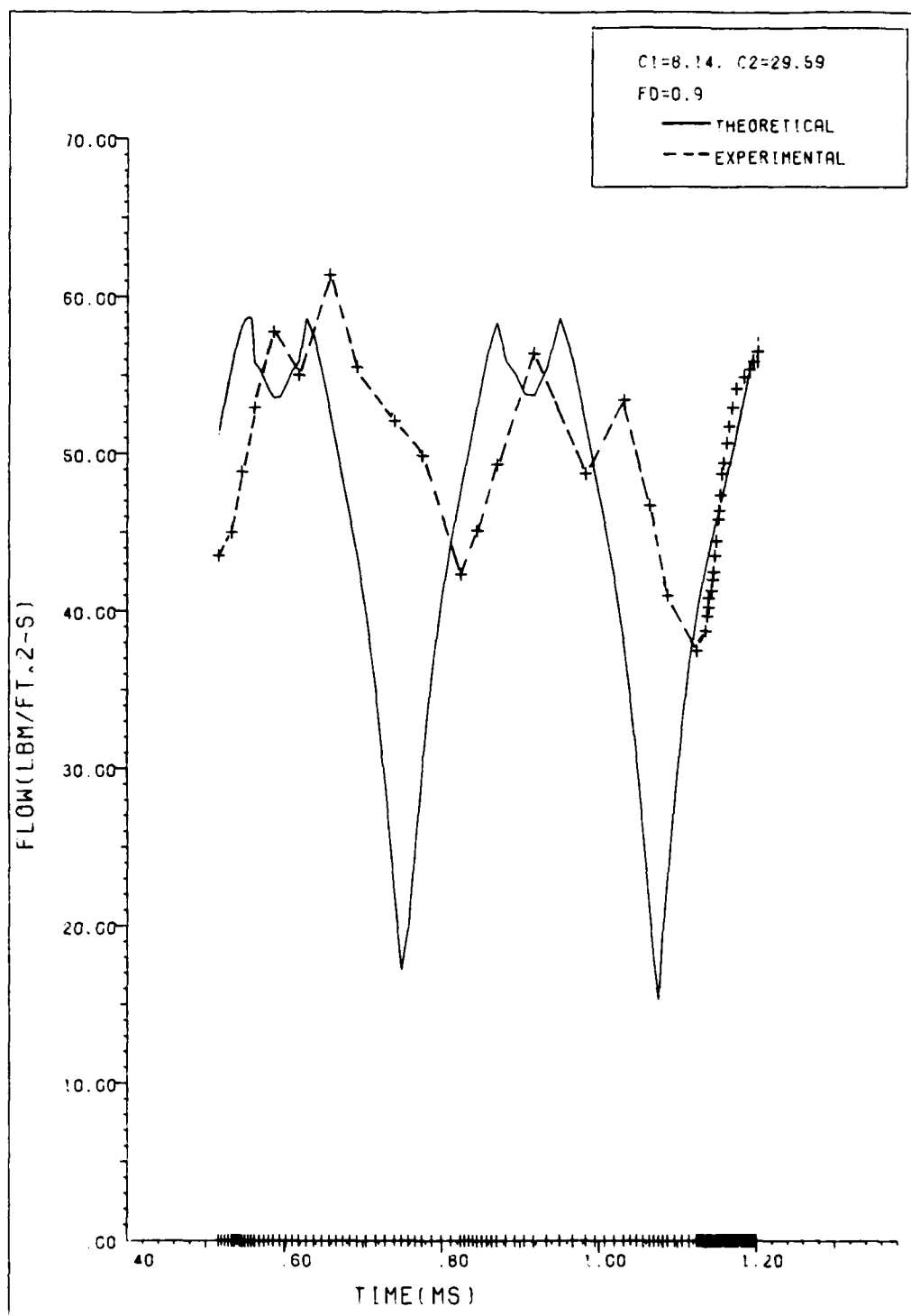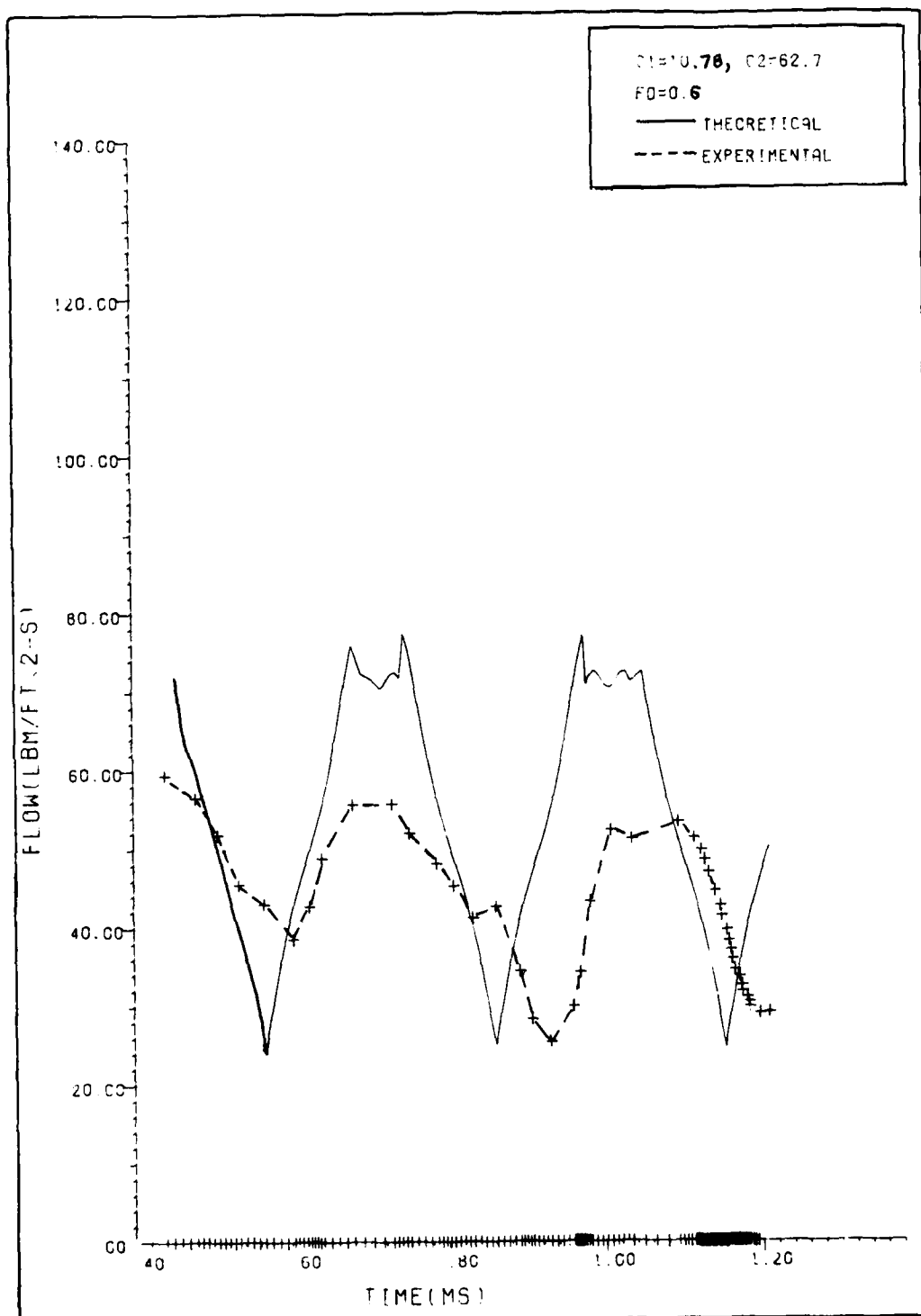Fig. 40. Run 092601--Theoretical and
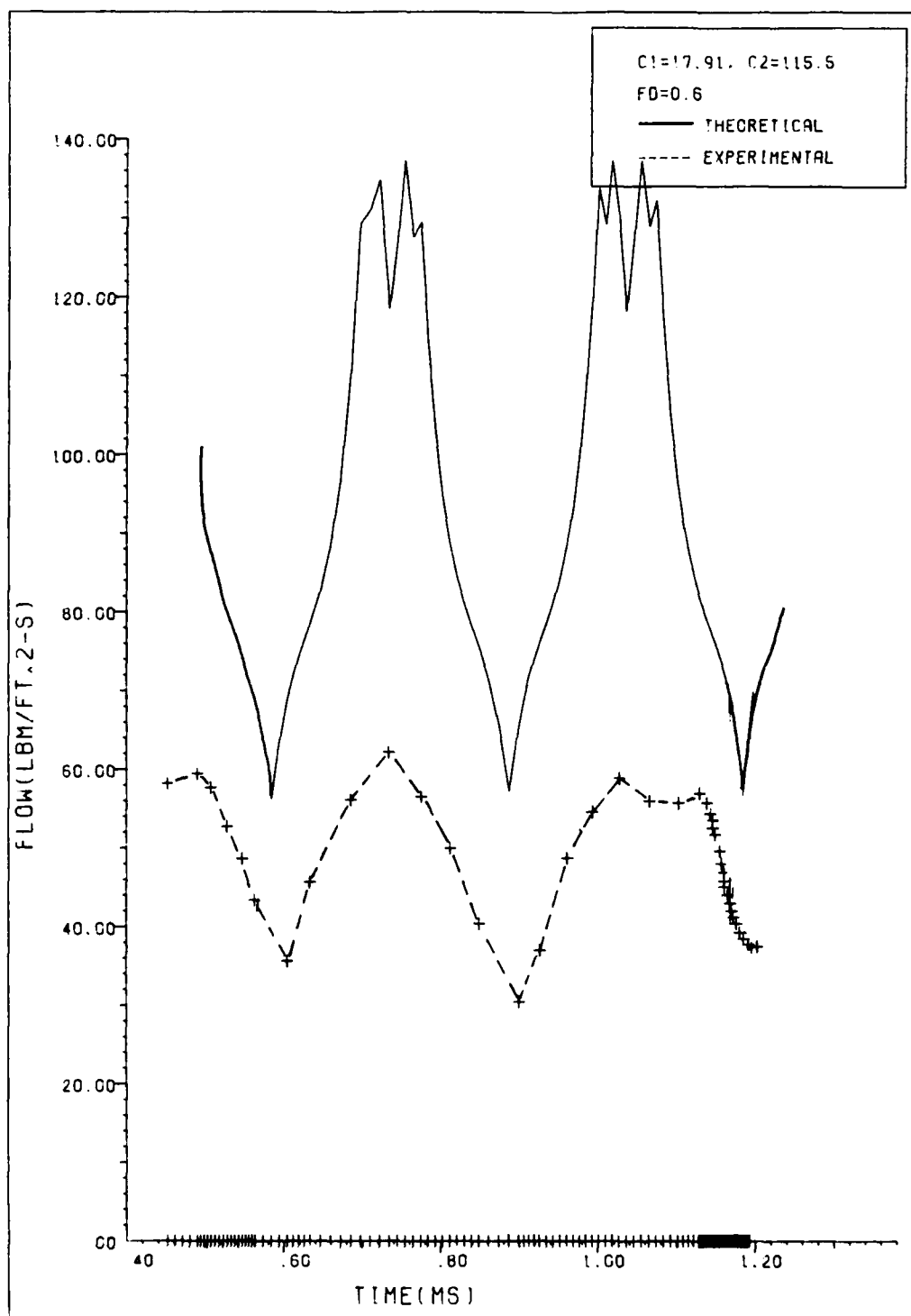Experimental Karman Streets
(Prandtl Tietjens Theory Used)

70
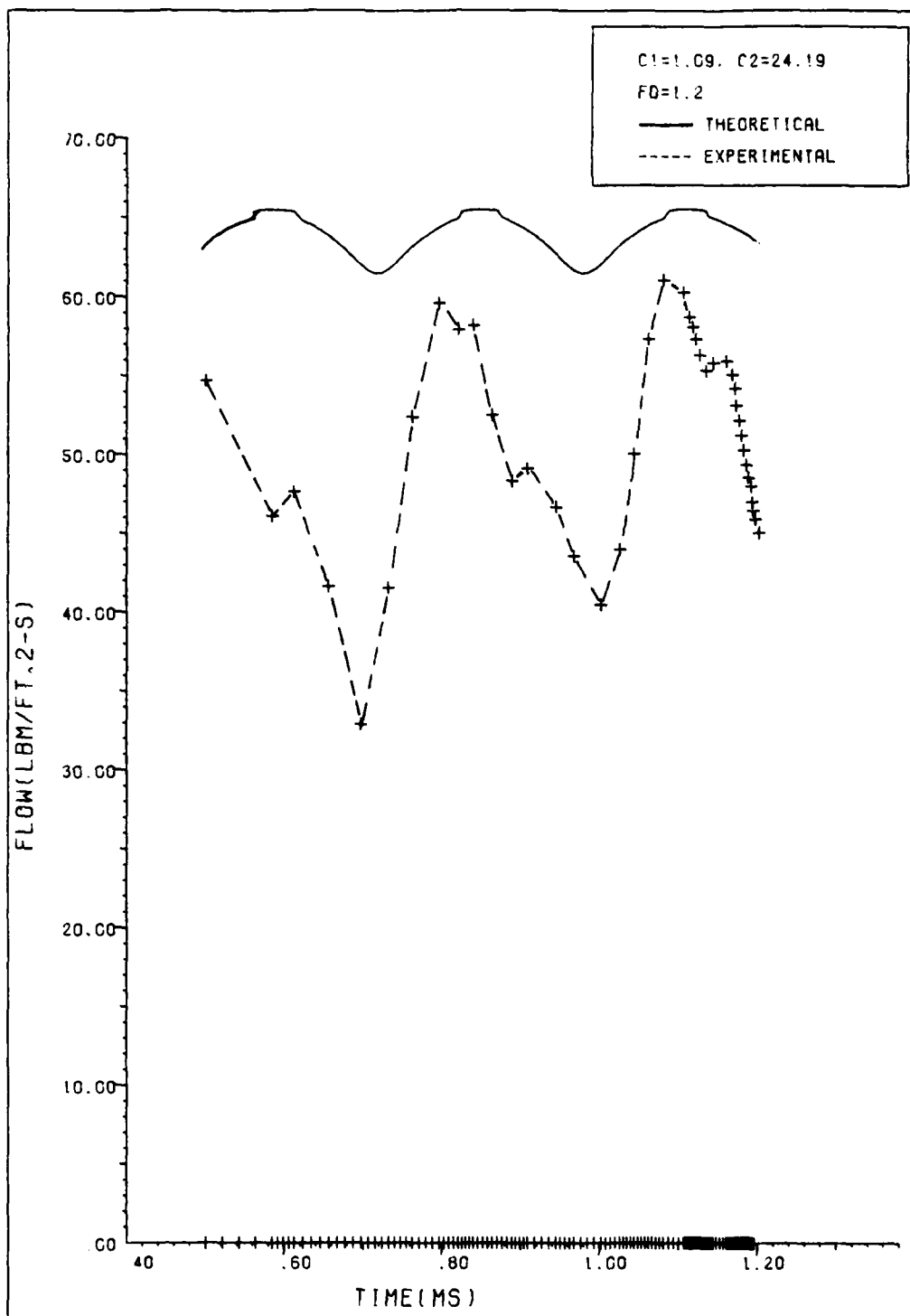
Fig. 41.   Run 092601--Theoretical and
Experimental Karman Streets

71
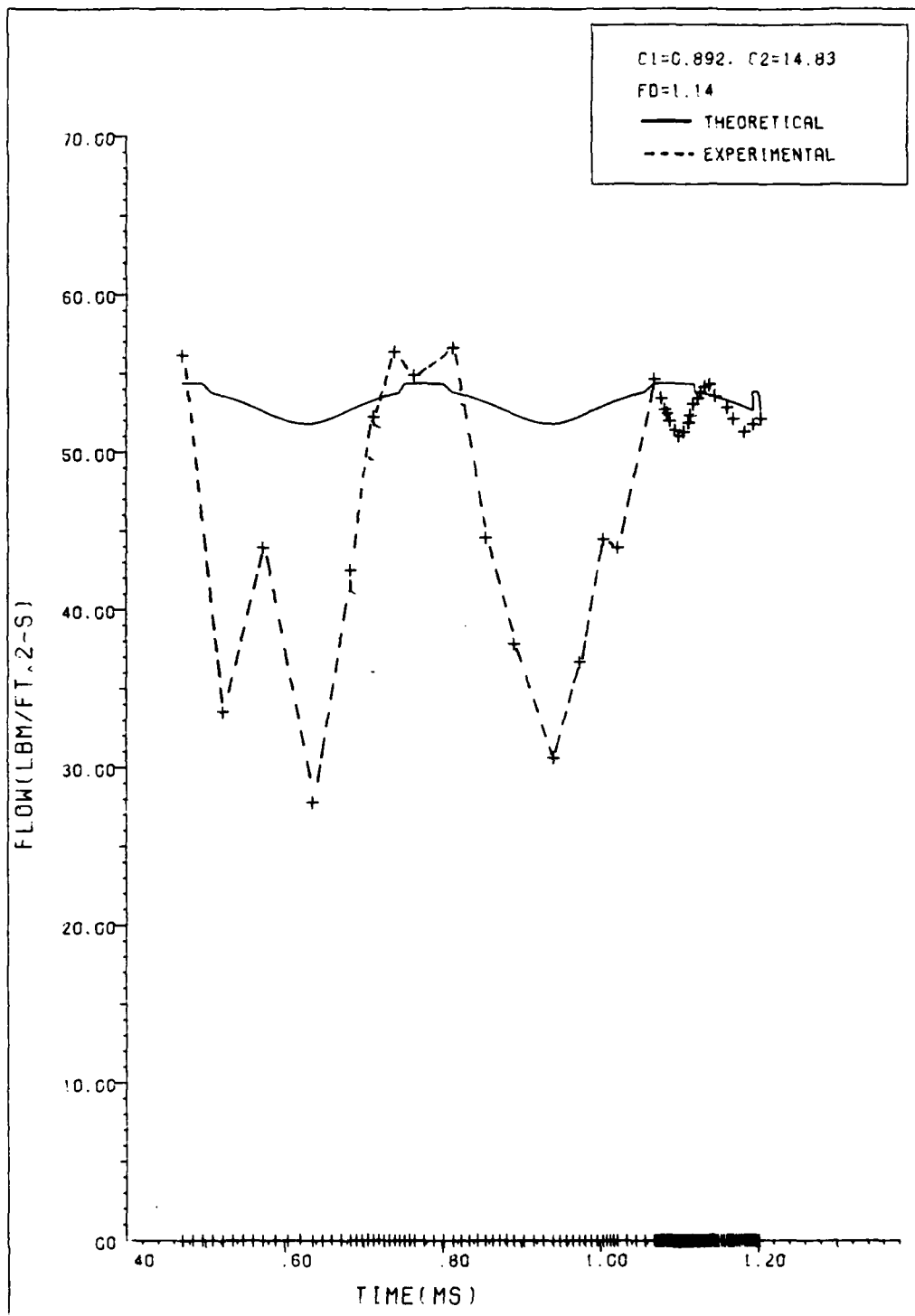
Fig. 42.   Run 092602--Theoretical and
            Experimental Karman Streets
            (Prandtl-Tietjens Theory Used)

72
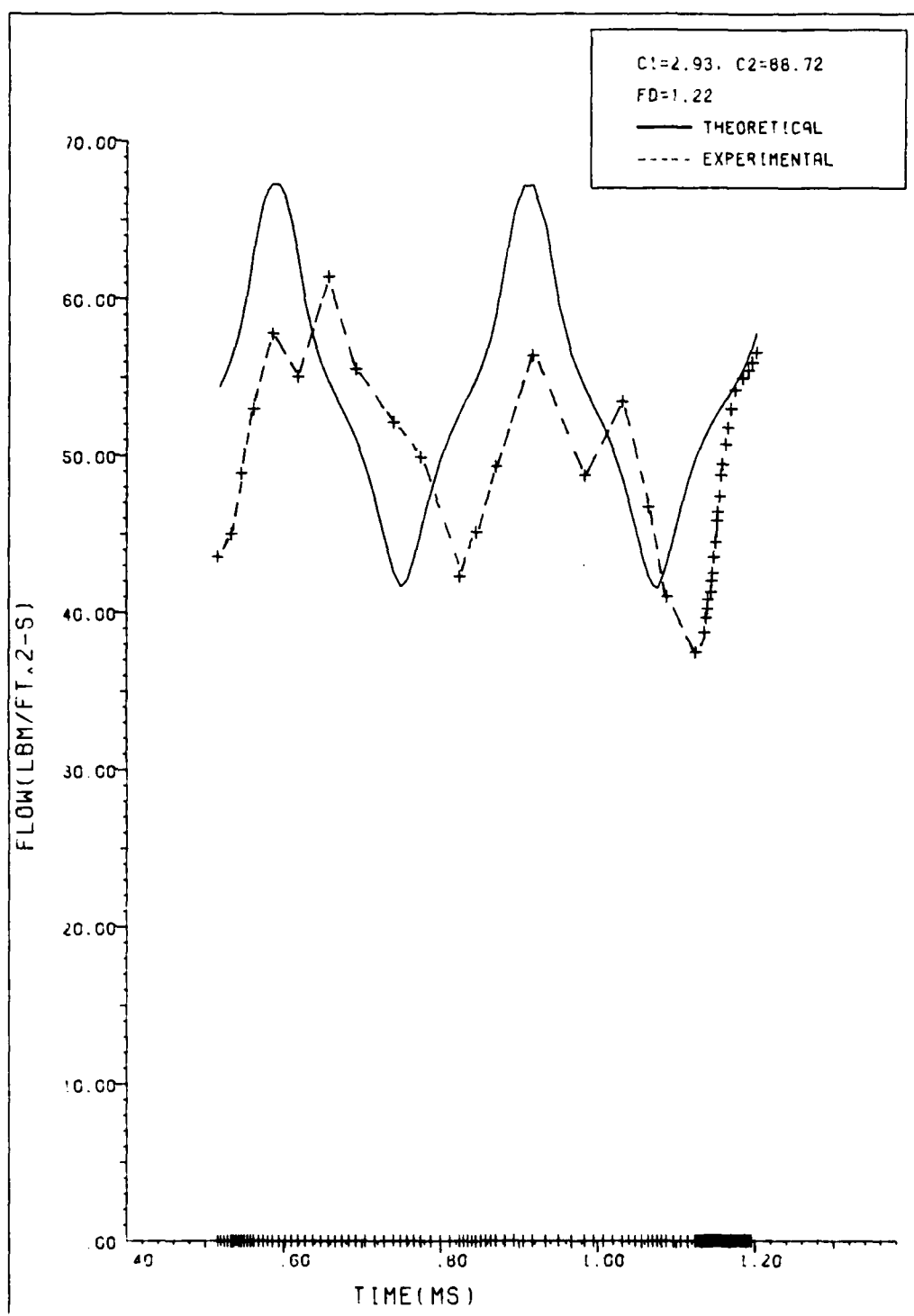
Fig. 43. Run 092606--Theoretical and
Experimental Karman Streets
(Prandtl-Tietjens Theory Used)

73
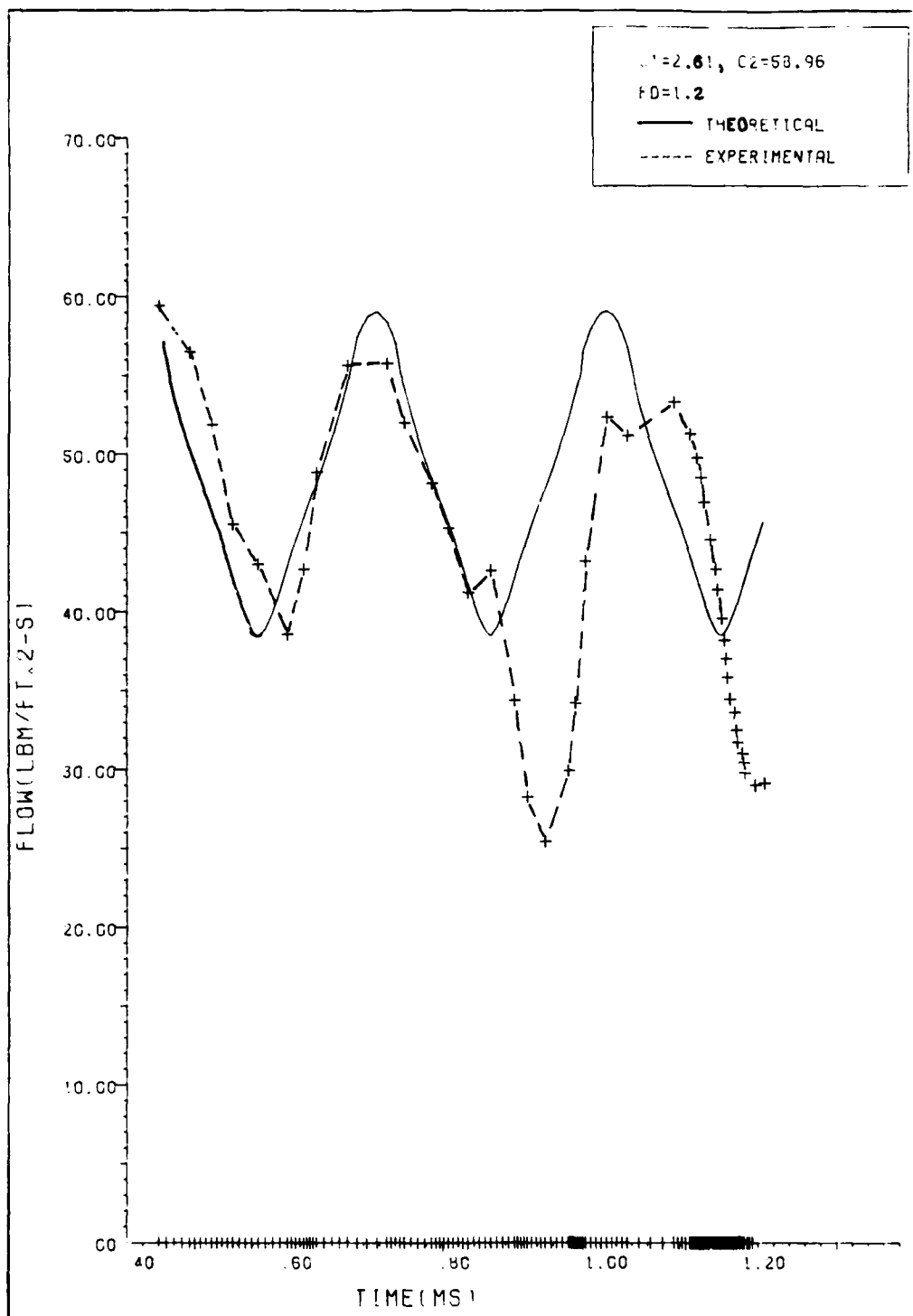
Fig. 44. Run 092609--Theoretical and
Experimental Karman Streets

74
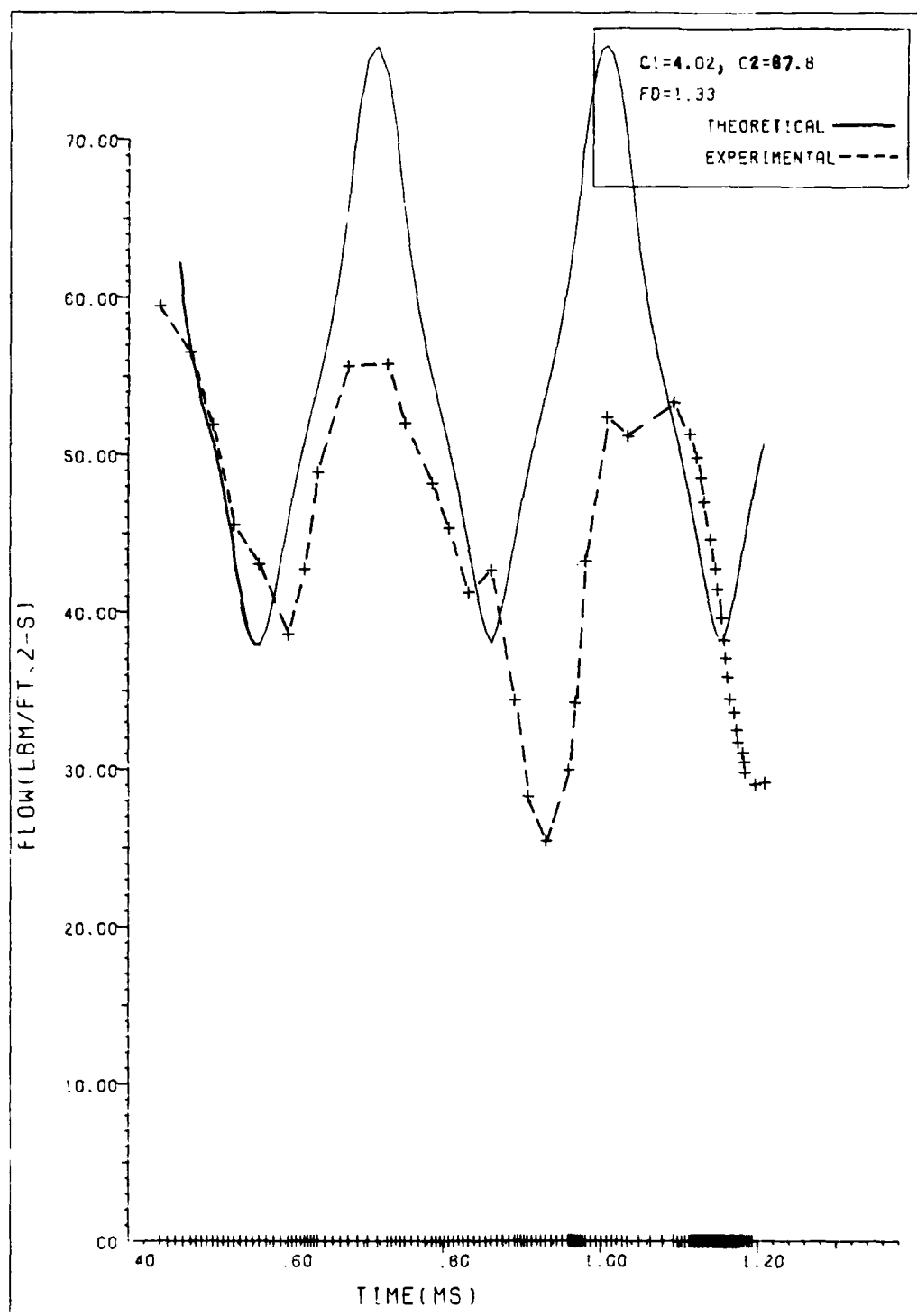
Fig. 45.   Run 092609--Theoretical and
Experimental Karman Streets
(Prandtl-Tietjens Theory Used)

75
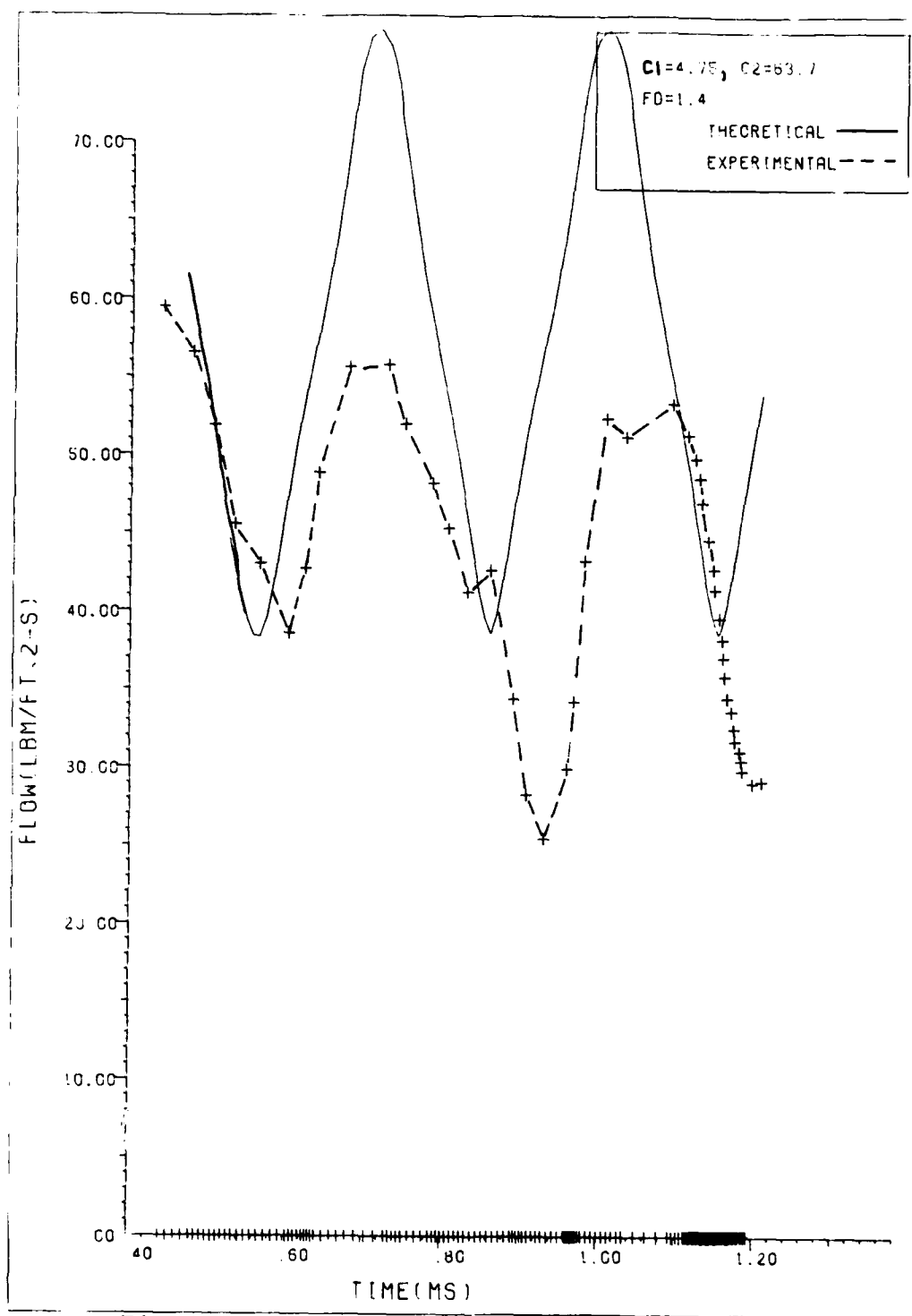
Fig. 46.   Run 092609--Theoretical and
            Experimental Karman Streets
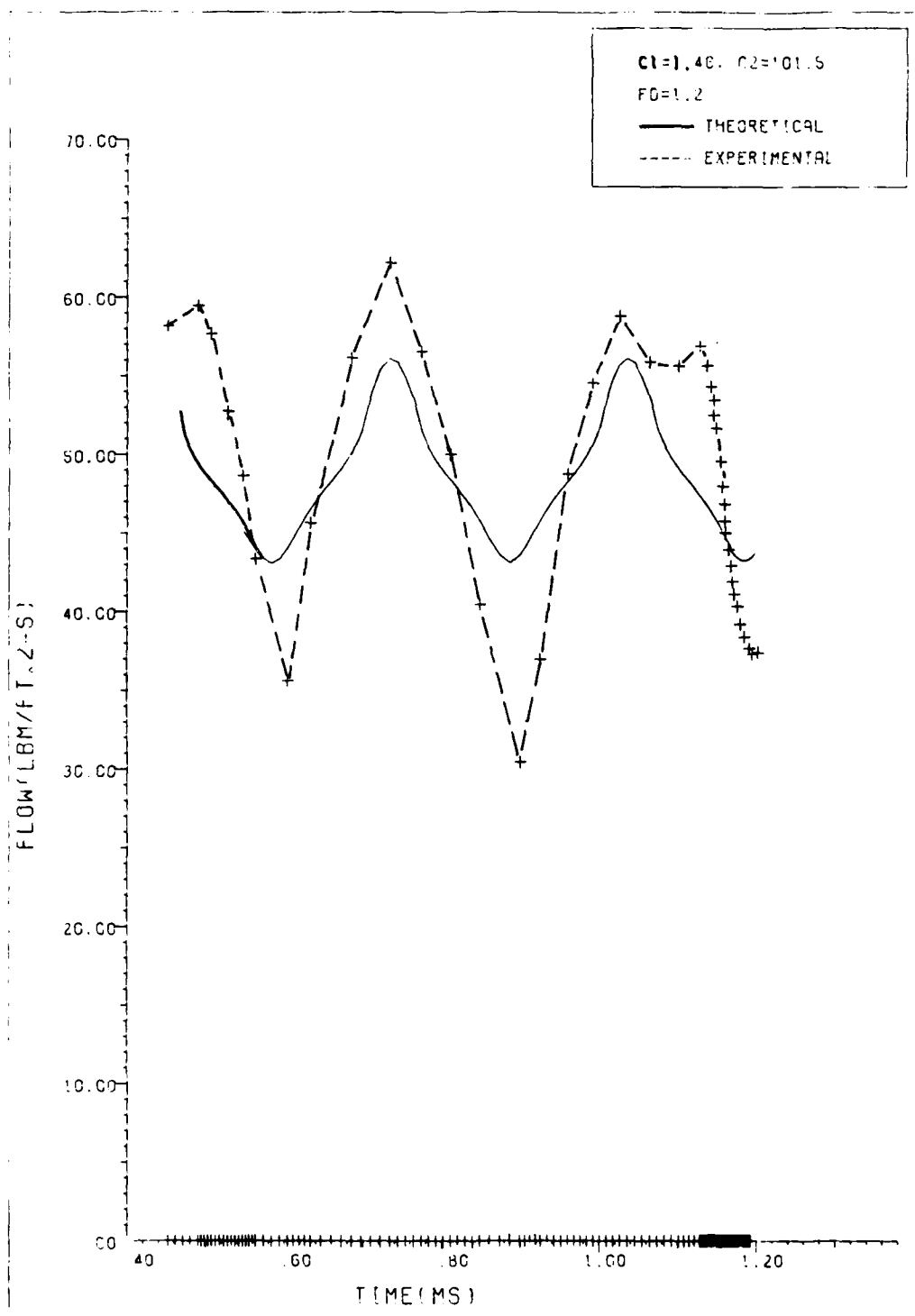
Fig. 47. Run 092611--Theoretical and
Experimental Karman Streets
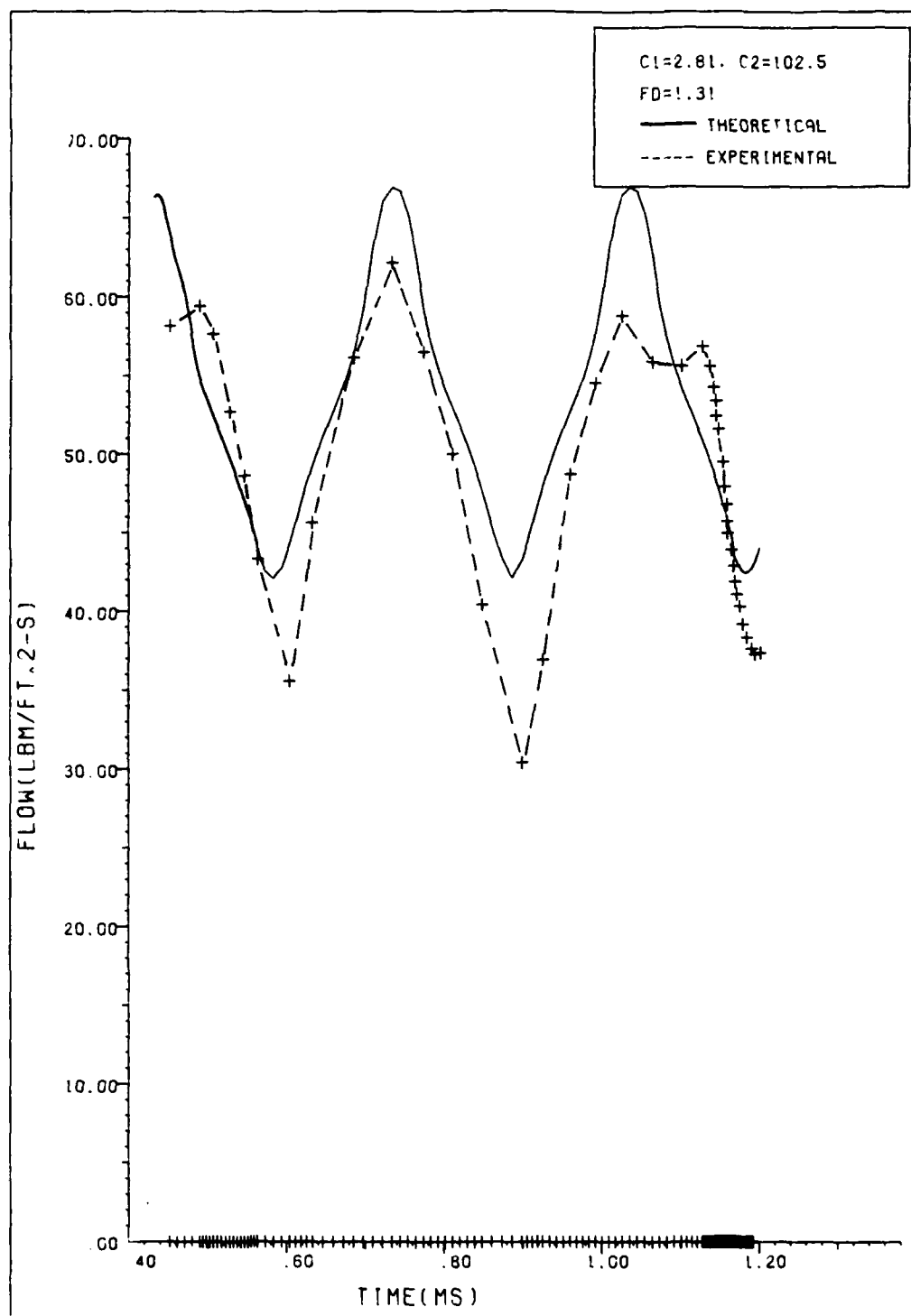
Fig. 48. Run 092611--Theoretical and
Experimental Karman Streets
(Prandtl-Tietjens Theory Used)

desirable (Figures 44, 46, and 47). It is probable that a combination of density gradients as well as the V_∞-vortex superposition apply to the Karman vortex street phenomena and its analysis, especially since the free-stream Mach number is of the order of 0.43.

The criteria for physically realistic values of c_1 and c_2 were simply that they be non-negative and that they be such that a ρu profile of the vortex exhibited a peak at a radius of 0.15 to 0.20 inches, which was the range of core radius observed in the schlieren pictures. Figure 49 shows some sample profiles for various acceptable values of c_1 and c_2. As with all optimization techniques, frequently the answers providing the best approximation to the experimental data did not satisfy the above criteria for physically correct answers. If c_1 becomes negative, that implies that the vortices are in effect spinning backwards (Figure 50) which is a physical impossibility with Karman vortex streets. If c_2 becomes negative, then, as r increases, (ρu) increases without bound in a negative direction, also an impossibility.

SYMBOL	C1	C2
SQUARE	12.71	27.73
OCT	3.7	66.89
TRI	9.2	55.19
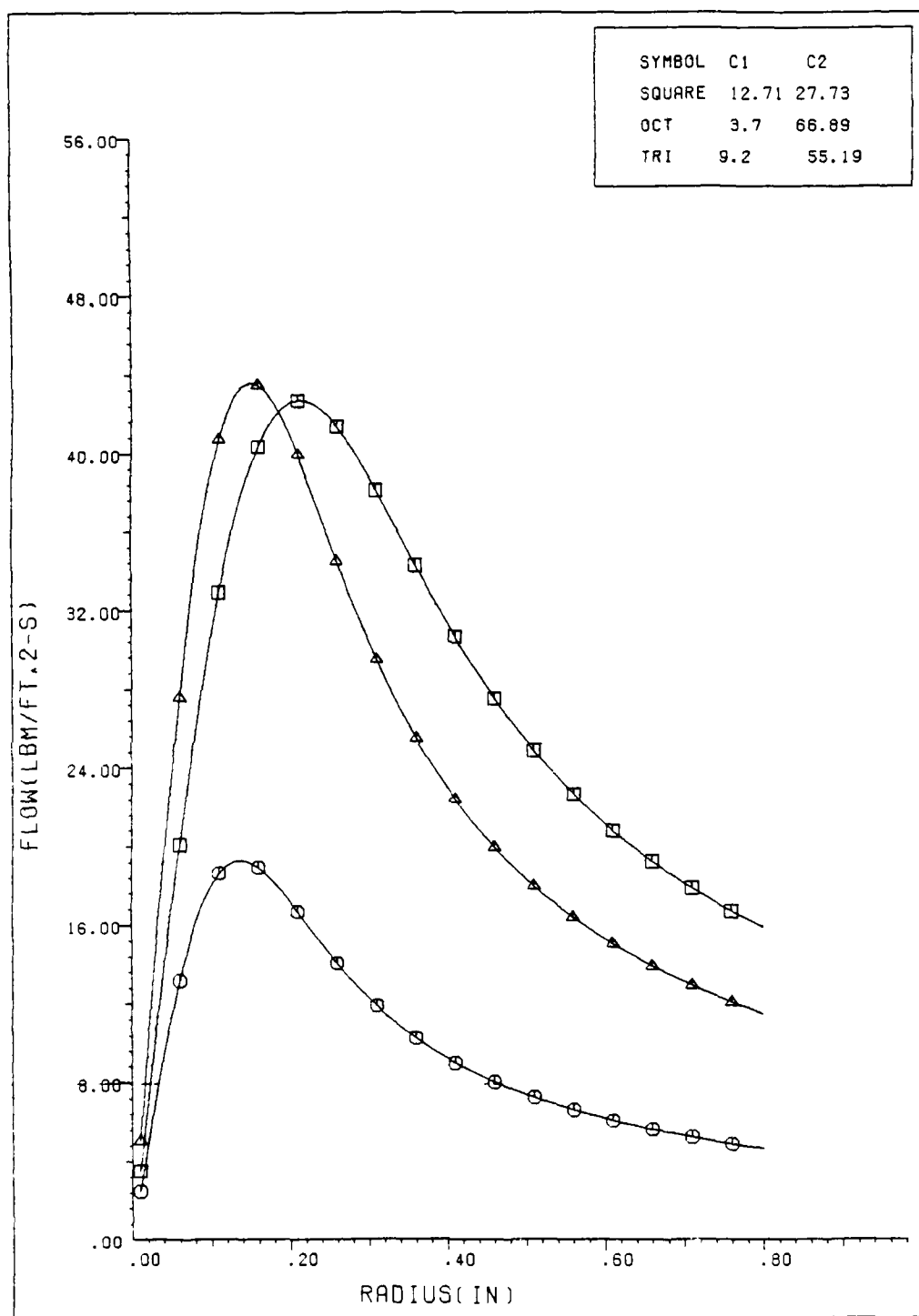
Fig. 49. Sample Vortex Profiles for
Acceptable Values of c_1 and c_2

80
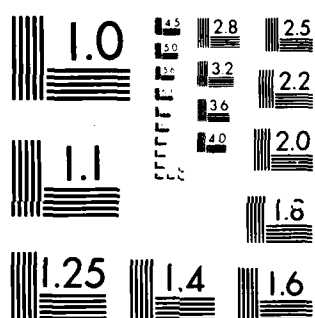
MICROCOPY RESOLUTION TEST CHART
NATIONAL BUREAU OF STANDARDS 1963 A
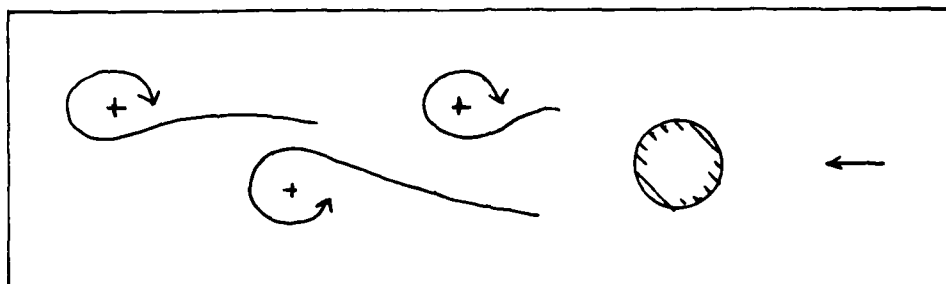
Fig. 50.   Karman Street Showing Effect of Negative c_1

VI. Conclusions

The following conclusions may be drawn from the previously discussed research effort:

1. It is possible, using the ideal, theoretical vortex equation and the ideas of superposition and core supremacy, to characterize the vortices in a Karman vortex street given anemometer and schlieren data. Considering the fact that the experimental flow is highly chaotic and the vortex shedding unstable, one can generate an experimentally based theoretical vortex street which bears reasonably close resemblance to the actual street.

2. The assumption that density is constant across the vortices is not valid in all cases. For true generality, it is necessary to take compressibility and density gradients into account in the analysis. If the flow is actually incompressible, then the analysis must be able to collapse to an incompressible solution.

3. The theoretical analysis by Prandtl and Tietjens, showing that the superposition phenomenon is between the free-stream and the vortex field has merit in efforts to experimentally characterize the individual vortices in the Karman street. It does not yield good results in all cases, however. It is clear that there are values of the density

factor which yield optimum solutions; these values are not always equal to $V_\infty/\overline{V}$, as the Prandtl-Tietjens theory would indicate. The best solutions appear to occur for values of density factor in the range of 0.8 to 1.4, depending on the test run. The analysis program in its current form cannot precisely determine the optimum value of density factor.

VII. Recommendations

Even though this thesis was itself a follow-on effort, there are several possible directions for future follow-on work to it.

1. Use a different optimization technique to find the c_1, c_2 solution. The Newton-Raphson Method, while it is rapid when it does converge, is not reliable in all cases. In addition, the new method should incorporate constraints which prevent the method from iterating to a nonphysical solution, for example, with c_1 and/or c_2 negative.

2. Extend the study to include planar shock waves interacting with vortices by completing the design and fabrication of the slider valve.

3. Use an airfoil pulsed in the pitch mode to produce a single starting vortex and then subject the vortex to a shock wave.

4. Because density is an important parameter in vortex characterization, interferometry instead of schlieren techniques should be used. Since interferometry measures density directly, it is a more sensitive technique and can measure smaller changes in density than can schlieren techniques. Thus, tests can be made at lower Reynolds numbers,

and hence lower turbulence levels. The quantitative infor-
mation available from the interferometer would also enable
the actual density across the vortex to be plotted as a
final check of the density variation across the vortices
in the vortex street.

5. Incorporate a digital computer with the IFA-100
anemometer system so as to automate the acquisition of flow
data. The most feasible means of doing this is to use the
IFA-100 in conjunction with a transient recorder, which
in turn stores and then sends the data to the computer.
The microcomputer can then be used to store the data on
diskette as well as perform the processing tasks.

6. Reformulate the method to take into account the
variation of density across the vortex street. Since the
density would no longer be constant, it is reasonable to
assume that the point value rather than the average value
of density is to be used in the convective mass flow calcu-
lation at each point in the vortex.

7. Using lower Reynolds number flows, investigate
further the applicability of the Prandtl-Tietjens super-
position concept to the technique of vortex characterization.

8. Verify that the vortices do indeed shed from
the cylinder in a two-dimensional manner by taking schlieren
photographs with the light path perpendicular to the
cylinder axis. Verification can also be done with a three
channel hot-film anemometer and correlation techniques.

Appendix A: Development of the Two-Vortex Assumption

Development of the Two-Vortex Assumption is composed of two smaller developments: derivation of more than one data point from a single anemometer trace and incorporation of the theoretical Equation (1) into the Two-Vortex Model.

Expansion of Data

As mentioned earlier, the anemometer provides a complete time history of the flow past the wire. As a vortex moves in space, its angle and radius to the anemometer change as its position changes.

Pictorally, we see that at two different times i_1 and i_2 for a vortex j, we have an $(r_j(i_1),\ \theta_j(i_1))$ and $(r_j(i_2),\ \theta_j(i_2))$ describing where the vortex is in relation to the anemometer (Figure 51).
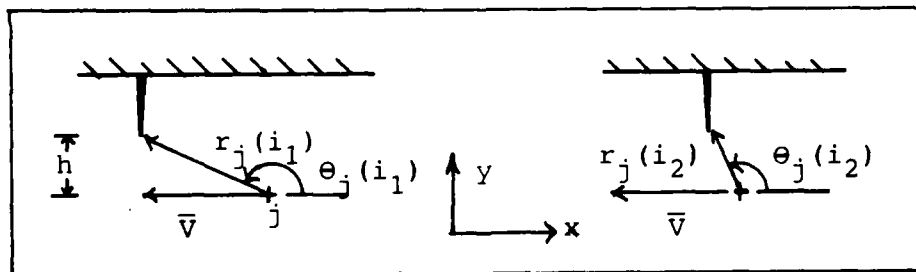
Fig. 51.   Temporal Expansion of Data

If the vortex is at time i_1 when the schlieren picture is taken, the $r_j(i_1)$ and $\theta_j(i_1)$ may be read from the picture. Also, noting vortex separation and frequency of passage gives the average convective velocity $\overline{V}$. If one considers a different time i_2, and assumes the $\overline{V}$ is constant and in the negative x-direction only, then one can mathematically move the vortex to any new location $r_j(i_2)$ and $\theta_j(i_2)$. Using simple geometry,

$$h = r_j(i_1)\sin\theta_j(i_1) = r_j(i_2)\cos\theta_j(i_2)$$

$$r_j(i_1)\cos\theta_j(i_1) = r_j(i_2)\cos\theta_j(i_2) - \overline{V}(i_2-i_1)$$

$$r_j(i_2) = \{[r_j(i_2)\cos\theta_j(i_2)]^2 + h^2\}^{\frac{1}{2}}$$

Therefore,

$$r_j(i_2) = \{[r_j(i_1)\cos\theta_j(i_1) + \overline{V}(i_2-i_1)]^2 \\ + [r_j(i_1)\sin\theta_j(i_1)]^2\}^{\frac{1}{2}}$$

and

$$\theta_j(i_2) = \tan^{-1}\{[r_j(i_1)\sin\theta_j(i_1)] \\ / [r_j(i_1)\cos\theta_j(i_1) + \overline{V}(i_2-i_1)]\}$$

Note that the - sign in front of $\overline{V}$ takes care of its negative direction and that, as drawn, $\cos\theta_j$ is negative. Thus, we have calculated a new (r,θ) position for the anemometer at a different time i_2.

87

The anemometer data is obtained by moving a time increment i_2-i_1 on the trace and reading the voltage at that point. The voltage value can then be applied to the calibration curve.

Development of the Two-Vortex Equations

The analysis begins with the elimination of time dependency from the vortex equation

$$\rho u = (c_1/r)(1-\exp(-r^2/4\nu(t_o+\Delta t))).$$

Considering the exponent term, one can make an order of magnitude estimate as to what t_o should be (t_o is defined as the time period which started when the vortex would have been an ideal $1/r$ type vortex and decayed to a more realistic free vortex form; Δt is on the order of .001 seconds, or the time the vortex is in the test section).

For a typical profile shown in Figure 2,

$$\nu(t_o+\Delta t)/r_o^2 = 0.04$$

where ν = dynamic viscosity = $1.155+10^{-4}$ ft^2/sec. Using $r_o = 0.02604$ ft (cylinder diameter) we can rewrite the equation above as

$$t_o + \Delta t = 0.04 r_o^2/\nu$$

$$t_o + \Delta t = 0.235 \text{ sec}$$

88

Since $\Delta t = 0.001$ sec, in the space of time the test takes place, $t_o + \Delta t$ is essentially constant. Therefore, we can assume the vortices are time independent, and

$$\rho u = (c_1/r)(1-\exp(-c_2 r^2))$$

Considering a generalized two-vortex system shown in Figure 52, one can write the total x-component of velocity at the anemometer as:

$$(\rho V)_x = (\rho u)_1 \sin\theta_1 + (\rho u)_2 \sin\theta_2 - (\overline{\rho V})$$

where

$$(\rho u)_1 = (-D_1 c_1/r_1)(1-\exp(-c_2 r_1^2))$$

$$(\rho u)_2 = (-D_2 c_1/r_2)(1-\exp(-c_2 r_2^2))$$

D_1, D_2 = direction of rotation; +1 counterclockwise, -1 clockwise

c_1, c_2 = unknown coefficients
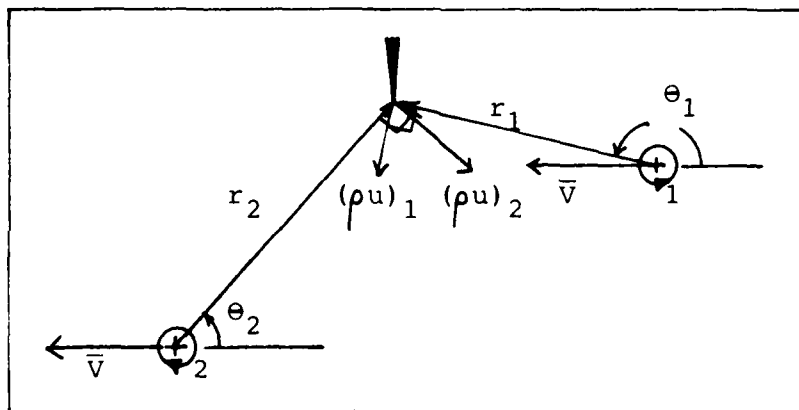
Fig. 52. Vortex Pair

Similarly, the total y-component is:

$$(\rho V)_y = (\rho u)_1 \cos\theta_1 + (\rho u)_2 \cos\theta_2$$

assuming that the convective transport is only in the negative x-direction.

The magnitude of the flow felt by the anemometer, then, is:

$$(\rho V) = [(\rho V)_x^2 + (\rho V)_y^2]^{\frac{1}{2}}$$

$$= \{ [\frac{-D_1 c_1}{r_1}(1-\exp(-c_2 r_1^2)) \sin\theta_1$$

$$- \frac{D_2 c_1}{r_2}(1-\exp(-c_2 r_2^2)) \sin\theta_2$$

$$- (\overline{\rho V})]^2 + [\frac{-D_1 c_1}{r_1}(1-\exp(-c_2 r_1^2)) \cos\theta_1$$

$$- \frac{D_2 c_1}{r_2}(1-\exp(-c_2 r_2^2) \cos\theta_2]^2 \}^{\frac{1}{2}}$$

or, eliminating the -1 factor:

$$(\rho V) = \{ [\frac{D_1 c_1}{r_1}(1-\exp(-c_2 r_1^2)) \sin\theta_1$$

$$+ \frac{D_2 c_1}{r_2}(1-\exp(-c_2 r_2^2)) \sin\theta_2$$

$$+ (\overline{\rho V})]^2 + [\frac{D_1 c_1}{r_1}(1-\exp(-c_2 r_1^2)) \cos\theta_1$$

$$+ \frac{D_2 c_1}{r_2}(1-\exp(-c_2 r_2^2)) \cos\theta_2]^2 \}^{\frac{1}{2}}$$

Defining a function f as the difference between the
right- and left-hand sides, we get

$$f = \{ [\frac{D_1 c_1}{r_1}(1-\exp(-c_2 r_1^2)) \sin\theta_1$$

$$+ \frac{D_2 c_1}{r_2}(1-\exp(-c_2 r_2^2)) \sin\theta_2$$

$$+ (\overline{\rho V})^2] + [\frac{D_1 c_1}{r_1}(1-\exp(-c_2 r_1^2)) \cos\theta_1$$

$$+ \frac{D_2 c_1}{r_2}(1-\exp(-c_2 r_2^2)) \cos\theta_2]^2 \}^{\frac{1}{2}} - (\rho V)$$

By multiplying out the terms, we get the form of Equation
(11).

Under ideal conditions where all measurements are
exact and there is no turbulence, for each data point, f
would equal zero. But, there are errors associated with
each data point, thus preventing an exact solution.
Therefore, an error minimization is needed, wherein we try
to obtain a "best fit" solution (c_1, c_2) which makes f as
small as possible. A feasible way to do this is by taking
many data points, each having its own f, and summing the
squares of f:

$$z = - \sum_i f_i^2$$

91

where i represents each data point. Following the Newton-Raphson procedure in the Schaum's Outline: Operations Research (16:122) we can find the values of c_1 and c_2 which minimize the sum of the errors, squared. Using matrices, we define

$$\vec{c} = [c_1, c_2]^T$$

$$\vec{H}_f = [\partial^2 z / \partial c_i \, \partial c_j]_{j=1,2}^{i=1,2}$$

$$z = -\sum_{i=1}^{N} f_i^2 \quad \text{(N= number of data points)}$$

Therefore,

$$\vec{c}_{NEW} = \vec{c}_{OLD} = (\vec{H}_f)^{-1}|_{OLD}(\partial z / \partial c_1, \partial z / \partial c_2)$$

defines a recursive relationship (16:112) which permits an iterative type solution. One then iterates until successive z values are within an acceptable error limit ε:

$$|z_{NEW} - z_{OLD}| / z_{OLD} < \varepsilon$$

This is best done using a computer since it requires lengthy calculations. The derivations of the first and second partial derivatives of z with respect to c_1 and c_2 are long and algebraically involved, but are not difficult and will not be repeated here.

The BASIC computer program "DATANAL8" used to perform the Newton-Raphson routine is shown below. The program begins by asking for the run number and if the raw data is stored on disk. If the data is on disk, the program asks for the filename (in MMDDRR format; M=month, D=day, R=run) and then retrieves the file and begins processing. If the data is not on disk, then the program asks for the information. After obtaining the raw data, the program requests initial starting points for c_1 and c_2. After the starting points are inputted, the program computes the first and second partial derivatives of the function z with respect to c_1 and c_2 and, through the Newton-Raphson algorithm computes new values for c_1 and c_2. If the error terms z for the old and new (c_1, c_2) pair are within 1 percent of each other, the program terminates execution; if the errors are different by more than 1 percent, then the program conducts another iteration.

```
1 REM DATANAL8
10 REM DEFINE TERMS
20 REM ARRAYS
30 REM E       ANEM VOLT
40 REM T       TIME
50 REM O1,O2 ANGLE THETA1 AND THETA2
60 REM R1,R2 RADII
70 REM F       FUNCTION FOR EACH DATA PT REFLECTING SUM OF
VORTICES AND MEAN FLOW
80 REM F1 TO F4   COMPONENTS OF F
90 REM G,G1 TO G4  DF/DC1 AND COMPONENTS
100 REM H,H1 TO H4  DF/DC2 AND COMPONENTS
110 REM W,W1 TO W4  D2F/DC1**2 AND COMPONENTS
120 REM X,X1 TO X4  D2F/DC2**2 AND COMPONENTS
130 REM Y,Y1 TO Y4  D2F/DC1DC2 AND COMPONENTS
140 REM I1( , )      COMPONENTS OF HESSIAN INVERSE
150 REM  M           MEASURED MASS FLOW/AREA IN LBM/FT**2-SEC
160 DIM
E(70),T(70),O1(70),O2(70),R1(70),R2(70),M(70),B(70),F1(70),F2(
70),F3(70)
165 DIM
F4(70),G(70),G1(70),G2(70),G3(70),G4(70),H(70),H1(70),H2(70),H
3(70)
170 DIM
H4(70),W(70),W1(70),W2(70),W3(70),W4(70),X(70),X1(70),X2(70),X
3(70)
175 DIM X4(70),Y(70),Y1(70),Y2(70),Y3(70),Y4(70)
190 REM VARIABLES
200 REM Z       SUM OF -F**2
210 REM Z1,Z2   FIRST DERIV WRT C1,C2
220 REM Z3,Z4   2ND DERIV WRT C1,C2
230 REM Z5      D2Z/DC1DC2
240 REM C1,C2   UNKNOWNS TO BE FOUND USING THE NEWTON-RAPHSON
METHOD
250 REM C3,C4   NEW C1,C2
260 REM C5,C6  C3=C1-C5,C4=C2-C6
270 REM P,T1,R BARO PRESS,TEMP,DENSITY
290 DIM I1(2,2),Q1(30),Q2(30),Q3(30)
300 REM INPUT VALUES************************************
305 Z9=100
310 INPUT"RUN NU.";N
311 INPUT"IS INPUT DATA ON DISK(Y/N)";D$
315 IF D$="Y" THEN GOSUB 3000
317 IF D$="Y" THEN GOTO 410
320 INPUT"NU. OF DATA PTS";I9
330 INPUT"T(SCHL)IN MSEC,E(SCHL) IN VOLTS";T(1),E(1)
340 FOR I=2 TO I9
350 PRINT"INPUT T(";I;")MSEC AND E(";I;") VOLTS":INPUT
T(I),E(I)
360 NEXT  I
370 INPUT"THETA1,R1,DIR(DEG,IN,+1=CCW";O1(1),R1(1),D1
```

```
380 INPUT"THETA2,R2,DIR";O2(1),R2(1),D2
390 INPUT"VTRANS IN FPS";V1
400 INPUT"PBARO,TEMP(INHG,DEGF)";P,T1
408 IF D$="N" THEN GOSUB 4000
410 T1=(T1+459.67)*((14+P)/(P+20))**((1.4-1)/1.4)
420 R=((P+14)*.4898*144)/(53.3*T1)
425 INPUT "DENSITY FACTOR";FD:R=FD*R
426 REM DENSITY ACCOUNTS FOR AVERAGE DENSITY BEING LOWER THAN
FREE S EAM
430 REM SOURCE SCHRIEIR,P. 150
440 REM DENS R IN LBM/FT**3
450 REM CALCULATE OTHER TEST POINTS**********************
460 O1(1)=O1(1)*π/180:O2(1)=O2(1)*π/180
470 V1=V1*12/1000:REM CONV TO IN/MSEC
480 FOR I=2 TO 20
490
R1(I)=((R1(1)*COS(O1(1))+V1*(T(I)-T(1)))**2+(R1(1)*SIN(O1(1)))
**2)**0.5
500
R2(I)=((R2(1)*COS(O2(1))+V1*(T(I)-T(1)))**2+(R2(1)*SIN(O2(1)))
**2)**0.5
510
O1(I)=ATN(R1(1)*SIN(O1(1))/(R1(1)*COS(O1(1))+V1*(T(I)-T(1))))
520
O2(I)=ATN(R2(1)*SIN(O2(1))/(R2(1)*COS(O2(1))+V1*(T(I)-T(1))))
530 REM ADJUST O1(I),O2(I)
540 IF NOT(O1(1)>0 AND O1(I)<0) THEN GOTO 550
545 O1(I)=π-ABS(O1(I)):GOTO 570
550 IF NOT(O1(1)>π AND O1(1)<3*π/2) THEN GOTO 560
555 O1(I)=π+O1(I):GOTO570
560 IF NOT(O1(1)<0 AND O1(I)>0) THEN GOTO 570
565 O1(I)=π+O1(I):GOTO 570
570 IF NOT(O2(1)>0 AND O2(I)<0) THEN GOTO 580
575 O2(I)=π-ABS(O2(I)):GOTO 640
580 IF NOT(O2(1)>π AND O2(1)<3*π/2) THEN GOTO 590
585 O2(I)=π+O2(I):GOTO 640
590 IF NOT(O2(I)<0 AND O2(I)>0) THEN GOTO 640
595 O2(I)=π+O2(I):GOTO 640
640 NEXT I
650 REM CALC M IN LBM/FT**2-SEC******************************
660 PRINT"ASSUMING HOT FILM USED IS K746"
670 M0=-887.645211:M1=2237.04893
680 M2=-1927.51774:M3=694.103018
690 M4=-87.5672976
700 FOR I=1 TO 20
710 M(I)=M0+M1*E(I)+M2*E(I)**2+M3*E(I)**3+M4*E(I)**4
720 NEXT I
730 PRINT"IGNORE 1ST DATA POINT AS BEING OUTSIDE THE BOUNDS OF
TWO VORTICES?"
740 PRINT"2=YES,1=NO":INPUT I8
750 V1=V1*1000/12:REM CONV BACK TO FPS
```

```
760 REM PICK INITIAL C1,C2**********************************
770 PRINT"INPUT INITIAL C1,C2 IN IN-LBM/FT**2-SEC &
IN**-2":INPUT C1,C2
780 REM CALCULATE F AND DERIVS(G,H,W,X,Y)*******************
785 RS=(5/16)/2:REM FIX CORE AT CYLINDER DIAMETER FOR
EXCLUSION OF FAR VORTEX
790 FOR I=I8 TO 20
795 IF (R1(I)<RS OR R2(I)<RS) THEN GOSUB 8200
797 IF(R1(I)<RS OR R2(I)<RS)THEN GOTO910
800 GOSUB 7000:REM CALC F(I) AND B(I)
810 Q1(I)=SIN(O1(I))*SIN(O2(I))+COS(O1(I))*COS(O2(I))
820 Q2(I)=1-EXP(-C2*R1(I)**2)
830 Q3(I)=1-EXP(-C2*R2(I)**2)
840 GOSUB 7200:REM CALCULATE G(I)
910 NEXT I
920 REM CALC Z'S AND DERIVS(Z1,Z2,Z3,Z4,Z5)****************
930 Z=0:Z1=0:Z2=0:Z3=0:Z4=0:Z5=0
940 FOR I=I8 TO 20
950 Z=Z-(B(I)-M(I))**2
960 Z1=Z1-(1-M(I)/B(I))*G(I)
970 Z2=Z2-(1-M(I)/B(I))*H(I)
980 Z3=Z3-(G(I)**2*M(I)/(2*B(I)**3)+W(I)*(1-M(I)/B(I)))
990 Z4=Z4-(H(I)**2*M(I)/(2*B(I)**3)+X(I)*(1-M(I)/B(I)))
1000 Z5=Z5-(G(I)*H(I)*M(I)/(2*B(I)**3)+Y(I)*(1-M(I)/B(I)))
1010 NEXT I
1020 REM CALCULATE
I1(1,1),I1(1,2),I1(2,1),I1(2,2)****************
1030 I1(1,1)=Z4/(Z3*Z4-Z5**2)
1040 I1(1,2)=Z5/(Z5**2-Z3*Z4)
1050 I1(2,1)=I1(1,2)
1060 I1(2,2)=Z3/(Z3*Z4-Z5**2)
1070 REM CALCULATE C5,C6*******************************
1080 C5=I1(1,1)*Z1+I1(1,2)*Z2
1090 C6=I1(2,1)*Z1+I1(2,2)*Z2
1100 REM CALCULATE C3,C4(NEW C1,C2)*********************
1110 C3=C1-C5
1120 C4=C2-C6
1130 REM COMPARE NEW AND OLD*****************************
1140 IF Z9>50 THEN GOTO 1170
1150 IF((ABS((Z9-Z)/Z9)>.01))THEN GOTO 1170
1155 PRINT C1;C2;SQR(ABS(Z)/(20-I8+1))
1160 GOTO1250:REM FINAL RESULTS
1170 PRINT C1;C2;SQR(ABS(Z)/(20-I8+1))
1180 C1=C3:C2=C4:Z9=Z
1190 GOTO 780:REM RETURN TO START FOR NEXT INTERATION********
1250 INPUT "HARD COPY?1=YES";P8
1260 IF P8<>1 THEN GOTO 1500
1270 OPEN 1,4
1275 PRINT#1,"RUN NUMBER   ";N
1280 PRINT#1,"C1= ";C1;"(LBM/FT**2-SEC)IN"
1290 PRINT#1,"C2= ";C2;"IN**-2"
```

96

```
1300 PRINT#1,"RMS OF ERRORS IS ";SQR(ABS(Z)/(20-I8+1))
1310 PRINT#1,"DENSITY FACTOR IS ";FD
1400 REM CHECK OF ERRORS AND PRINT
1410 PRINT#1,"TIME(MS)";TAB(12);"ACT FLOW";TAB(12);"EXP
FLOW";TAB(12);"ERROR%"
1420 PRINT#1,""
1430 FOR I=I8 TO 20
1440
PRINT#1,T(I);TAB(10);M(I);TAB(10);B(I);TAB(10);(B(I)-M(I))/M(I
)*100
1450 NEXT I
1455 PRINT#1,"FLOWS IN IN-LBM/FT**2-SEC"
1460 CLOSE1
1500 PRINT"TEST PT     ACT FLOW    EXP FLOW   %ER"
1510 FOR I=I8 TO 20
1520 PRINT I;"   ";M(I);"    ";B(I);"    ";(B(I)-M(I))/M(I)*100
1530 NEXT I
1540 PRINT"WOULD YOU LIKE TO GO AGAIN? IF SO Y=YES,N=NO":INPUT
G$
1560 IF G$="N" THEN GOTO 2000
1570 PRINT"WOULD YOU LIKE TO USE THE SAME INPUT DATA?":INPUT
G$
1580 IF G$="Y" THEN GOTO 770
1590 GOTO 310
2000 END
3000 REM RETRIEVE DATA FROM DISK FILE
3010 INPUT"DATA FILE MMDDRR FORMAT";N1$
3020 DO$="0:DF"+N1$+",S,R"
3030 OPEN2,8,9,DO$
3050 INPUT#2,I9,T(1),E(1)
3060 FOR I=2 TO I9
3070 INPUT#2,T(I),E(I)
3080 NEXT I
3090 INPUT#2,O1(1),R1(1),D1
3100 INPUT#2,O2(1),R2(1),D2
3110 INPUT#2,V1,P,T1
3150 CLOSE2
3160 RETURN
4000 REM  PUTS DATA ONTO DISK FOR LATER USE
4010 INPUT"DATAFILE MMDDRR FORMAT";N1$
4020 DO$="0:DF"+N1$+",S,W"
4030 OPEN2,8,9,DO$
4040 PRINT#2,I9;",";T(1);",";E(1);CHR$(13);
4050 FOR I=2 TO I9
4060 PRINT#2,T(I);",";E(I);CHR$(13);
4070 NEXT I
4080 PRINT#2,O1(1);",";R1(1);",";D1;CHR$(13);
4090 PRINT#2,O2(1);",";R2(1);",";D2;CHR$(13);
4100 PRINT#2,V1;",";P;",";T1;CHR$(13);
4150 CLOSE2
4160 RETURN
```

```
7000 REM SUBR CALC F(I) TO B(I)
7010 F1(I)=C1**2/R1(I)**2*(1-EXP(-C2*R1(I)**2))**2
7020
F2(I)=-2*(SIN(O1(I))*SIN(O2(I))+COS(O1(I))*COS(O2(I)))/(R1(I)*
R2(I))
7030
F2(I)=F2(I)*C1**2*(1-EXP(-C2*R1(I)**2))*(1-EXP(-C2*R2(I)**2))
7040 F3(I)=C1**2/R2(I)**2*(1-EXP(-C2*R2(I)**2))**2
7050 F4(I)=D1*SIN(O1(I))/R1(I)*(1-EXP(-C2*R1(I)**2))
7060 F4(I)=F4(I)+D2*SIN(O2(I))/R2(I)*(1-EXP(-C2*R2(I)**2))
7070 F4(I)=F4(I)*2*R*V1*C1+(R*V1)**2-M(I)**2
7080 B(I)=SQR(F1(I)+F2(I)+F3(I)+F4(I)+M(I)**2)
7090 RETURN
7200 REM SUBR CALC G(I)=DF/DC1
7210 G1(I)=2*C1/R1(I)**2*Q2(I)**2
7220 G2(I)=-4*Q1(I)/(R1(I)*R2(I))*C1*Q2(I)*Q3(I)
7230 G3(I)=2*C1/R2(I)**2*Q3(I)**2
7240
G4(I)=2*R*V1*(D1*SIN(O1(I))/R1(I)*Q2(I)+D2*SIN(O2(I))/R2(I)*Q3
(I))
7250 G(I)=G1(I)+G2(I)+G3(I)+G4(I)
7400 REM SUBR CALC H(I)=DF/DC2
7410 H1(I)=2*C1**2*EXP(-C2*R1(I)**2)*Q2(I)
7420 H2(I)=R1(I)/R2(I)*EXP(-C2*R1(I)**2)*Q3(I)
7430 H2(I)=H2(I)+R2(I)/R1(I)*EXP(-C2*R2(I)**2)*Q2(I)
7440 H2(I)=H2(I)*(-2)*Q1(I)*C1**2
7450 H3(I)=2*C1**2*EXP(-C2*R2(I)**2)*Q3(I)
7460 H4(I)=D1*R1(I)*SIN(O1(I))*EXP(-C2*R1(I)**2)
7470 H4(I)=H4(I)+D2*R2(I)*SIN(O2(I))*EXP(-C2*R2(I)**2)
7480 H4(I)=H4(I)*2*R*V1*C1
7490 H(I)=H1(I)+H2(I)+H3(I)+H4(I)
7600 REM SUBR CALC W(I)=D2F/DC1**2
7610 W1(I)=2/R1(I)**2*Q2(I)**2
7620 W2(I)=-4*Q1(I)/(R1(I)*R2(I))*C1
7630
W2(I)=W2(I)*(R1(I)**2*EXP(-C2*R1(I)**2)*Q3(I)+R2(I)**2*EXP(-C2
*R2(I)**2)*Q2(I))
7640 W3(I)=2/R2(I)**2*Q3(I)**2
7650 W4(I)=0
7660 W(I)=W1(I)+W2(I)+W3(I)+W4(I)
7800 REM SUBR CALC X(I)=D2F/DC2**2
7810
X1(I)=2*C1**2*R1(I)**2*EXP(-C2*R1(I)**2)*(2*EXP(-C2*R1(I)**2)-
1)
7820 X2(I)=R2(I)**2*EXP(-C2*(R1(I)**2+R2(I)**2))
7830 X2(I)=X2(I)-R1(I)**2*EXP(-C2*R1(I)**2)*Q3(I)
7840 X2(I)=X2(I)*R1(I)/R2(I)
7850
U8=R1(I)**2*EXP(-C2*(R1(I)**2+R2(I)**2))-R2(I)**2*EXP(-C2*R2(I
)**2)*Q2(I)
7860 X2(I)=X2(I)+R2(I)/R1(I)*U8
```

```
7870 X2(I)=X2(I)*C1**2*Q1(I)*(-2)
7880
X3(I)=2*C1**2*R2(I)**2*EXP(-C2*R2(I)**2)*(2*EXP(-C2*R2(I)**2)-
1)
7890 X4(I)=D1*R1(I)**3*SIN(O1(I))*EXP(-C2*R1(I)**2)
7900 X4(I)=X4(I)+D2*R2(I)**3*SIN(O2(I))*EXP(-C2*R2(I)**2)
7910 X4(I)=-2*X4(I)*R*V1*C1
7920 X(I)=X1(I)+X2(I)+X3(I)+X4(I)
8000 REM SUBR CALC Y(I)=D2F/DC1DC2
8010 Y1(I)=4*C1*EXP(-C2*R1(I)**2)*Q2(I)
8020 Y2(I)=R1(I)/R2(I)*EXP(-C2*R1(I)**2)*Q3(I)
8030 Y2(I)=Y2(I)+R2(I)/R1(I)*EXP(-C2*R2(I)**2)*Q2(I)
8040 Y2(I)=-4*Q1(I)*C1*Y2(I)
8050 Y3(I)=4*C1*EXP(-C2*R2(I)**2)*Q3(I)
8060 Y4(I)=D1*R1(I)*SIN(O1(I))*EXP(-C2*R1(I)**2)
8070 Y4(I)=Y4(I)+D2*R2(I)*SIN(O2(I))*EXP(-C2*R2(I)**2)
8080 Y4(I)=2*R*V1*Y4(I)
8090 Y(I)=Y1(I)+Y2(I)+Y3(I)+Y4(I)
8100 RETURN
8200 REM SUBR CALCULATES DERIVS FOR W/IN CORE.    USES
ASSUMPTION
8201 REM THAT FOR POINTS WITH IN THE CORE ONLY THE NEAREST
VORTEX
8202 REM AFFECTS THE FLOW;SUPER POSITION DOES NOT HOLD
8210 IF R1(I)<R2(I) THEN GOTO 8230
8220 RC=R2(I):OC=O2(I):DC=D2:GOTO8240
8230 RC=R1(I):OC=O1(I):DC=D1
8240 F1(I)=(DC*C1/RC*(1-EXP(-C2*RC**2)))**2
8250 F2(I)=2*DC*C1*(R*V1)/RC*(1-EXP(-C2*RC**2))*SIN(OC)
8260 F2(I)=F2(I)+(R*V1)**2-M(I)**2
8270 B(I)=SQR(F1(I)+F2(I)+M(I)**2)
8280 G1(I)=2*(DC/RC*(1-EXP(-C2*RC**2)))**2*C1
8290 G2(I)=2*DC*R*V1/RC*(1-EXP(-C2*RC**2))*SIN(OC)
8300 G(I)=G1(I)+G2(I)
8310 H1(I)=2*C1**2*(1-EXP(-C2*RC**2))*EXP(-C2*RC**2)
8320 H2(I)=2*DC*R*V1*C1*RC*SIN(OC)*EXP(-C2*RC**2)
8330 H(I)=H1(I)+H2(I)
8340 W1(I)=2*(DC/RC*(1-EXP(-C2*RC**2)))**2
8350 W2(I)=0
8360 W(I)=W1(I)+W2(I)
8370 X1(I)=2*C1**2*RC**2*EXP(-C2*RC**2)
8380 X1(I)=X1(I)*(2*EXP(-C2*RC**2)-1)
8390 X2(I)=-2*DC*C1*R*V1*RC**3*SIN(OC)
8400 X2(I)=X2(I)*EXP(-C2*RC**2)
8410 X(I)=X1(I)+X2(I)
8420 Y1(I)=4*C1*(1-EXP(-C2*RC**2))*EXP(-C2*RC**2)
8430 Y2(I)=2*DC*R*V1*RC*SIN(OC)*EXP(-C2*RC**2)
8440 Y(I)=Y1(I)+Y2(I)
8500 RETURN
```

99

Appendix B: <u>Data</u> <u>Display</u> <u>Program</u> "DISP4"

       The following program accepts a c_1 and c_2 pair as
well as the quantitative data for a particular run and
generates a theoretical Karman vortex street to compare
to the experimental Karman vortex street over several
cycles. It uses the same basic ideas on expansion of data
as "DATANAL8." The program is written in BASIC and outputs
the theoretical and experimental street data to an output
file, on diskette, as directed by the user. The data can
then be plotted for a direct comparison between theory and
experiment.

```
1 REM PROGRAM DISP4
10 REM VARIABLE DEFN
20 REM ARRAYS
30 REM SINGLE SUBSCRIPT
40 REM TF     THEORETICAL FLOW
50 REM M      ACTUAL FLOW
60 REM T      TIME (MSEC)
70 REM E    ANEMOMETER VOLTAGE
80 REM DOUBLE SUBSCRIPT
90 REM R(I,J)  RADIUS OF VORTEX I AT TIME J FROM HOTWIRE
100 REM O(I,J) ANGLE "        "         "      "        "
110 REM Fl(I,J) TANGENTIAL FLOW OF VORTEX I AT TIME J LINED UP
WITH VORTEX 1
120 REM F2(I,J) "         "       "         "         "         "
              " 2
160 REM VARIABLES
170 REM V1       TRANS VEL (FPS)
180 REM P,T1,D  BARO PRESS(INHG),TEMP(DEGF),DENSITY(LBM/FT**3)
190 REM M0 TO M4  CONSTANTS FOR HOT WIRE CAL
200 REM  D1,D2  DIR OF ROTATION FOR VORTEX 1 AND VORTEX 2
210 REM  C1,C2  VORTEX CHARACTERISTIC CONSTANTS
220 REM X1   AVG VORTEX SPACING
250 REM DIMENSION ARRAYS
260 DIM M(50),T(50,5),E(50)
265 DIM TF(50,5),R(6,50,5),O(6,50,5)
270 REM INPUT DATA
290 REM INPUT DATA
300 INPUT"RUN NU.";N$
310 INPUT"IS INPUT DATA ON DISK(Y/N)";D$
320 IF D$="Y" THEN GOSUB 3000:REM SUBR WILL INPUT DATA
330 IF D$="Y" THEN GOTO 380
340 PRINT"IF DATA NOT ON DISK, THEN IT HASN'T BEEN PROCESSED
AND C1,C2 ARE UNK"
350 PRINT"STOP AND PROCESS DATA FOR C1,C2"
360 GOTO 2000
380 INPUT "C1 IN (IN-LBM/FT**2-SEC)";C1
390 INPUT "C2 IN (IN**-2)";C2
395 INPUT "DENSITY FACTOR(0 TO 1)";FD
400 INPUT"AVG VORTEX SPACING IN INCHES";X1
410 FOR I=1TOI9-1
415 FOR K=1 TO 4
420 T(I,K)=T(I,0)+K/4*(T(I+1,0)-T(I,0))
422 PRINT"LN 422  K=";K
425 NEXT K
430 NEXT I
435 REM K=0 CORRESPONDS TO A TEST DATA PT.
440 REM CALC NEW R'S AND THETA'S AT EACH TIME INC.
450 O(1,1,0)=O(1,1,0)*ᴨ/180:O(2,1,0)=O(2,1,0)*ᴨ/180
460 H1=R(1,1,0)*SIN(O(1,1,0)):H2=R(2,1,0)*SIN(O(2,1,0))
470 R(3,1,0)=SQR(H1**2+(X1+R(2,1,0)*COS(O(2,1,0)))**2)
480 R(4,1,0)=SQR(H2**2+(2*X1+R(2,1,0)*COS(O(2,1,0)))**2)
490 R(5,1,0)=SQR(H1**2+(3*X1+R(2,1,0)*COS(O(2,1,0)))**2)
```

101

```
500 R(6,1,0)=SQR(H2**2+(4*X1+R(2,1,0)*COS(O(2,1,0)))**2)
510 O(3,1,0)=ATN(H1/(X1+R(2,1,0)*COS(O(2,1,0))))
520 O(5,1,0)=ATN(H1/(3*X1+R(2,1,0)*COS(O(2,1,0))))
530 O(4,1,0)=ATN(H2/(2*X1+R(2,1,0)*COS(O(2,1,0))))
540 O(6,1,0)=ATN(H2/(4*X1+R(2,1,0)*COS(O(2,1,0))))
550 REM CALCULATE EXP FLOWS
560 PRINT"ASSUMING HOT FILM USED IS K746"
570 M0=-887.645211:M1=2237.04893
580 M2=-1927.51774:M3=694.103018
590 M4=-87.5672976
600 FOR I=1 TO I9
610 M(I)=M0+M1*E(I)+M2*E(I)**2+M3*E(I)**3+M4*E(I)**4
620 NEXT I
630 PRINT"JUST CALC M(I)'S. I9= ";I9
700 REM CALCULATE NEW R'S AND THETA'S
710 V1=V1*12/1000:REM CONV TO IN/MSEC
720 FOR J=1 TO 6:REM VORTEX LOOP
730 FOR I=2 TO I9:REM TIME LOOP
735 FOR K=0 TO 4:REM INTERMEDIATE TIME LOOP
740 R(J,I,K)=(R(J,1,0)*COS(O(J,1,0))+V1*(T(I,K)-T(1,0)))**2
742 R(J,I,K)=(R(J,I,K)+(R(J,1,0)*SIN(O(J,1,0)))**2)**.5
743 IF (R(J,1,0)*COS(O(J,1,0))+V1*(T(I,K)-T(1,0)))<>0 THEN
GOTO 750
745 O(J,I,K)=π/2:GOTO 770
750 O(J,I,K)=R(J,1,0)*SIN(O(J,1,0))
751
O(J,I,K)=O(J,I,K)/(R(J,1,0)*COS(O(J,1,0))+V1*(T(I,K)-T(1,0)))
760 O(J,I,K)=ATN(O(J,I,K))
770 NEXT K
775 NEXT I
780 NEXT J
790 REM ADJUST O(J,I,K)
800 GOSUB 4000
900 REM CALCULATE MEAN FLOW
910 REM DENSITY IN LBM/FT**3
915 RS=(5/16)/2
920 T1=(T1+459.67)*((14+P)/(P+20))**((1.4-1)/1.4)
930 D=((P+14)*.4898*144)/(53.3*T1)
935 D=FD*D
940 REM CLACULATE THEORETICAL FLOW AT EACH TIME
950 FOR I=1 TO I9:REM TIME LOOP
955 FOR K=0TO 4
960 GOSUB 5000:REM SELECT 2 SMALLEST R'S
965 IF RL<RS THEN GOTO 1015
966 IFRL=0THEN AL=0:IF RL=0 THENGOTO 980
970 AL=DL*C1/RL*(1-EXP(-C2*RL**2))
980 AH=DH*C1/RH*(1-EXP(-C2*RH**2))
990 AS=AL*SIN(OL)+AH*SIN(OH)
1000 AC=AL*COS(OL)+AH*COS(OH)
1010 GOTO 1030
1015 IF RL<>0 THEN GOTO 1020
1017 AL=0:GOTO 1025
```

```
1020 AL=DL*C1/RL*(1-EXP(-C2*RL**2))
1025 AS=AL*SIN(OL):AC=AL*COS(OL)
1030 TF(I,K)=SQR((AS+D*V1*1000/12)**2+AC**2)
1035 NEXT K
1040 NEXT I
1050 PRINT"RESULTS:TIME,EXP,THEO"
1060 FOR I=1 TO I9
1065 FOR K=0 TO 4
1067 IF   K<>0 THEN GOTO 1080
1070 PRINT T(I,K);M(I);TF(I,K):GOTO1085
1080 PRINT T(I,K);"-------------";TF(I,K)
1085 NEXT K
1088 NEXT I
1090 INPUT"WRITE TO DISK(Y/N)";Y1$
1095 IF Y1$="N" THEN GOTO 1270
1100 REM OUTPUT TO PRINTER,DISK
1110 OPEN 1,4
1120 INPUT "HARD COPY(Y/N)";Y$
1130 DO$="0:RESF"+N$+",S,W"
1140 OPEN 2,8,9,DO$
1150 IF Y$="Y"THEN PRINT#1,"RUN# ";N1$
1160 PRINT#2,I9;",";C1;",";C2;",";FD;",";CHR$(13);
1170 IF Y$="Y" THEN PRINT#1,"NO. OF PTS IS ";I9
1180 IF Y$="Y" THEN PRINT#1,"C1= ";C1;" INLBM/FT**2-SEC"
1190 IF Y$="Y" THEN PRINT#1,"C2= ";C2;" IN**-2      DENSITY
FACTOR=";FD
1200 IF Y$="Y" THEN PRINT#1,"TIME(MS)";TAB(12);"ACT
FLOW";TAB(12);"THEO FLOW";
1205 IF Y$="Y" THEN PRINT#1,TAB(12);"ERROR(%)"
1210 FOR I=1 TO I9
1212 FOR K=0 TO 4
1213 IF K<>0 THEN GOTO1240
1215 PE=(TF(I,K)-M(I))/M(I)*100
1220 IFY$="Y"THEN
PRINT#1,T(I,K);TAB(10);M(I);TAB(10);TF(I,K);TAB(10);PE
1230 PRINT#2,T(I,K);",";M(I);",";TF(I,K);CHR$(13);
1235 GOTO 1245
1240 PRINT#2,T(I,K);",";-100;",";TF(I,K);",";CHR$(13);
1245 NEXT K
1250 NEXT I
1260 CLOSE1:CLOSE2
1270 PRINT"WOULD YOU LIKE TO GO AGAIN?"
1280 PRINT"INPUT N IF NO, ANO FOR ANOTHER OUTPUT OF  RESULTS"
1290 PRINT"AND SO FOR NEW INPUT OF RUN DATA"
1300 INPUT E$
1310 IF E$="N" THEN GOTO2000
1320 IF E$="ANO" THEN GOTO 1050
1330 IF E$="SO" THEN GOTO 250
2000 END
3000 REM PULL DATA OFF DISK
3010 INPUT"DATA FILE IN MMDDRR FORMAT";N1$
3020 RO$="0:DF"+N1$+",S,R"
```

```
3030 OPEN 2,8,9,RO$
3050 INPUT#2,I9,T(1,0),E(1)
3060 FOR I=2 TO I9
3070 INPUT#2,T(I,0),E(I)
3080 NEXT I
3090 INPUT#2,O(1,1,0),R(1,1,0),D1
3100 INPUT#2,O(2,1,0),R(2,1,0),D2
3110 INPUT#2,V1,P,T1
3130 CLOSE 2
3140 RETURN
4000 REM ADJUST THETA'S
4010 FOR J=1 TO 6:REM VORTEX LOOP
4020 FOR I=1 TO I9:REM TIME LOOP
4025 FOR K=0 TO 4
4030 IF O(J,I,K)<0 THEN O(J,I,K)=π-ABS(O(J,I,K))
4035 NEXT K
4040 NEXT I
4050 NEXT J
4060 RETURN
5000 REM SUBR SELECT 2 SMALLEST R'S
5010 RL=R(1,I,K)
5020 FOR J=1 TO 6:REM VORTEX LOOP
5030 IF R(J,I,K)>RL THEN GOTO 5060
5040 RL=R(J,I,K):OL=O(J,I,K):JL=J
5060 NEXT J
5080 IF JL<>1 THEN GOTO 5095
5085 RH=R(JL+1,I,K):OH=O(JL+1,I,K):GOTO 5160
5095 IF JL<>6 THEN GOTO 5105
5100 RH=R(JL-1,I,K):OH=O(JL-1,I,K):GOTO 5160
5105 IF R(JL+1,I,K)>R(JL-1,I,K) THEN GO TO 5115
5110 RH=R(JL+1,I,K):OH=O(JL+1,I,K):GOTO 5160
5115 RH=R(JL-1,I,K):OH=O(JL-1,I,K)
5160 REM GET DL,DH
5170 FOR J=1 TO 6
5180 IF RL<>R(J,I,K) THEN GOTO 5270
5190 IF J/2=INT(J/2) THEN GOTO 5240
5200 DL=D1:DH=D2:GOTO 5270
5240 DL=D2:DH=D1
5270 NEXT J
5300 RETURN
```

Appendix C: Equipment List

TABLE I

EQUIPMENT LIST

Item Number	Name	Serial Number
1	Anemometer, TSI, Inc. IFA-100	134D
2	Camera, Poloroid, Type 47 Film	-
3	Camera, Oscilloscope, Tektronix C30	B029890
4	Computer, HP85	-
5	Counter, CMC Model 726C	3957
6	Digitizer, HP9874A	-
7	Gauge, Wallace & Tiernan Model FA145 30 in Hg	HH10973
8	Hot Film Probe, TSI, Inc. 1214-10	K746
9	Manometer, Meriam Instrument Co. Model 33KA35-2, 30 inHg	L62931
10	Mirror, 40-inch focal length parabolic (2 each)	-
11	Oscilloscope, AN/USM-425	49300/ 4H4033
12	Power Supply, Cordin Model 5205	6-263
13	Power Supply, Cordin Model 5205 (modified for use with Cooke Spark Lamp)	6-261
14	Spark Lamp, Cooke Model 596-4116	8
15	Spark Lamp, Cordin Model 5401	8-256
16	Temperature Indicator, Fluke Model 2100A (Type K)	3957

Appendix D: <u>Schlieren</u> <u>and</u> <u>Anemometer</u> <u>Measurements</u>

Although a great many test runs were made, only
those with clear street definition were analyzed. Table II
and Figures 53 through 58 summarize the data from those
runs. Included are the c_1, c_2 and density factor values
derived from the data analysis. It should be noted that
the zero trace level on the anemometer trace is actually
2 volts due to the offset feature of the IFA-100. The
voltage levels were converted to flow levels via the cali-
bration equation:

$$\rho u \, (lbm/ft^2 \, sec) = -887.65 + 2237.05E - 1927.52E^2$$
$$+ 694.10E^3 - 87.57E^4$$

where E is the anemometer output in volts.

In Table II, those entries with a * by them indi-
cate that the density factor was equal to:

$$fd = V_\infty / \overline{V}$$

so as to use the Prandtl-Tietjens superposition theory in
the analysis program.

TABLE II

DATA SUMMARY

Run	Density Factor	c_1	c_2	Trans Vel (fps)
092502	0.6	12.7	27.2	423
	1.0	0.0	0.0	
	1.14*	2.85	57.64	
092504	0.4	5.84	58.21	453.4
	0.6	3.70	58.21	
	1.0*	0.01	8.74	
	1.2	0.0	0.0	
	1.4	0.01	7.60	
092601	0.4	10.21	68.40	484
	0.6	9.2	55.2	
	0.85	1.52	151.6	
	1.0*	2.56	39.65	
	1.2	1.09	24.19	
092602	0.76	15.6	8.76	426
	0.9	0.0	0.0	
	1.0	0.0	0.0	
	1.14*	0.892	14.83	
092606	0.76	9.59	26.64	398
	0.9	8.14	29.59	
	1.22*	2.93	88.72	

TABLE II--Continued

Run	Density Factor	c_1	c_2	Trans Vel (fps)
092609	0.6	10.78	62.7	363
	1.0	3.30	1.40	
	1.2	2.61	58.96	
	1.33*	4.02	87.8	
	1.4	4.75	63.70	
092611	0.6	17.91	115.5	369.6
	1.0	0.0	0.0	
	1.2	1.48	101.5	
	1.31*	2.81	102.5	
	1.4	3.91	123.2	
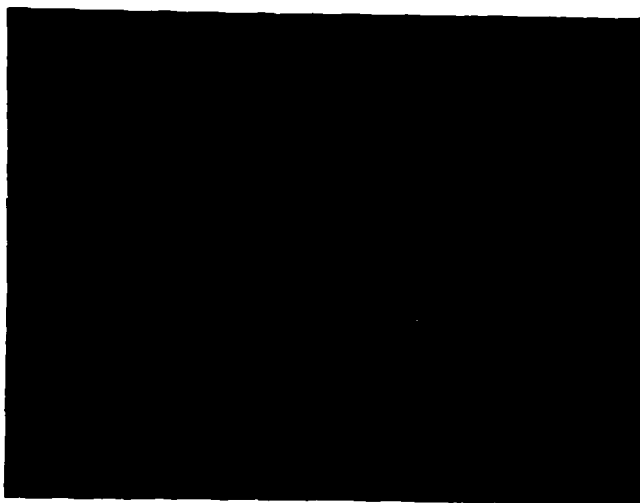
Baro. Press. = 29.164 in Hg
Total Temp. = 70°F
0.2 msec/div horizontal
0.1 v/div vertical
Spark lamp delay = 1.202 ms

Fig. 53.   Data for Run 092502

109

Baro. Press. = 29.164 in Hg
Total Temp. = 71.3°F
0.2 msec/div horizontal
0.1 v/div vertical
Spark lamp delay = 1.2026 ms

Fig. 54.   Data for Run 092504

110

Baro. Press. = 28.990 in Hg
Total Temp = 72° F
0.2 msec/div horizontal
0.1 v/div vertical
Spark lamp delay = 1.2022 ms

Fig. 55. Data for Run 092601

111

Baro. Press. = 28.990 in Hg
Total Temp = 72.3° F
0.2 msec/div horizontal
0.1 v/div vertical
Spark lamp delay = 1.2045 ms

Fig. 56. Data for Run 092606

112
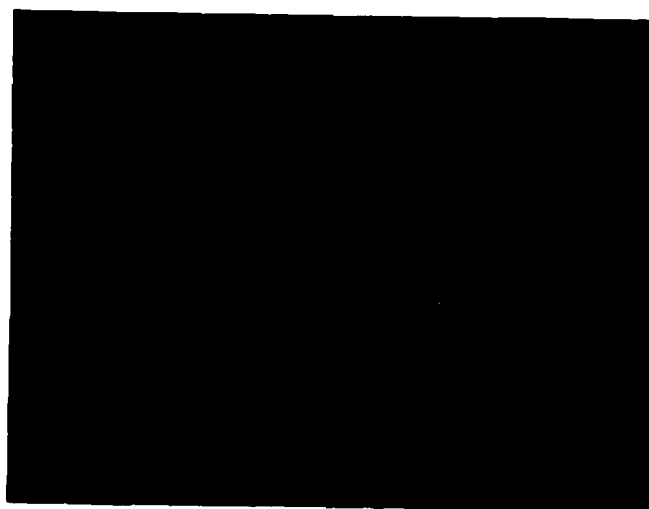
Baro. Press. = 28.990 in Hg
Total Temp = 72.5° F
0.2 msec/div horizontal
0.1 v/div vertical
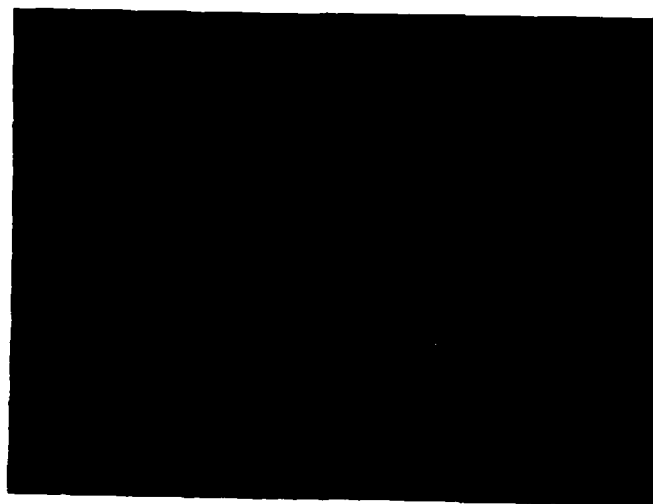Spark lamp delay = 1.2054 ms

Fig. 57. Data for Run 092609

113

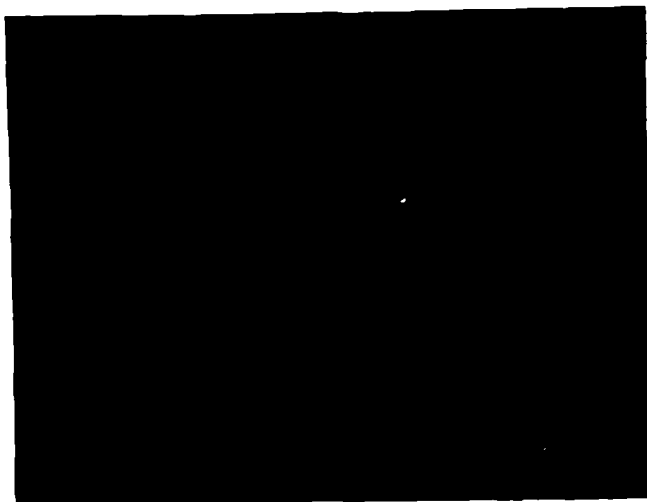Baro. Press. = 28.990 in Hg
Total Temp = 72.5° F
0.2 msec/div horizontal
0.1 v/div vertical
Spark lamp delay = 1.2057 ms

Fig. 58.   Data for Run 092611

114

Bibliography

1. Fage, A., A. R. C. Sci, and F. C. Johanson, B. Sc. "The Structure of Vortex Sheets," Reports and Memoranda No. 1143 (Ae 311), *Philosophical Magazine, V*: 1-27 (February 1928).

2. Relf, E. F., A. R. C. Sci, and L. F. G. Simmons, B.A., A.R.C. Sc. "The Frequency of the Eddies Generated by the Motion of Circular Cylinders Through a Fluid," Reports and Memoranda No. 917, *Royal Society Proceedings* (June 1924).

3. Roshko, A. "On the Development of Turbulent Wakes from Vortex Streets." *Fortieth Annual Report of the NACA*: 801-825, NACA TR 1191. U.S. Government Printing Office, 1956.

4. Schlichting, H. *Boundary Layer Theory*. New York: McGraw-Hill Co., 1979.

5. Weston, C. P. *Influence of Periodic Compressible Vortices on Laser Beam Intensity*. MS thesis. Wright-Patterson Air Force Base OH: Air Force Institute of Technology, December 1982.

6. Clark, G. C. *Effects of Multiple Cylinders on the Formation of von Karman Vortex Streets*. MS thesis. Wright-Patterson Air Force Base OH: Air Force Institute of Technology, December 1983.

7. Luttges, M. W. and M. C. Robinson. "Unsteady Separated Flow: Forced and Common Vorticity About Oscillating Airfoils." Unpublished paper, University of Colorado, Boulder CO, 117-126.

8. Dosanjh, D. S. and T. M. Weeks. "Interaction of a Starting Vortex as Well as a Vortex Street with a Traveling Shock Wave," *AIAA Journal, 3*(2): 216-223 (February 1965).

9. Cornish, J. J. III. "Vortex Flows." Lecture presented at Eight Quick-Goethert Lecture Series, University of Tennessee Space Institute, Tullahoma TN, 21 October 1982.

115

10. Naumann, A. and E. Hermanns. "On the Interaction Between a Shock Wave and a Vortex Field," AGARD Conference Proceedings No. 131, Noise Mechanisms, 19-21 September, 1973: 23-1 to 23-10.

11. Pao, S. P. and M. D. Salas. "A Numerical Study of Two-Dimensional Shock-Vortex Interaction," AIAA Paper 81-1205, 1981.

12. Bradshaw, P. An Introduction to Turbulence and Its Measurement. New York: Pergamon Press, 1971, 107-133.

13. McQueen, Stephen M. Velocity and Transient Measurements in a Shock Tube Using a Hot-Wire Anemometer. MS thesis. Wright-Patterson Air Force Base OH: Air Force Institute of Technology, December 1984.

14. Kuethe, Arnold M. and Chuen-Yen Chow. Foundations of Aerodynamics: Bases of Aerodynamic Design (Third Edition). New York: John Wiley and Sons, 1976.

15. Miller, Alan R. BASIC Programs for Scientists and Engineers. Berkeley: Sybex, Inc., 1981, 179-182.

16. Bronson, Richard. Operations Research. New York: McGraw-Hill Book Company, 1982, 110-114.

17. Prandtl, L. and O. G. Tietjens. Applied Hydro- and Aeromechanics. New York: Dover Publications, Inc., 1934, 130-135.

VITA

First Lieutenant John B. Wissler was born on
7 January 1958 in Bremerton, Washington. He graduated
from Radford High School in Honolulu, Hawaii in 1976 and
went to the U.S. Naval Academy (1976-1978), George Wash-
ington University (1978-1980), and the University of
Maryland (1980-1981) where he received a degree of Bachelor
of Science in Mechanical Engineering in December, 1981.
Upon graduation, he attended Air Force Officer Training
School, receiving his commission in the USAF in April,
1982. He then served as an R&D Munitions Test Engineer
with the 3246th Test Wing, Eglin AFB, Florida, until
entering the School of Engineering, Air Force Institute of
Technology, in May, 1984.

      Permanent address: P.O. Box 660

                            Madera, California 93639

AD-A164 01

REPORT DOCUMENTATION PAGE

1a. REPORT SECURITY CLASSIFICATION	1b. RESTRICTIVE MARKINGS
UNCLASSIFIED	

2a. SECURITY CLASSIFICATION AUTHORITY	3. DISTRIBUTION/AVAILABILITY OF REPORT
	Approved for public release;
2b. DECLASSIFICATION/DOWNGRADING SCHEDULE	distribution unlimited

4. PERFORMING ORGANIZATION REPORT NUMBER(S)	5. MONITORING ORGANIZATION REPORT NUMBER(S)
AFIT/GAE/AA/85D-18	

6a. NAME OF PERFORMING ORGANIZATION	6b. OFFICE SYMBOL (If applicable)	7a. NAME OF MONITORING ORGANIZATION
School of Engineering	AFIT/ENY	

6c. ADDRESS (City, State and ZIP Code)	7b. ADDRESS (City, State and ZIP Code)
Air Force Institute of Technology	
Wright-Patterson AFB, OH 45433	

8a. NAME OF FUNDING/SPONSORING ORGANIZATION	8b. OFFICE SYMBOL (If applicable)	9. PROCUREMENT INSTRUMENT IDENTIFICATION NUMBER

8c. ADDRESS (City, State and ZIP Code)	10. SOURCE OF FUNDING NOS.			
	PROGRAM ELEMENT NO.	PROJECT NO.	TASK NO.	WORK UNIT NO.

11. TITLE (Include Security Classification)
see box 19

12. PERSONAL AUTHOR(S)
John B. Wissler, B.S., 1st Lt, USAF

13a. TYPE OF REPORT	13b. TIME COVERED	14. DATE OF REPORT (Yr., Mo., Day)	15. PAGE COUNT
MS Thesis	FROM _____ TO _____	1985, December 13	132

16. SUPPLEMENTARY NOTATION

17.	COSATI CODES		18. SUBJECT TERMS (Continue on reverse if necessary and identify by block number)
FIELD	GROUP	SUB. GR.	Vortices, Schlieren Photography, Hot-Wire Anemometers,
20	04		Vortex Streets

19. ABSTRACT (Continue on reverse if necessary and identify by block number)

Title: A Schlieren and Hot-Wire Investigation of Karman Vortex Streets

Thesis Chairman: Eric J. Jumper, Lieutenant Colonel, USAF
Professor of Aerospace Engineering

Approved for public release: IAW AFR 190-1.

LYNN E. WOLAVER 16 JAN 86
Dean for Research and Professional Development
Air Force Institute of Technology (AIC)
Wright-Patterson AFB OH 45433

20. DISTRIBUTION/AVAILABILITY OF ABSTRACT	21. ABSTRACT SECURITY CLASSIFICATION
UNCLASSIFIED/UNLIMITED XX SAME AS RPT ☐ DTIC USERS ☐	UNCLASSIFIED

22a. NAME OF RESPONSIBLE INDIVIDUAL	22b. TELEPHONE NUMBER (Include Area Code)	22c. OFFICE SYMBOL
Eric J. Jumper, Lieutenant Colonel, USAF	(513)255-2998	AFIT/ENY

DD FORM 1473, 83 APR EDITION OF 1 JAN 73 IS OBSOLETE.

→ This investigation involved taking schlieren and hot-film anemometer data on Karman vortex streets, then developing a means of characterizing the individual vortices in a street using a schlieren picture and the corresponding anemometer trace. A ThermoSystems, Inc. IFA-100 anemometer system, with a Tektronix 425 oscilloscope, was used to record an anemometer trace. The trace was captured on photographic film. The oscilloscope also fired a Cordin Model 5401 spark lamp, which provided, via a schlieren optical system, a physical picture of the Karman streets formed behind a 5/16-inch dia cylinder in a 2-inch by 2-inch square cross-section test region with a Mach 0.43 flow. Distance and angle information were obtained from the schlieren photographs, and timing and anemometer output voltage were obtained from the anemometer trace photograph using an HP-9874A digitizer. The data were analyzed using a Newton-Raphson method to solve for two constants, c_1 and c_2, which should have completely characterized the vortices in the vortex street, assuming the vortices followed the theoretical equation for a combined free and forced vortex. It was assumed that the superposition of two vortices plus the mean flow were the parameters influencing the flow at any point in space and time. The core supremacy principle, which says that in a vortex core only one vortex contributes to the flow, was used in the data analysis. It was found that generally close fits between the theoretical data using the solved for constants c_1 and c_2, and the experimental data from the anemometer were possible, thus indicating reasonable vortex characterization.

END

FILMED

3-86

DTIC